

Summer 8-11-2015

Adaptive Online Transient Stability Assessment of Power Systems for Operational Purposes

Hussain Hassan Al Marhoon
University of New Orleans, halmaroo@uno.edu

Follow this and additional works at: <https://scholarworks.uno.edu/td>



Part of the [Power and Energy Commons](#)

Recommended Citation

Al Marhoon, Hussain Hassan, "Adaptive Online Transient Stability Assessment of Power Systems for Operational Purposes" (2015). *University of New Orleans Theses and Dissertations*. 2036.
<https://scholarworks.uno.edu/td/2036>

This Dissertation-Restricted is protected by copyright and/or related rights. It has been brought to you by ScholarWorks@UNO with permission from the rights-holder(s). You are free to use this Dissertation-Restricted in any way that is permitted by the copyright and related rights legislation that applies to your use. For other uses you need to obtain permission from the rights-holder(s) directly, unless additional rights are indicated by a Creative Commons license in the record and/or on the work itself.

This Dissertation-Restricted has been accepted for inclusion in University of New Orleans Theses and Dissertations by an authorized administrator of ScholarWorks@UNO. For more information, please contact scholarworks@uno.edu.

Adaptive Online Transient Stability Assessment of Power Systems for Operational Purposes

A Dissertation

Submitted to the Graduate Faculty of the
University of New Orleans
in partial fulfillment of the
requirements for the degree of

Doctor of Philosophy
in
Engineering and Applied Sciences
Electrical Engineering

By

Hussain Hassan Al Marhoon

M.S., University of New Orleans, 2010

B.S., University of New Orleans, 2008

August, 2015

© 2015
Hussain H. Al Marhoon

All Rights Reserved

Dedication

I dedicate my work to the loving memory of my father, Hassan Ali Al Marhoon, who I love and miss dearly! God bless his soul. I also dedicate my dissertation with a special feeling of gratitude to my loving mother whose words of encouragement and continuous support ring in my ears. Mom, I love you so much! Additionally, my sister has always encouraged me to become who I am on personal and professional levels. My brothers, Ali, Mohammed, Moayad and Ahmed, have never left my side and have always been supportive throughout this journey.

Acknowledgements

This dissertation would not have been possible without the guidance and help of several individuals who in one way or another contributed and extended their valuable assistance in the preparation and completion of this study.

First and foremost, I would like to express my utmost gratitude to my major advisor, Dr. Parviz Rastgoufard for his valuable guidance and selfless support during my graduate studies. His patience and unfailing encouragement have been the major contributing factors in the completion of my dissertation research. I am truly thankful to the members of the supervisory committee: Dr. Ittiphong Leevongwat, Dr. Vesselin Jilkov, Dr. George Ioup, and Dr. Norma Jean Mattei for their great support throughout the process to complete this research. I would like to thank Dr. Rasheed Azzam for being on my Masters supervisory committee, as he was an essential person to complete this research. I would like to thank the Entergy-UNO Power and Research Laboratory for providing the appropriate tools to finish this research.

I express my heartfelt thankful to my parents, sister and brothers for their never ending love and support. I am thankful to all my friends and co-workers for their knowledgeable feedback and moral support.

Finally, I would like to thank all the professors and staff at the University of New Orleans who contributed in providing quality education. I would also like to thank the Saudi Ministry of Higher Education for supporting me financially throughout my studies.

Table of Contents

List of Figures.....	viii
List of Tables	ix
Abstract.....	x
Chapter 1	1
1 Introduction	1
1.1 Power System Stability	1
1.2 Forms of Power Instability.....	2
1.3 Classification of Stability	2
1.4 Historical Review of Power System Stability Problems.....	5
1.5 Review of Rotor Angle Stability.....	7
1.6 Review of Rotor Angle Stability Analysis Methods.....	8
1.7 Review of Online Dynamic Security Assessment Methods.....	11
1.8 Scope	14
Chapter 2	17
2 Power System Stability Formulation.....	17
2.1 Basic Concept and Variables in Transient Stability.....	17
2.1.1 Rotor Angle Stability	18
2.1.2 Small-Signal Stability	23
2.1.3 Transient Stability.....	25
2.2 Formulation of Existing Methods of Transient Stability	26
2.2.1 Swing Equation.....	27
2.2.2 Equal-Area Criterion.....	28
2.2.3 Numerical Integration Methods	30
2.2.4 Direct Methods for Transient Stability Analysis	31
2.3 Power System Models.....	33
2.3.1 Single-Machine Infinite-Bus Classical System Model.....	33
2.3.2 Single-Machine Infinite-Bus Detailed System Model (6 th Order).....	34
2.3.3 Multi-Machine Classical System Model.....	36
2.4 Summary	38
Chapter 3	40
3 Transient Stability Using Numerical Methods	40
3.1 Overview	40
3.2 Numerical Integration Methods	40
3.2.1 Euler Method	40
3.2.2 Runge-Kutta (R-K) Methods	42
3.2.3 Implicit Integration Methods	43
3.3 Simulation of Power System Dynamic Response	44
3.3.1 Overall System Equations.....	44
3.3.2 Solution of Overall System Equations Using Implicit Integration Methods	45
3.4 Summary	47

Chapter 4	48
4 Transient Stability Analysis Using Direct Methods	48
4.1 Overview	48
4.2 Lyapunov’s Method [7].....	48
4.3 Transient Energy Function (TEF) Formulation	49
4.3.1 Main Idea	49
4.3.2 Mathematical Development	50
4.3.3 Mathematical Development of TEF of Multi-Machine Power System	51
4.4 Multi-machine Transient Stability Measure Using TEF	54
4.4.1 Individual Machine Energy Function for Synchronous Reference Frame [18].....	54
4.4.2 Individual Machine Energy Function for COI Reference Frame	55
4.4.3 Equal Area Criterion for Multi-Machine System [20].....	57
4.5 Proof of Concept Proposed Method	61
4.6 Summary	62
Chapter 5	63
5 Problem Statement, Objective, and Methodology	63
5.1 Problem Statement	63
5.2 Objective	66
5.3 Methodology	66
5.3.1 Modeling and Simulation of the Test System (Phase I)	67
5.3.2 Identification of Critical Machine(s) (Phase II).....	69
5.3.3 Online Transient Stability Assessment (Phase III)	74
5.3.4 Critical Clearing Time Calculations (Phase IV)	77
5.4 Summary	79
Chapter 6	80
6 Test System.....	80
6.1 IEEE 39-Bus Test System.....	80
6.1.1 Transmission Lines	81
6.1.2 Transformers	81
6.1.3 Generators	82
6.1.4 Loads.....	83
6.2 Summary	84
Chapter 7	85
7 Simulation Results.....	85
7.1 Modeling and Simulation of IEEE 39 Bus System (Phase I).....	85
7.2 Identification of Critical Machine(s) (Phase II)	90
7.2.1 Determination of the Severely Disturbed Unit (SDU) Using Accelerating Power	90
7.2.2 Finding Coherent Generators with the SDU	92
7.2.3 Finding SDU Using During-Fault Rotor Angles	94
7.2.4 Finding SDU Using During-Fault Rotor Speed.....	99
7.2.5 Finding SDU Using Change in Rotor Angle	105
7.3 Online Transient Stability Assessment (Phase III)	107
7.4 Critical Clearing Time Calculation (Phase IV)	115

7.5	Results Discussion.....	120
7.6	Summary	121
Chapter 8	123
8	Concluding Remarks and Future Work	123
8.1	Concluding Remarks	123
8.2	Future Work	125
Appendix A	126
Bibliography	136
Vita	140

List of Figures

Figure 1.1: Classification of power system stability [5]	4
Figure 2.1: Single line diagram and equivalent circuit of a two-machine system [5]	19
Figure 2.2: Phasor diagram or power transfer characteristic of a two-machine system [5]	20
Figure 2.3: Power-angle characteristic of a two-machine system [5].....	21
Figure 2.4: Nature of small-disturbance response with constant field voltage [5]	24
Figure 2.5: Nature of small-disturbance response with excitation control [5]	24
Figure 2.6: Rotor angle response to a transient disturbance. Redrawn from [5]	26
Figure 2.7: Simple SMIB System [18]	28
Figure 2.8: Power-angle characteristic of the system in Figure 2.7.....	29
Figure 2.9: A ball rolling on the inner surface of a bowl.....	31
Figure 2.10: Single-machine infinite-bus system	33
Figure 3.1: Euler’s method illustration	41
Figure 4.1: Potential energy plot. Redrawn from [14].....	50
Figure 5.1: Power System Operational States [50].....	65
Figure 5.2: Effect of Prefault Loading Condition on CCT [42]	66
Figure 5.3: Phase I – Modeling and Simulation	68
Figure 5.4: Phase II – Identification of Critical Machine(s).....	70
Figure 5.5: Phase III – Online Transient Stability Assessment	75
Figure 5.6: Phase IV – Critical Clearing Time Calculations	78
Figure 6.1: IEEE 39-Bus System	80
Figure 7.1: Generator rotor speeds for a fault on Bus 25.....	86
Figure 7.2: Generator rotor angles for a fault on Bus 25	86
Figure 7.3: Generator rotor speeds for a fault on Bus 25 for Phase I	87
Figure 7.4: Generator rotor angles for a fault on Bus 25 for Phase I.....	87
Figure 7.5: Generator rotor speeds for a fault on Bus 35.....	88
Figure 7.6: Generator rotor angles for a fault on Bus 35	88
Figure 7.7: Generator rotor speeds for a fault on Bus 35 for Phase I	89
Figure 7.8: Generator rotor angles for a fault on Bus 35 for Phase I.....	89
Figure 7.9: Generator rotor speeds for a fault on Bus 9.....	93
Figure 7.10: Rotor angle distance for fault on Bus 25 cleared in 0.1 sec	95
Figure 7.11: Rotor angle distance for fault on Bus 25 cleared in 0.23 sec	96
Figure 7.12: Rotor angle distance for fault on Bus 35 cleared in 0.10 sec	97
Figure 7.13: Rotor angle distance for fault on Bus 35 cleared in 0.23 sec	99
Figure 7.14: Rotor speed distance for fault on Bus 25 cleared in 0.1 sec.....	100
Figure 7.15: Rotor speed distance for fault on Bus 25 cleared in 0.23 sec.....	101
Figure 7.16: Rotor speed distance for fault on Bus 35 cleared in 0.10 sec.....	103
Figure 7.17: Rotor speed distance for fault on Bus 35 cleared in 0.23 sec.....	104
Figure 7.18: The difference between PE and KE for different clearing times	115

List of Tables

Table 6.1: Transmission Line Data.....	81
Table 6.2: Transformers Data	82
Table 6.3: Generators' Initial Load Flow	83
Table 6.4: Generators Details	83
Table 6.5: Loads Data	84
Table 7.1: Accelerating Power for fault on Bus 25 cleared in 0.10 sec.....	90
Table 7.2: Accelerating Power for fault on Bus 25 cleared in 0.23 sec.....	91
Table 7.3: Accelerating Power for fault on Bus 35 cleared in 0.1 sec.....	91
Table 7.4: Accelerating Power for fault on Bus 35 cleared in 0.23 sec.....	91
Table 7.5: During-Fault Rotor Angles Distance Measure (Bus 25 $t_c = 0.10$ sec)	94
Table 7.6: During-Fault Rotor Angles Distance Measure (Bus 25 $t_c = 0.23$ sec)	96
Table 7.7: During-Fault Rotor Angles Distance Measure (Bus 35 $t_c = 0.10$ sec)	97
Table 7.8: During-Fault Rotor Angles Distance Measure (Bus 35 $t_c = 0.23$ sec)	98
Table 7.9: During-Fault Rotor Speeds Distance Measure (Bus 25 $t_c = 0.10$ sec)	100
Table 7.10: During-Fault Rotor Speeds Distance Measure (Bus 25 $t_c = 0.23$ sec)	101
Table 7.11: During-Fault Rotor Speed Distance Measure (Bus 35 $t_c = 0.10$ sec).....	102
Table 7.12: During-Fault Rotor Speeds Distance Measure (Bus 35 $t_c = 0.23$ sec)	104
Table 7.13: Rotor Angle Change Measure (Bus 25 $t_c = 0.10$ sec)	105
Table 7.14: Rotor Angle Change Measure (Bus 25 $t_c = 0.23$ sec)	105
Table 7.15: Rotor Angle Change Measure (Bus 35 $t_c = 0.10$ sec)	106
Table 7.16: Rotor Angle Change Measure (Bus 35 $t_c = 0.23$ sec)	106
Table 7.17: Potential Energy per Group of Machines Investigation Result	108
Table 7.18: TSA Results (Stable Cases Pre- = Post-Fault).....	110
Table 7.19: TSA Results (Unstable Cases Pre- = Post-Fault)	111
Table 7.20: TSA Results (Stable Cases Pre- \neq Post-Fault).....	112
Table 7.21: TSA Results (Unstable Cases Pre- \neq Post-Fault)	113
Table 7.22: Average Simulation Time of Proposed Method	114
Table 7.23: CCT Calculation Comparison (pre-fault = post-fault).....	116
Table 7.24: CCT Calculation Comparison (pre-fault \neq post-fault).....	118
Table 7.25: Average Simulation Time for Calculating CCT	119

Abstract

Online stability assessment is an important problem that has not been solved completely yet. The purpose of this research is to tackle online transient stability assessment. Currently, most utility companies use step-by-step integration in order to set protective equipment so that they effectively work for critical contingencies. However, there are times an unforeseen contingency may occur which may cause the system to transit and the protective equipment to misoperate and does not isolate the disturbed part of the system. This research introduces a method that automatically determines a group of generators that participate in system separation and hence transient instability. The method consists of four phases: modeling and simulation, critical machines identification, online transient stability assessment, and critical clearing time calculation. In the modeling and simulation phase, the power system is built and the generators' rotor angles and speeds are captured. In the critical machines identification phase, the average instantaneous rotor accelerating powers, coherency measures, the during-fault rotor angles and speeds characteristics, and the pre- and post-fault rotor angles are used to identify the Severely Disturbed Group (SDG) of machines. The results of this phase are used to calculate the kinetic energy of the SDG and potential energy of another (or possibly the same) group of generators. Utilization and success of the proposed method will be documented using results from the IEEE 39-Bus test system. Each step of each phase will be demonstrated as needed. The proposed method is compared to step-by-step integration and two direct methods. The suitability of the proposed method for operation will be shown in cases where the Y-Bus matrix and rotor angles and speeds are given. The proof of concept of the proposed method was used in simulating the test system and encouraging results of the simulation were published in [1] and [2]. The proof of

concept is the foundation of the method proposed in this dissertation to determine transient stability of large-scale power systems.

Key Words: Transient stability, online stability, direct methods, numerical methods, energy function, critical machine, kinetic energy, potential energy

Chapter 1

1 Introduction

1.1 Power System Stability

Power systems generally consist of three stages: generation, transmission, and distribution. In the first stage, generation, the electric power is generated mostly by using synchronous generators. Then the voltage level is raised by transformers before the power is transmitted in order to reduce the line currents which consequently reduce the power transmission losses. After the transmission, the voltage is stepped down using transformers in order to be distributed accordingly.

Power systems are designed to provide continuous power supply that maintains voltage stability. However, due to undesired events, such as lightning, accidents or any other unpredictable events, short circuits between the phase wires of the transmission lines or between a phase wire and the ground may occur. This is called a *fault*. Due to a fault, one or more generators may be severely disturbed causing an imbalance between generation and demand. If the fault persists and is not cleared in a pre-specified time frame, it may cause severe damages to the equipment which in turn may lead to a power loss and power outage. Therefore, protective equipment are installed to detect faults and clear/isolate faulted parts of the power system as quickly as possible before the fault energy is propagated to the rest of the system.

Power system stability is a very important aspect to supply continuous power. It is defined as the property of a power system that enables it to remain in a state of operating equilibrium under normal operating conditions and to regain an acceptable state of equilibrium after being subjected to a disturbance [5]. Instability of power system can occur in many

different situations depending on the system configuration and operating mode. One of the stability problems is maintaining synchronous operation or synchronism, especially where that power system relies on synchronous machines. This aspect is influenced by the dynamic of generator rotor angles and power-angle relationships. Another instability problem that may be encountered is voltage collapse that is mostly related to load behavior and not synchronous speed of generators.

1.2 Forms of Power Instability

There are three different forms of power system instability: rotor angle instability, voltage instability and voltage collapse, and mid-term and long-term instability. *Rotor angle stability* is the ability of interconnected synchronous machines of a power system to remain in synchronism. *Voltage stability* is the ability of a power system to maintain acceptable voltages at all buses in the system under normal operating conditions and after being subjected to a disturbance. For the voltage to be stable, the synchronous machines must run in synchronism. The *long-term* and *mid-term stability* are relatively more recent to the literature on power system stability [5]. Long-term stability is associated with the slower and longer-duration phenomena that accompany large-scale system upsets and on the resulting large, and sustained mismatches between generation and consumption of active and reactive power. In mid-term stability, the focus is on synchronizing power oscillations between machines, including the effects of some of the slower phenomena and possibly large voltage or frequency excursions [5].

1.3 Classification of Stability

Figure 1.1 provides a comprehensive categorization of power system stability. As depicted by Figure 1.1, there are two main classes of stability: *angle stability* and *voltage stability*. Angle stability has two main subclasses: *small-signal (steady-state) stability* and

transient stability. A power system is considered to be *steady-state stable* if, after any small disturbance, it reaches a steady state operating condition which is identical or close to the pre-disturbance operating condition. A power system is transient stable for a large disturbance or sequence of disturbances if, following a disturbance(s) it reaches an acceptable steady-state operating condition. Unlike steady-state stability which is a function only of the operating condition, transient stability is more complicated since it is a function of both operating condition and the disturbance [6]. Voltage stability also has two main subclasses: *large-disturbance voltage stability* and *small-disturbance voltage stability*. There is some overlap between mid-term/long-term stability and voltage stability. With appropriate models for loads, Under-Load Tap Changer (ULTC) transformer and generator reactive power limits, mid-term/long-term stability simulations are ideally suited for dynamic analysis of voltage stability. Similarly, there is overlap between transient, mid-term and long-term stability: all three use similar analytical techniques for simulation of the nonlinear time domain response of the system to large disturbances. It can be seen that the three categories are concerned with different aspects of the stability problem, but, in terms of analysis and simulation, they are extensions of one another.

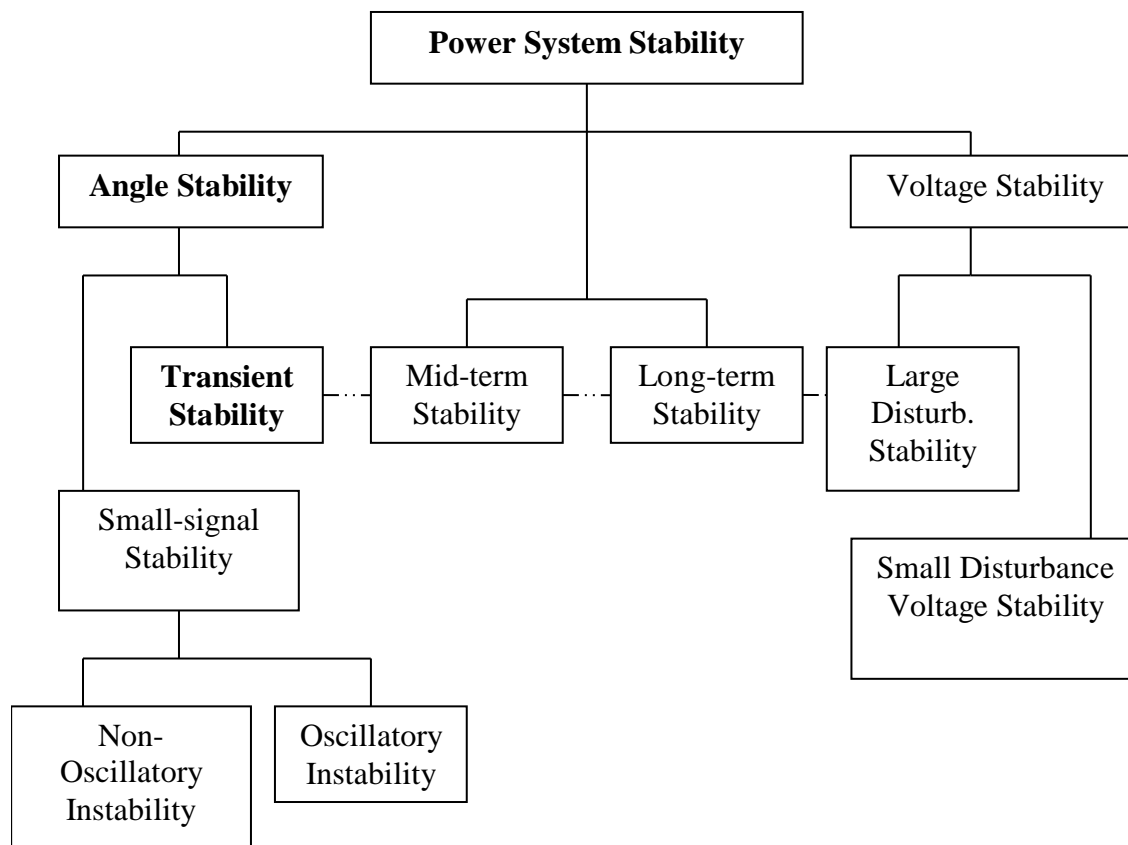


Figure 1.1: Classification of power system stability [5]

Apart from different categories of power system stabilities, this research will focus on transient stability. For transient stability, it is usually when the power system experiences a large disturbance caused by an imbalance between the mechanical input and the electrical output powers. In order to study this type of stability, the focus is only on the first swing periodic drift. Therefore, only a fraction of a second is enough to observe the transients and several simulation time seconds to study the system. As of the small-signal stability, it occurs when the system lacks synchronizing torque or when an unstable control action occurs. This type of stability requires a study of more than a minute to several hours.

1.4 Historical Review of Power System Stability Problems

Different forms of instability have emerged over the last century. The methods of power system stability problems analysis were influenced by the development of computational tools, stability theories, and power system control technologies. Therefore, it is very essential to present a review of the history of the subject to better understand the methods used in industries with regard of system stability and how these developments relate to the proposed practical method in this research.

Power system stability is a complex problem that has challenged power system engineers for many years. It was first recognized as an important problem in 1920s (Steinmetz, 1920; Evans and Bergvall, 1924; Wilkins 1926) [7]. The first field tests on the stability on a practical power system were conducted in 1925 ([11], [12]). The early stability problems were associated with remote power plants feeding load centers over long transmission lines. With slow exciters and non-continuously acting voltage regulators, power transfer capability was often limited by steady-state as well as transient rotor angle instability due to insufficient synchronizing torque [13].

In the early years, graphical methods such as Equal Area Criterion (EAC) and the power circle diagrams were developed. These methods were successfully applied to early systems that could be represented as two-machine systems. As the systems become larger and more interconnected (which was found to be economically better), the complexity of the systems grew and therefore the stability problems became more complex. This voided the treatment of the systems as two-machine systems. A significant step towards the improvement of stability calculations was the development in 1930 of the network analyzer which was capable of power flow analysis of multi-machine power systems ([5], [13]). A network analyzer is essentially a

scaled model of an AC power system with adjustable resistors, inductors and capacitors to represent the transmission network and loads, voltage sources whose magnitude and angle are adjustable, and meters to measure voltages, currents, and power anywhere in the network. However, system dynamic still had to be solved by hand by solving the swing equations using step-by-step numerical integration. During this period, classical models were used for the swing equations, that is, by representing the generators as fixed transient reactances with a fixed power supply behind these reactances.

In the early 1950s, electronic analog computers were used for analysis of special problems requiring detailed modeling of the synchronous machine, excitation system, and speed governor. Also during that period, development of digital computers was seen, and specifically about 1956, the first digital program for power system stability analysis was developed. In the 1960s, most of the power systems in the United States and Canada were joined as part of one of two large interconnected systems, one in the east and the other in the west. In 1967, low capacity HVDC ties were also established between the east and west systems. Nowadays, the power systems in the United States and Canada form virtually one large system. This interconnection between the two systems results in operating economy and increased reliability, though, it increased the complexity of stability problems and increased the consequences of instability [5].

Until recently, most industry effort and interest has been concentrated on transient (rotor angle) stability [5]. Powerful transient stability simulation programs have been developed that are capable of modeling large complex systems using detailed models. In the early 1990s, the focus was on small-signal stability which then led to the development of special study techniques, such as modal analysis using eigenvalue techniques.

In the 1970s and 1980s, frequency stability problems were experienced following major system upsets. This led to an investigation of the underlying causes of such problems and to the development of long-term dynamic simulation programs to assist in their analysis. In 1983, guidelines were developed for enhancing power plant response during major frequency disturbance.

Recently, power systems are being operated under increasingly stressed conditions due to the prevailing trend to make the most of existing facilities. Increased competition, open transmission access, and construction and environmental constraints are shaping the operation of electric power systems which present greater challenges for secure system operation. This is clear from the increasing number of major power-grid blackouts that have been experienced in recent years such as Northeast USA-Canada blackout of August 14, 2003. Planning and operation of today's power systems require a careful consideration of all forms of system instability. Significant advances have been made in recent years in providing better tools and techniques to analyze instability in power systems.

1.5 Review of Rotor Angle Stability

Rotor angle stability is the ability of interconnected synchronous machines of a power system to remain in synchronism [5]. The stability problem involves the study of the electromechanical oscillations inherent in power systems. A fundamental factor in this problem is how the outputs of synchronous machines vary with respect to their rotor oscillations. A brief discussion of synchronous machine characteristics is helpful to develop the basic concepts of stability.

A synchronous machine has two essential circuits: the field, which is on the rotor, and the armature, which is on the stator. The field winding is supplied by direct current power while the

terminals of the armature provide the load power. The rotating magnetic field of the field winding induces alternating voltages when the rotor is driven by a prime mover (turbine). The frequency of the induced voltages depends on the speed of the rotor and the number of poles of the machine. The frequency of the electrical voltage and the rotor mechanical speed are synchronized (or in synchronism) at 60 Hz in the United States, Canada and South America, and 50 Hz in most other countries. When two or more synchronous machines are interconnected, the stator voltages and currents must have the same frequency and the rotor mechanical speed of each machine is synchronized to this frequency. To change the electrical torque (or power) output of the generator, the mechanical torque input is changed to advance the rotor to a new position relative to the revolving magnetic field of the stator.

1.6 Review of Rotor Angle Stability Analysis Methods

In this section, a brief summary of the available methods to analyze rotor angle stability is discussed.

In the early years, graphical methods such as EAC and the power circle diagrams were developed. These methods were successfully applied to early systems that could be represented as two-machine systems [6]. As the systems became larger, the complexity of the systems grew and therefore the stability problems became more complex. This voided the treatment of the systems to be two-machine systems [5]. Transient Energy Function (TEF) is used to determine Critical Clearing Time (CCT) and therefore transient stability of multi-machine power systems [6]. Application of TEF is based on classical model of a power system with which the CCT can be determined accurately with significantly less computational time than the time required for numerical methods. However, the TEF methods still have some modeling limitations which affect simulation of large-scale power systems. Xue [15] proposed a method that

decomposes a multi-machine power system into two subsystems. The machines in each subsystem are replaced by an equivalent machine. The two-machine system is further reduced to a single-machine infinite-bus (SMIB) model for which the Extended Equal Area Criterion (EEAC) is used to determine the CCT and therefore the system's transient stability. In [16], EAC is used without a need for finding equivalents of two groups in the system. In [17], the authors proposed a direct method that uses individual machine or group of machines energy function. The energy function of individual machine is compared to a critical energy, which is found using Potential Energy Boundary Surface (PEBS) method. If the individual machine's energy is greater than the critical energy, then the system is considered unstable. Based on this phenomenon, the CCT is determined for different fault locations. Haque [18] proposed another direct method of finding the existence of the peak of the post fault rotor's angle of the most severely disturbed machine (SDM) through comparing two areas: accelerating and decelerating areas. The method calculates the accelerating and decelerating energies of the SDM which further are compared to determine the transient stability of the power system. This method conceptually has the same framework of the EAC of a SMIB system; however, the method can be applied to multi-machine power systems. The method can provide a fair estimation of CCT, but sometimes more than one machine is severely disturbed which limits the method of determining the transient stability in some cases. In [21], the authors treat the transient stability problem as a boundary value problem while in [22], critical trajectory method is applied to determine kinetic and potential energies leading to stability decisions. Energy function methods and their variations are used extensively with limited success in analysis of large scale power systems. Reference [23] documents utilization of transient energy function to assess first swing stability of power systems including Static Var Compensators (SVCs). In [24], the authors use PEBS to determine critical group

energy function and use the potential energy function and the sum of energy functions for the generators which belong to the critical group to determine transient stability. The authors of [25] proposed the use of catastrophe theory by which the sudden changes of the power system operation are found. This is further used to determine the maximum swing angle between two generator clusters which can be used to find the transient stability margin, and therefore the transient stability of the system.

In [47], the authors proposed a method that uses distance measures to draw boundaries and pattern recognition concepts to identify coherent generators in a power system. The method classifies the generators to three different classes: inner circle generators, middle circle generators, and outer circle generators. The inner circle is drawn around the group of generators to be studied for stability. The middle circle is drawn with the use of distance measures to separate generators which will be represented individually and in detail from those which will be equivalized (those are the important group). The outer circle defines the boundary of the system beyond which no machine representation is necessary. Also, in [48], the authors proposed a method to cluster generators based on their physical characteristics to be used for transient stability analysis. Their proposed method is based on equivalent network reduction techniques. The electromechanical equivalent system is found by finding clusters of coherent generators. The rotor speed deviations of the synchronous generators are used as a criterion to perform the grouping. After finding the coherent generators, an equivalencing technique is used to make that portion of the system to a one-machine equivalent which then is used to perform further analysis for transient stability using EAC method.

In [1] – [3], we proposed a systemic fast algorithm to apply direct and transient energy function methods to determine the CCT of transient stability in power system. Our proposed

method is a hybrid method that uses both numerical step-by-step integration and direct methods. The method requires three points: the *stable equilibrium point* (SEP), *rotor angles at the clearing time*, and the estimate of *unstable equilibrium points* (UEP). The framework of that method is used to search for the CCT for particular faults. The algorithm uses a search technique that increments the clearing time until it converges to a solution. The solution, based on our previous manuscript, occurs when the kinetic energy of the fault-clearing instant of the Severely Disturbed Group (SDG) of machines is equal to the lowest combined group of machines' potential energy of the post-fault configuration. Notice that the SDG is found by comparing the maximum accelerating power for a certain fault to all the other machines' accelerating power.

1.7 Review of Online Dynamic Security Assessment Methods

Recently, pattern recognition techniques have been used to determine dynamic security of a power system online. In [34], the authors proposed an online dynamic security assessment scheme for large-scale interconnected power systems using phasor measurements (PMU) and decision trees (DT's). The scheme builds and updates decision trees offline to determine critical attributes (CA's) to be used as security indicators. DT's provide online security assessment and preventive control guidelines based on real-time measurements. Classification involves finding the whole path of DT instead of only classification results at terminal nodes. The authors use transient stability and damping problem as the security criteria for testing the proposed method. They selected the power flow (MW-flows) and angle differences between voltage phase angles of the buses as features to the DT algorithm. The authors of [35] expanded the findings in [34] to determine the timing of controlled islanding in real-time by using PMU's. In addition, a slow coherency based approach is used to determine where to island. The scheme is tested to demonstrate the cascading phenomenon. The cascading phenomenon is the loss of power by

means of relay reactions to a contingency which may overload another line, causing its relays to disconnect the line, and so on. This cascading phenomenon very likely causes loss of power. At the initiation of the loss of transient stability, generators tend to form coherent groups with their rotor angles swinging against each other. When the power transfers at the interfaces are blocked due to the faults, the generators in a generation rich area will speed up while the ones in a load populated area will slow down, governed by their swing equations. Low voltages may occur at electrical centers during the out of step swings since voltage and current magnitudes on buses and branches are all closely coupled. The resulting low voltage may violate the settings of protective impedance relays that detect an unstable swing as a fault, causing the line to trip. Tripping branch injects an additional perturbation to the already disturbed system which increases the power transfer burden to the surrounding lines and deteriorates the unstable swing. Therefore, controlled islanding is considered to be the last line of defense to stabilize the system by separating the system into two or more pre-designed islands before cascading events occur. The same authors of [35] perform exhaustive time-domain transient stability simulation to identify critical contingencies. With the obtained data, they train DT's offline to obtain the desired predication performance. Post-contingency system states are used as transient predictors.

In [36], the authors present an online voltage security assessment scheme that uses PMU measurements to update DT's. The DT's are first trained offline using detailed voltage security analysis conducted using the past representative and forecasted 24-hour ahead operating conditions. The DT's are then updated every hour by including newly predicted system conditions to improve robustness. The proposed method focuses on voltage collapse problems. The offline training of DT's uses different groups of predictors which includes faulted bus, voltage phase angle differences, current magnitudes on branches, MVA_r flows on branches,

square of voltage magnitudes, and absolute value of current magnitude multiplied by branch impedance.

The authors of [37] proposed a method to enhance the dynamic security of power systems against credible contingencies. Preventive and corrective controls are developed based on security regions and boundaries based on the rules of DT's. This work also involves improving the accuracy of security boundaries as well as the optimal solution for the fuel cost (generation rescheduling) and load shedding optimization problems encountered in the preventive and corrective controls. Decoupled Optimal Power Flow (DCOPF) method is utilized to determine optimal values of decision variables subject to various constraints, including stability related. The authors' primary contribution is the effective method that utilizes DT's to determine transient stability related security regions and their boundaries in the space of critical attributes and preventive control methods applied to a realistic large power system with a systematic approach based on the security regions defined by the DT rules, sensitivity analysis and OPF calculations.

In [38], Support Vector Machines (SVM) is applied to assess the transient stability of power system after faults occur on transmission lines. Reactive and active powers of all generators after fault clearing and abstract attributes consisted of the inputs of the SVM algorithm. An effective feature selection technique is used to refine the inputs and increase the accuracy of SVM.

In [4], N. Beeravolu developed a systemic algorithm to detect voltage collapse ahead of time by analyzing the dynamic behavior of a stressed power system. The proposed algorithm utilizes pattern recognition methods such as Regularized Least-Squared Classifier (RLSC) and DT's.

1.8 Scope

It is very important for electric utilities to provide continuous power supply with minimal interruption. In order to do that, it is essential to install protective equipment such as, circuit breakers and protective relays which protect the synchronous generators and transmission lines. The purpose of this dissertation is to find new ways to help in transient stability assessment for multi-machine power systems during planning and operation (online assessment) phases. For this purpose, direct methods are the most appropriate and the fastest methods to determine stability of power systems. However, due to the complication of these methods when applied to larger systems, they may not be suitable to be used for online applications. Essentially, these methods are all based on *transient energy function* (TEF) phenomena.

In this dissertation, the author proposes a faster and more accurate way to apply TEF on a multimachine power system by utilizing the benefits of the traditional numerical methods. The proposed method requires the fault profile for generators' rotor angles and speeds in addition to the pre-fault and post-fault network's admittance matrices. Also, the pre-fault rotor angles are needed which can be found from the power flow solution. In traditional direct methods, the UEP is estimated by using only simulation results up to the clearing time. However, in the proposed methodology, the simulation up to critical clearing time is continued to be used, a longer simulation time than clearing time but much smaller than the simulation time that is used in step-by-step integration of the model. The method is based on simulating the system from the moment of a fault occurrence until the critical clearing of that fault using numerical methods. Then, the results of the numerical integration are used to: first determine the unstable equilibrium points, then, calculate the potential and kinetic energies for the relevant generators. By relevant, the method refers to the critical machines, that is called the Severely Disturbed Group (SDG) of

machines, need to have their kinetic energies calculated while the same or another group that need to have their smallest potential energies calculated. Once the relevant energies are calculated, then the kinetic energy of the SDG is compared to the potential energy of the other group. If the potential energy is greater than the potential energy, then the system is stable. Otherwise, the system is unstable. This can be interpreted by energy conversion phenomena. When the system is at a steady-state equilibrium point, the potential energy and kinetic energy are equal. Once the system is disturbed, the system starts to transit by some change in the kinetic and potential energies. In this case, the potential energy decreases while the kinetic energy increases due to the external force. Once the force is removed, the system tries to come back to a stable equilibrium point if there is enough potential energy to absorb the additional kinetic energy that occurred due to the external force. Otherwise, the kinetic energy will keep increasing making the total energy to be equal to the kinetic energy (no more potential energy).

This dissertation compares the proposed methodology to a selected direct method and numerical methods. In the comparison, the suitability of the proposed method to online application is verified by capturing the simulation time and how accurate it is with respect to a benchmark method (step-by-step integration). The proposed method and the previous methods will be simulated and tested on the IEEE 39 Bus (New England) equivalent power system. This system has a total of 39 Buses of which 10 Buses are generator buses. The data of this system will be provided in Chapter 6.

Matlab is a numerical computing environment that can be used for transient stability analysis using the *Power System Analysis Toolbox* (PSAT.) PSAT is a Matlab toolbox for static and dynamic analysis and control of electric power systems [51]. PSAT includes all the required

tools such as, power flow and time domain simulation, to simulate and analyze the methods in this dissertation.

In brief, in this dissertation, an introduction to stability of a power system is introduced. The stability problems are further discussed to then focus on transient stability problems for multi-machine power systems. Some historical review for traditional methods and direct methods are presented and the weakness of each method is discussed. Also, a brief review for some of pattern recognition techniques to be used for online transient stability assessment is presented.

The remainder of this dissertation discusses power system stability formulation in Chapter 2, numerical methods in Chapter 3, direct methods in Chapter 4, dissertation objective and methodology are outlined in Chapter 5, modeling of the test system in Chapter 6, simulation results in Chapter 7, and concluding remarks and future work in Chapter 8.

Chapter 2

2 Power System Stability Formulation

2.1 Basic Concept and Variables in Transient Stability

Power system stability may be defined as that property of a power system that enables it to remain in a state of operating equilibrium under normal operating conditions and to regain an acceptable state of equilibrium after being subjected to a disturbance [5].

Instability of power system can occur in many different situations depending on the system configuration and operating mode. Traditionally, the stability problem has been to maintain synchronous operation or synchronism especially since power systems generation relies on operation of synchronous machines. Necessary condition for satisfactory system operation is that all synchronous machines operate in synchronism. This aspect is influenced by the dynamics of the generator rotor angles and power-angle relationship.

In the stability assessment, the concern is the behavior of the power system when subjected to transient disturbance. The disturbance may be small in the form of load changing conditions, or large in the form of short-circuit on a transmission line or other large disturbances such as, loss of large load or generator, or loss of tie-line between two subsystems. The system response to a disturbance involves much of the equipment. For example, a short-circuit on a critical element followed by its isolation by protective relays will cause variations in power transfers, machine rotor speeds, and bus voltages; the voltage variations will actuate both generator and transmission system voltage regulators; the speed variation will actuate prime mover governors; the change in tie line loading may actuate generation controls; the changes in voltage and frequency will affect loads on the system in varying degrees depending on their

individual characteristics [5]. Many assumptions are usually made to simplify the problem and to focus on factors influencing the specific type of stability problem.

To provide a framework for our proposed method, we briefly describe different form of power system instability and associated concepts. Analysis of small idealized system will be used to show each type of instability.

2.1.1 Rotor Angle Stability

Rotor angle stability is the ability of interconnected synchronous machines of a power system to remain in synchronism [5]. The stability problem involves the study of the electromechanical oscillations inherent in power systems. A fundamental factor in this problem is how the outputs of synchronous machines vary with respect to their rotors oscillations. A brief discussion of synchronous machines characteristics is helpful to develop the basic concepts of stability.

A synchronous machine has two essential circuits: the field, which is on the rotor, and the armature, which is on the stator. The field winding is supplied by direct current power while the terminals of the armature provide the load power. The rotating magnetic field of the field winding induces alternating voltages when the rotor is driven by a prime mover (turbine). The frequency of the induced voltages depends on the speed of the rotor and the number of poles of the machine. The frequency of the electrical voltage and the rotor mechanical speed are synchronized (or in synchronism), at 60 Hz in the United States, Canada and South America, and 50 Hz in most other countries.

When two or more synchronous machines are interconnected, the stator voltages and currents must have the same frequency and the rotor mechanical speed of each machine is synchronized to this frequency.

To change the electrical torque (or power) output of the generator, the mechanical torque input is changed to advance the rotor to a new position relative to the revolving magnetic field of the stator

Consider the system shown in Figure 2.1. It consists of two synchronous machines connected by a transmission line having an inductive reactance X_L but negligible resistance and capacitance. Assume that machine 1 represents a generator feeding power to a synchronous motor represented by machine 2.

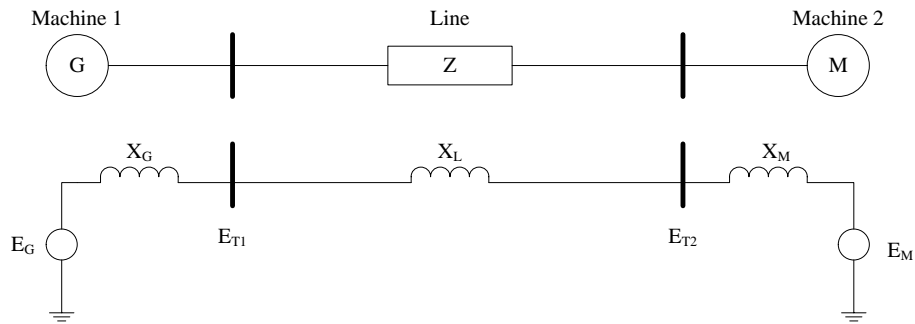


Figure 2.1: Single line diagram and equivalent circuit of a two-machine system [5]

The power transfer from the generator to the motor is a function of the angular separation δ between the rotors of the two machines. This angular separation is due to three components: generator internal angle δ_G , angular difference between the terminal voltages of the generator and motor, and the internal angle of the motor.

A phasor diagram identifying the relationships between generator and motor voltages is shown in Figure 2.2. The power transferred from the generator with reactance of X_G to the motor with reactance of X_M through a transmission line with reactance of X_L is given by (2.1).

$$P = \frac{E_G E_M}{X_T} \sin \delta \quad (2.1)$$

where

$$X_T = X_G + X_L + X_M$$

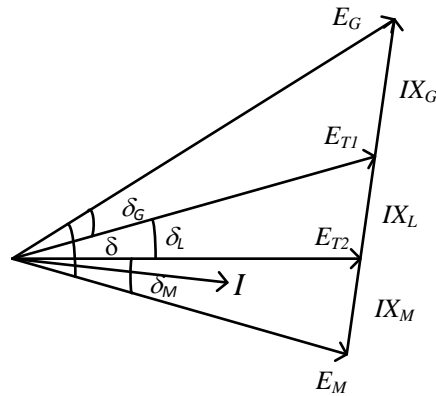


Figure 2.2: Phasor diagram or power transfer characteristic of a two-machine system [5]

The corresponding power versus angle relationship is plotted in Figure 2.3. In the equivalent model, an idealized model is used which makes the power varies as a sine of the angle. However, with a more accurate machine models including the effects of automatic voltage regulators, the variation in power with angle would deviate significantly from the sinusoidal relationship, but the general form would be similar. As the angle is increased, the power transfer increases up to a maximum. After a certain angle, normally 90° , a further increase in angle results in a decrease in power. When the angle is zero, no power is transferred.

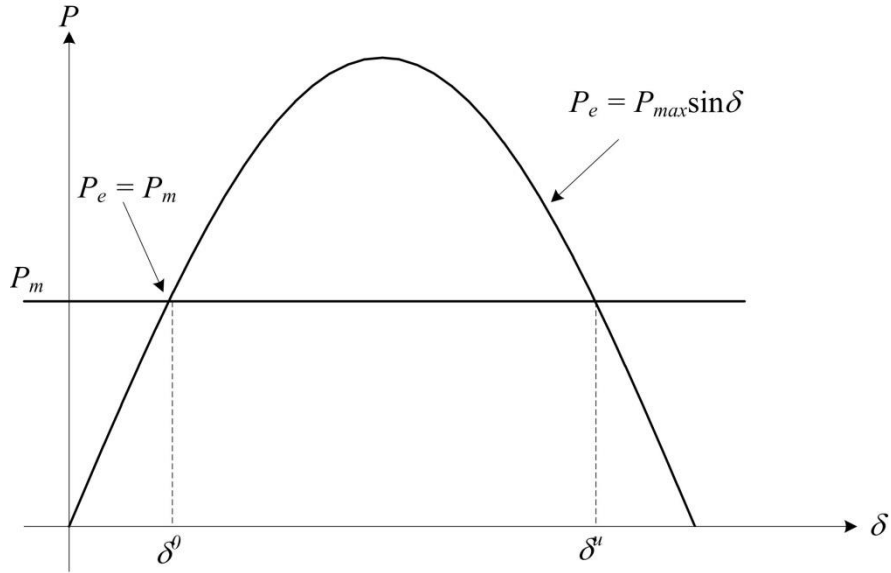


Figure 2.3: Power-angle characteristic of a two-machine system [5]

From Figure 2.3, there are two points of interest: stable equilibrium point δ^o (SEP), and the unstable equilibrium point δ^u (UEP). In the steady-state status, the system rests on the SEP where the mechanical power is equal to the electrical power. However, if the system *swings* to the UEP, where the mechanical power is equal to the electrical power graphically, the synchronous machine loses synchronism (unstable). Note that the system is assumed to be lossless.

When there are more than two machines, their relative angular displacements affect the interchange of power in a similar manner. However, limiting values of power transfers and angular separation are a complex function of generation and load distribution.

Stability is a condition of equilibrium between opposing forces. The mechanism by which interconnected synchronous machines maintain synchronism with one another is through restoring forces, which act whenever there are forces tending to accelerate or decelerate one or more machine with respect to other machines. In steady-state, there is equilibrium between the input mechanical torque and the output electrical power of each machine, and the speed remains

constant. However, if the system is perturbed, this equilibrium is disturbed resulting in acceleration or deceleration of the rotors of the machines according to the laws of motion of a rotating body [5]. If one generator runs faster than the other, the rotor angle of the faster machine relative to the rotor angles of the slower machines will change and that particular machine may lose synchronism causing disturbance to the other machines. As previously discussed, beyond a certain limit, an increase in angular separation is accompanied by a decrease in power transfer; this increases the separation further which leads to instability. For any given situation, the stability of the system depends on whether or not the deviations in angular positions of the rotors result in sufficient restoring torque.

Loss of synchronism can occur between one machine and the rest of the system or between groups of machines. In this case, synchronism may be maintained within each group after its separation from the others.

The change in electrical torque of a synchronous machine following a perturbation can be resolved into two components:

$$\Delta T_e = T_s \Delta \delta + T_D \Delta \omega \quad (2.2)$$

where in (2.2)

$T_s \Delta \delta$ is the component of torque change in phase with the rotor angle perturbation $\Delta \delta$ and is referred to as *synchronizing torque* component; T_s is the synchronizing torque coefficient.

$T_D \Delta \omega$ is the component of torque change in phase with the speed deviation $\Delta \omega$ and is referred to as the *damping torque* component; T_D is the damping torque coefficient.

Lack of sufficient synchronizing torque may result in instability through an *aperiodic drift* in rotor angle. On the contrary, lack of sufficient damping torque results in *oscillatory instability*.

Rotor angle stability phenomenon is categorized into two main categories: *small-signal stability*, and *transient stability*. In this report, transient stability is discussed and some of the relevant mathematical development to this research is shown.

2.1.2 Small-Signal Stability

It is the ability of the power system to maintain synchronism under small disturbances. These types of disturbances occur on the system because of small variation in loads and generation. Instability that may result can be of two forms: (i) steady increase in rotor angle due to lack of sufficient synchronizing torque, or (ii) rotor oscillations of increasing amplitude due to lack of sufficient damping torque. The system response to small disturbance depends on: initial operation, the transmission system strength, and the type of generator excitation controls used. For a generator connected radially to a large power system, in the absence of automatic voltage regulators (i.e. with constant field voltage) the instability is due to lack of sufficient synchronizing torque. This result is shown in Figure 2.4. With continuously acting voltage regulators, the small-signal stability is one of ensuring enough damping of system oscillations. Figure 2.5 shows this type of instability.

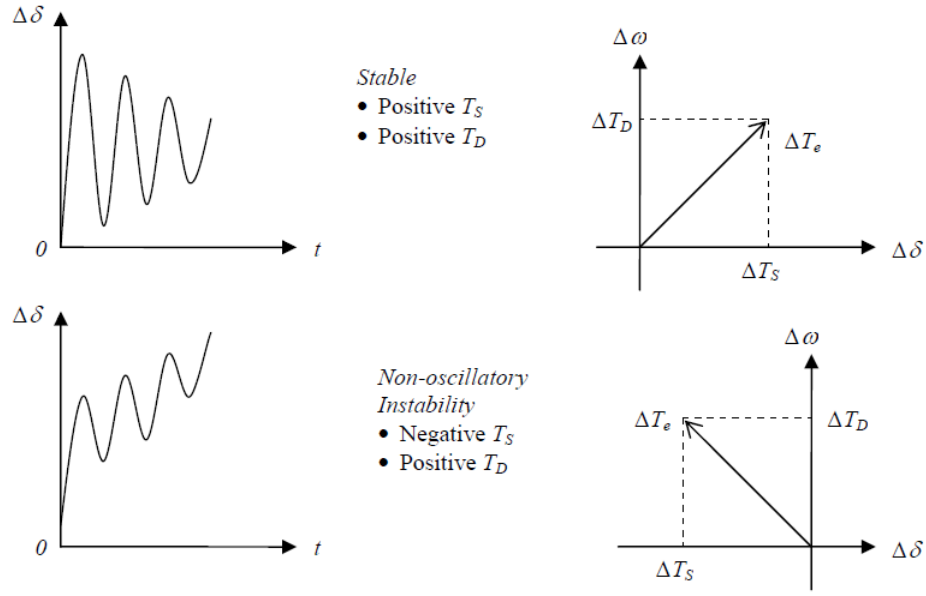


Figure 2.4: Nature of small-disturbance response with constant field voltage [5]

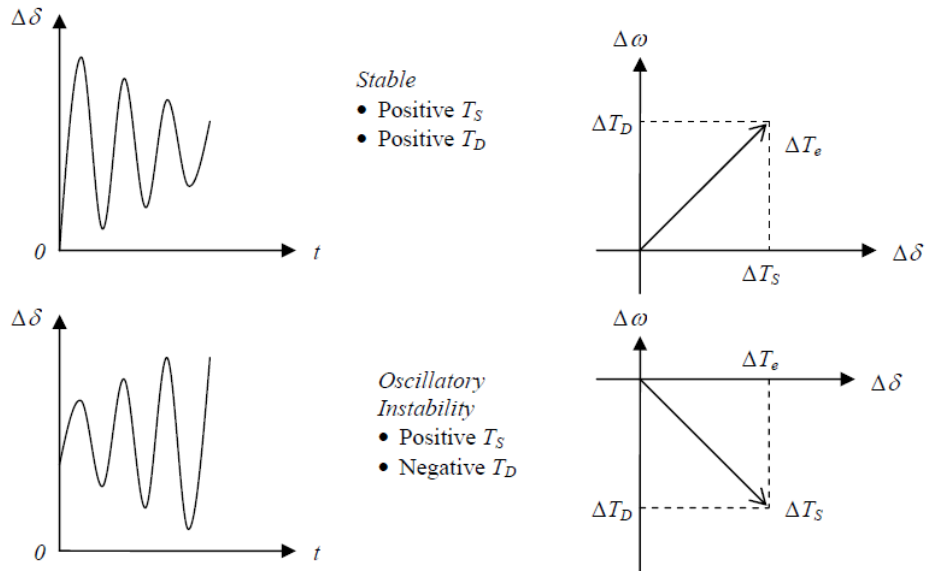


Figure 2.5: Nature of small-disturbance response with excitation control [5]

Nowadays, practical power system may experience small-signal instability due to insufficient damping of oscillations. The stability of the following types of oscillations is of concern:

- *Local modes or machine-system modes*: these are associated with the swinging of units at a generating station with respect to the rest of the power system.

- *Inter-area modes*: these are associated with the swinging of many machines in one part of the system against machines in other parts.
- *Control modes*: these are associated with generating units and other controls.
- *Torsional modes*: these are associated with the turbine-governor shaft system rotational components.

2.1.3 Transient Stability

Transient stability is the ability of the power system to maintain synchronism when subjected to severe transient disturbance. The response to this type of disturbance involves large excursions of rotor angles and is influenced by nonlinear power-angle relationship. Stability depends on the initial operating state of the system and the severity of the disturbance. The system usually altered after the disturbance which may cause the system to operate in a different steady-state status from that prior the disturbance.

Power systems are designed to be stable for a selected set of contingencies. The contingencies usually considered are short-circuits of different types: phase-to-ground, phase-to-phase-to-ground, or three-phase. They are usually assumed to occur on the transmission lines, but occasionally bus or transformer faults are also considered.

Figure 2.6 illustrates the behavior of a synchronous machine for stable and unstable situations. In Case 1, the rotor angle increases to a maximum, then decreases and oscillates with decreasing amplitude until it reaches a steady state. This case is considered transient stable. In Case 2, the rotor angle continues to increase steadily until synchronism is lost. This type of transient instability is referred to as *first-swing* instability. In Case 3, the system is stable in the first swing but becomes unstable as a result of growing oscillations as the end state is

approached. This form of instability occurs when the post-fault steady-state condition is itself is small-signal unstable.

In transient stability studies, the study period of interest is usually limited to 3 to 5 seconds following the disturbance, although it may extend to about ten seconds for very large systems with dominant interarea modes of oscillation.

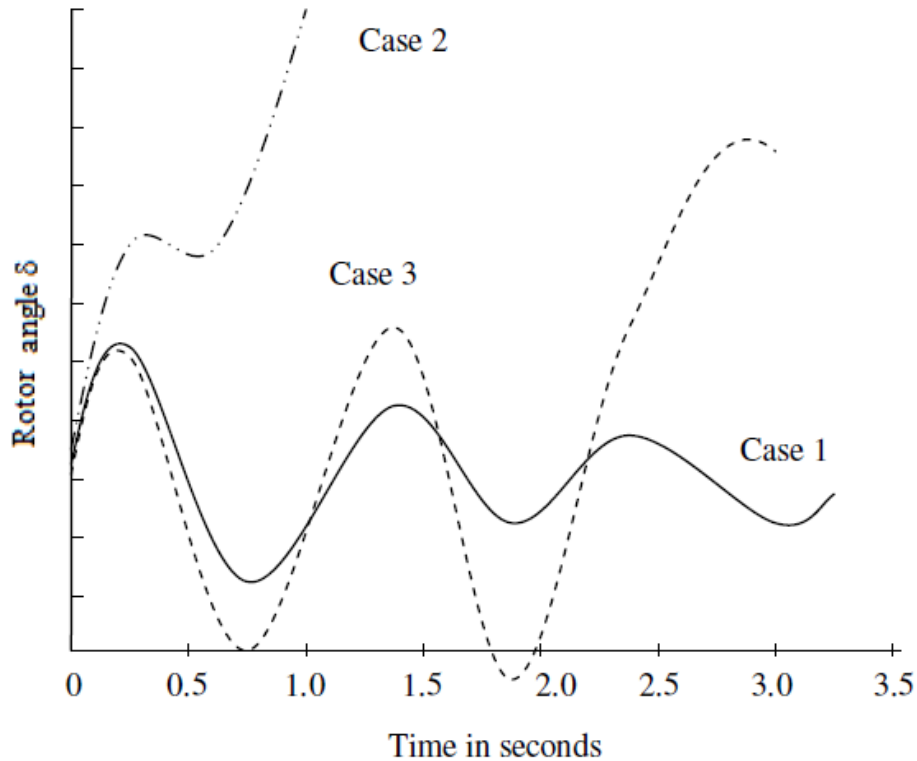


Figure 2.6: Rotor angle response to a transient disturbance. Redrawn from [5]

2.2 Formulation of Existing Methods of Transient Stability

As previously explained, transient stability is the ability of the power system to maintain synchronism when subjected to a severe transient disturbance such as a fault on transmission facilities, loss of generation, or loss of a large load. The system response to such disturbances involves large excursions of generator rotor angles, power flows, bus voltages, and other system variables. If the resulting angular separation between the machines in the system remains within

certain bounds, the system maintains synchronism. If loss of synchronism occurs, the transient instability will be evident within 2 to 3 seconds of the occurrence of the disturbance.

In this section, different methods of transient stability analysis are briefly introduced. Since the focus of this dissertation is transient stability analysis, small-signal stability analysis is not explained in this section. Also, before introducing some of the methods, it is essential to introduce the swing equation to represent the dynamic of a power system.

2.2.1 Swing Equation

The swing equation describes the rotational dynamics of a synchronous machine and is used in stability analysis to characterize that dynamic. During normal operation, the relative position of the rotor axis and the resultant axis is fixed. During disturbance to the machine, the rotor either accelerates or decelerates with respect to the synchronous rotating air gap MMF [14]. The swing equation describes this relation.

The swing equation of a power system is given as:

$$M\ddot{\delta} + D\dot{\delta} + P_G(\delta) = P_M^0 \quad (2.3)$$

where $M \triangleq H / \pi f_0$

H is the per unit inertial constant, $H \triangleq \frac{W_{kinetic}^0}{S_B^{3\phi}} = \frac{\text{kinetic energy}}{\text{3-phase apparent power}}$

$$D \triangleq 2k\omega_0 / S_B^{3\phi}$$

$P_G(\delta)$ is the electrical power in p.u

P_M^0 is the per unit mechanical power

δ is the relative angle of the electrical power

k is damping constant

ω_0 is the base electrical frequency in rad/sec

With the swing equation idea introduced, transient stability can be introduced in the following sections.

2.2.2 Equal-Area Criterion

Consider a single-machine infinite-bus (SMIB) system of Figure 2.7. For the system model considered in Figure 2.7, it is not necessary to formally solve the swing equation to determine whether the rotor angle increases indefinitely or oscillates about an equilibrium position. Assume that the system is a purely reactive, a constant P_m and constant voltage behind transient reactance for the system in Figure 2.7.

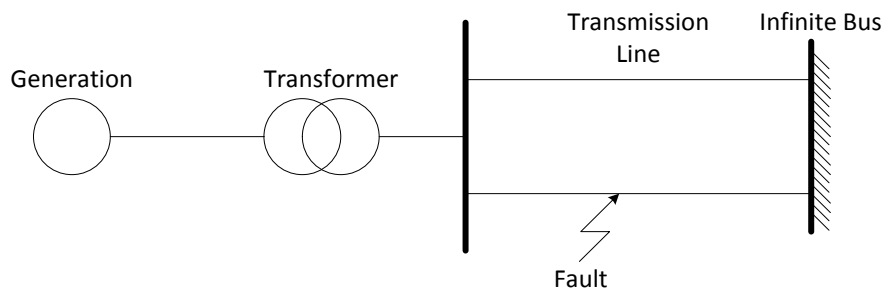


Figure 2.7: Simple SMIB System [18]

Assume that a 3-phase fault appears in the system at $t = 0$ and it is cleared by opening one of the lines. The power angle characteristics of the system are shown in Figure 2.8.

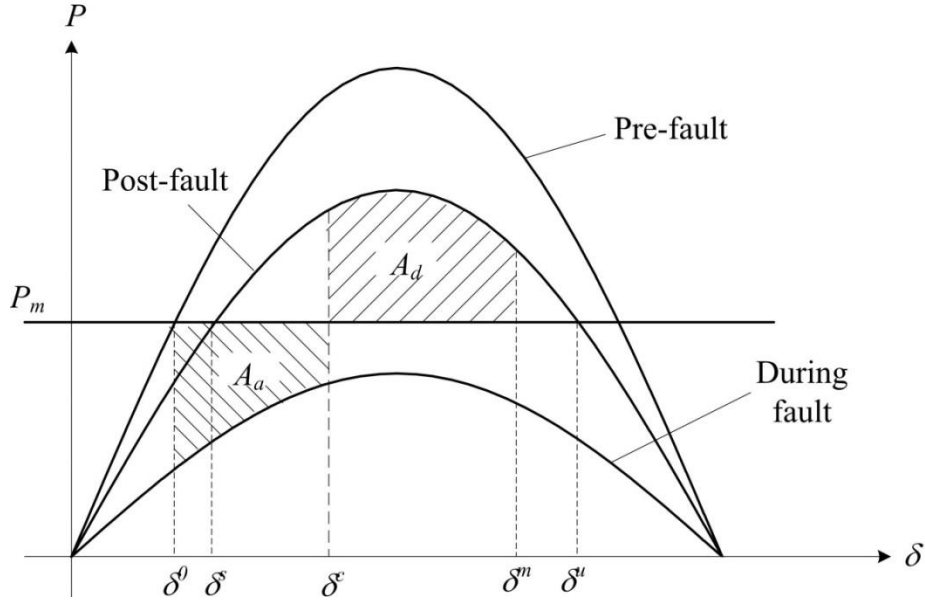


Figure 2.8: Power-angle characteristic of the system in Figure 2.7

Let δ^0 and δ^s be the pre-fault and post-fault operating or stable-equilibrium points, respectively, of the system. During the fault, the electrical output P_e of the generator reduces drastically (almost to zero) but the mechanical power P_m remains almost constant. Thus the generator accelerates and its angle δ increases. When the fault is cleared by disconnecting the faulted line at time t_c , the output power of the generator becomes greater than the mechanical power and the generator decelerates to bring its speed to normal as shown in Figure 2.8. If the system is stable, the generator will recover to its steady-state speed (or zero speed deviation) at some peak angle δ^m . At δ^m , $P_e > P_m$ and the generator will continue to decelerate. The angle δ decreases from δ^m and reaches a minimum value below δ^s before it starts to increase again. The generator angle will oscillate around δ^s and eventually it will settle down at δ^s because of the system damping. For a given clearing angle δ^c , the peak angle δ^m can be determined by equating the accelerating area A_a to decelerating area A_d . The expressions for A_a and A_d are

$$A_a = \int_{\delta^0}^{\delta^c} (P_m - P_e^f) d\delta \quad (2.4)$$

$$A_d = \int_{\delta^c}^{\delta^m} (P_e^p - P_m) d\delta \quad (2.5)$$

where

P_e^f is the during-fault electrical power

P_e^p is the post-fault electrical power

For a system to be transient stable, the maximum decelerating area is greater than the accelerating area. That is, $A_d > A_a$. For a clearing time t_{cl} when $A_d = A_a$, we reach the maximum clearing time referred to as the critical clearing time t_{cr} .

2.2.3 Numerical Integration Methods

The most commonly used method to solve the swing Equation 2.3 is the numerical integration. The initial condition of the differential equation to be solved is the swing angle δ^0 (SEP) of Figure 2.8.

Transient stability analysis is routinely performed in utility system planning. The industry standard for transient stability usually requires the ability of the system to withstand severe disturbances, including any “possible but improbable” three-phase fault close to a generator’s Bus. The method used for analysis is time-domain numerical integration. The time-domain numerical integration is not suitable for on-line security analysis due to the long CPU run times for simulation. A typical time-domain numerical integration of 2 seconds takes more than 120 seconds depending on the step size of the integration. Larger step size that reduce time causes inaccurate and less reliable results than smaller step size.

There are different algorithms to perform numerical integration such as trapezoidal rule and Euler integration. Mathematical derivation is illustrated in Chapter 3.

2.2.4 Direct Methods for Transient Stability Analysis

The direct methods determine stability without explicitly solving the system differential equations. This approach has received considerable attention since the early work of Magnusson [7] and Aylett [9] who used transient energy function for stability assessment.

The transient energy approach can be described by considering a ball rolling on the inner surface of a bowl generated by the equation describing the transient energy of the system as depicted in Figure 2.9. The area inside the bowl represents the region of stability and the area outside represents the region of instability. The rim of the bowl represents maximum elevation to δ^* , and hence, maximum potential energy for the traversed trajectory caused by the fault energy.

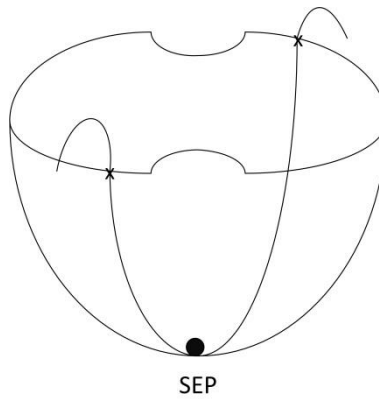


Figure 2.9: A ball rolling on the inner surface of a bowl

Initially, the ball is at rest at the bottom of the bowl, and this state is referred to as the stable equilibrium point (SEP). When the bowl is perturbed, some kinetic energy is injected into the ball causing it to move from its location at SEP in a particular direction. The ball will roll up the inside surface of the bowl along a path determined by the direction of initial motion, and the point where the ball will stop is determined by the amount of the initially injected kinetic energy. If the ball converts all its kinetic energy into potential energy before reaching the rim, then it will roll back and eventually settle down at the stable equilibrium point again. However, if the injected kinetic energy is high enough to cause the ball to go over the rim, then the ball will enter

the region of instability and will not return to the SEP. The surface inside the bowl represents the *potential energy surface* and the rim of the bowl represents the *potential energy boundary surface* (PEBS.)

The application of *transient energy function* (TEF) method to power systems is conceptually similar to that of a rolling ball in a bowl in the hyperspace (n-dimensional space). Initially, the system is operating at steady-state equilibrium point. If a fault occurs, the equilibrium is disturbed causing the synchronous machines to accelerate. The power system gains kinetic energy and potential energy during the fault-on period causing the system to move away from the SEP. After clearing the fault, the kinetic energy is converted to potential energy. For a system to avoid instability, the system must be capable of absorbing the kinetic energy at a time when the forces on the generators tend to bring them toward new equilibrium positions. For a given post-disturbance network configuration, there is a maximum or critical amount of transient energy that the system can absorb. For that reason, assessment of transient stability requires the following:

- a) Functions that adequately describe the transient energy responsible for separation of one or more synchronous machines from the rest of the system.
- b) An estimate of the critical energy required for the machine to lose synchronism.

Direct methods are suitable for on-line operation for dynamic security assessment because it only requires simple mathematical operations unlike numerical methods which involve solving differential equations numerically. Direct methods may require solving the differential equation up to the point where the fault is cleared. However, there are still some difficulties in applying direct methods to large power system. The mathematical formulation of the direct methods will be illustrated in Chapter 4.

2.3 Power System Models

In order to analyze any power system, a mathematical model is used to represent the system. It is very important to understand the various power system models before applying them in this dissertation. Therefore, several power system models are presented in this section. The models that are presented in this section include: SMIB classical and detailed models, and multi-machine classical model for both synchronous reference frame and center-of-inertia reference frame.

2.3.1 Single-Machine Infinite-Bus Classical System Model

Consider the *single-machine infinite-bus* (SMIB) system shown in Figure 2.10.

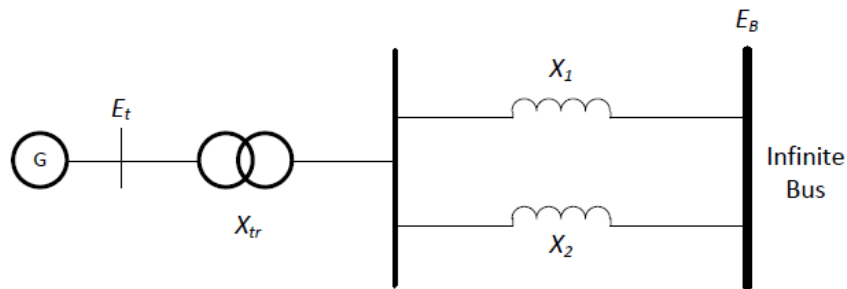


Figure 2.10: Single-machine infinite-bus system

The generator is represented by the classical model, which ignores saliency of round rotor, that is, for the purpose of transient stability, only the transient reactance X'_d is considered with the assumption that the direct and quadrature components are equal. Also, the speed governor effects are neglected. The generator's voltage is denoted by E' , and the infinite-bus voltage is denoted by E_B . The rotor angle δ represents the angle by which E' leads E_B . When the system experiences a disturbance, the magnitude of E' remains constant at its pre-disturbance value and δ changes as the generator rotor speed deviates from synchronous speed ω_0 .

The generator's electrical power output is:

$$P_e = \frac{E'E_s}{X_T} \sin \delta = P_{\max} \sin \delta \quad (2.6)$$

where

$$P_{\max} = \frac{E'E_s}{X_T} \quad (2.7)$$

The equation of motion or the *swing equation* may be written as:

$$\frac{2H}{\omega_0} \frac{d^2 \delta}{dt^2} = P_m - P_{\max} \sin \delta \quad (2.8)$$

where

P_m mechanical power input, in pu

P_{\max} maximum electrical power output, in pu

H inertia constant, in MW.s/MVA

δ rotor angle, in elec. rad

t time, in s

2.3.2 Single-Machine Infinite-Bus Detailed System Model (6th Order)

In this model of synchronous machine, the field coil on the direct axis (d-axis) and damper coil on the quadrature axis (q-axis) are considered. The machine differential equations are:

$$\frac{dE'_q}{dt} = \frac{1}{T'_{do}} \left[-E'_q + (X_d - X'_d)i_d + E_{fd} \right] \quad (2.9)$$

$$\frac{dE'_d}{dt} = \frac{1}{T'_{qo}} \left[-E'_d - (X_q - X'_q)i_q \right] \quad (2.10)$$

$$\frac{d\delta}{dt} = \omega_B (S_m - S_{m0}) \quad (2.11)$$

$$\frac{dS_m}{dt} = \frac{1}{2H} [T_m - DS_m - T_e] \quad (2.12)$$

$$T_e = E'_q i_q + E'_d i_d + (X_q - X'_q) i_d i_q \quad (2.13)$$

$$E'_q + X'_d i_d - R_a i_q = v_q \quad (2.14)$$

$$E'_d - X'_q i_q - R_a i_d = v_d \quad (2.15)$$

From Equations (2.14) and (2.15), i_d and i_q can be solved as

$$\begin{bmatrix} i_q \\ i_d \end{bmatrix} = \frac{1}{R_a^2 + X'_d X'_q} \begin{bmatrix} R_a & X'_d \\ -X'_q & R_a \end{bmatrix} \begin{bmatrix} E'_q - v_q \\ E'_d - v_d \end{bmatrix} \quad (2.16)$$

where

- T_m the mechanical torque in the direction of rotation
- T_e the electrical torque opposing the mechanical torque
- T'_{do} d-axis open circuit transient time constant
- T'_{qo} q-axis open circuit transient time constant
- S_m machine slip
- S_{m0} initial machine slip (= 0 in steady-state)
- ω_B the electrical angular frequency (or synchronous angular speed)
- R_a armature resistance
- E_{fd} control voltage
- X_d, X_q d- and q-axis reactance, respectively
- X'_d, X'_q d- and q-axis transient reactance, respectively
- E'_d, E'_q d- and q-axis generator's voltage, respectively

i_d, i_q d- and q-axis current, respectively

2.3.3 Multi-Machine Classical System Model

2.3.3.1 Synchronous Reference Frame Model [17]

For this model, the motion of the generators can be represented by the set of differential equations:

$$\left. \begin{aligned} M_i \dot{\omega}_i + D_i \omega_i &= P_i - P_{ei} \\ \dot{\delta}_i &= \omega_i, \quad i = 1, 2, \dots, n \end{aligned} \right\} \quad (2.17)$$

where, for machine i ,

- δ_i angle of voltage behind transient reactance, indicative of generator rotor position
- ω_i rotor speed
- M_i generator inertia constant
- D_i damping coefficient

The expressions for P_i and P_{ei} are given by

$$\left. \begin{aligned} P_i &= P_{mi} - E_i^2 G_{ii} \\ P_{ei} &= \sum_{\substack{i=1 \\ j \neq i}}^n \left[C_{ij} \sin(\delta_i - \delta_j) + D_{ij} \cos(\delta_i - \delta_j) \right] \end{aligned} \right\} \quad (2.18)$$

where

$$\begin{aligned} C_{ij} &= E_i E_j B_{ij} \\ D_{ij} &= E_i E_j G_{ij} \end{aligned}$$

and

- P_{mi} mechanical power input
- E_i magnitude of voltage behind transient reactance

G_{ii} real part of the i th diagonal element of the network's Y -matrix

G_{ij}, B_{ij} real and imaginary components of the ij th element of the network's Y -matrix

2.3.3.2 Center of Inertia (COI) Reference Frame [16]

Reference [17] provides a thorough description of the model used in development of Transient Energy Function of multi-machine power system using classical model referenced to center-of-inertia (COI) reference frame, such as by generators that are represented by constant voltage behind transient reactance, and by constant impedance loads. The COI model gives a good physical insight into the behavior of synchronous generators. The development in [17] is also used in describing transient energy function of individual machines with respect to COI.

Using the following notations:

P_{mi} mechanical power input

E_i magnitude of voltage behind transient reactance

G_{ij}, B_{ij} real and imaginary components, respectively, of the ij th element of the network's admittance matrix

G_{ii} self conductance of unit i

δ_i angle of voltage behind transient reactance, indicative of generator rotor position

ω_i rotor speed

M_i generator inertia constant

D_i damping coefficient

n number of generators

The equation of motion of the generators in the COI reference frame can be represented by:

$$\left. \begin{aligned} M_i \dot{\tilde{\omega}}_i &= P_i - P_{ei} - \frac{M_i}{M_T} P_{COI} - D_i \tilde{\omega}_i \\ \dot{\theta}_i &= \tilde{\omega}_i, \quad i = 1, \dots, n \end{aligned} \right\} \quad (2.19)$$

where,

$$M_T = \sum_{i=1}^n M_i \quad (2.20)$$

$$P_{COI} = \sum_{i=1}^n (P_i - P_{ei}) \quad (2.21)$$

$$P_i = P_{mi} - E_i^2 G_{ii} \quad (2.22)$$

$$P_{ei} = \sum_{\substack{i=1 \\ j \neq i}}^n [C_{ij} \sin(\delta_i - \delta_j) + D_{ij} \cos(\delta_i - \delta_j)] \quad (2.23)$$

$$C_{ij} = E_i E_j B_{ij} \quad (2.24)$$

$$D_{ij} = E_i E_j G_{ij} \quad (2.25)$$

In (2.19), the angle displacement θ_i and angular velocity $\tilde{\omega}_i$ are defined by:

$$\left. \begin{aligned} \theta_i &= \delta_i - \delta_0 \\ \tilde{\omega}_i &= \dot{\theta}_i = \omega_i - \omega_0 \end{aligned} \right\} \quad (2.26)$$

In (2.26),

$$\delta_0 = \frac{1}{M_T} \sum_{i=1}^n M_i \delta_i \quad (2.27)$$

$$\omega_0 = \frac{1}{M_T} \sum_{i=1}^n M_i \omega_i \quad (2.28)$$

This model is used throughout this dissertation to verify the proposed method with respect to the results of the numerical methods.

2.4 Summary

In this chapter, the basic concepts of stability in general are discussed. Then, the discussion is focused on the rotor angle stability with its two main types: small-signal stability, and transient stability. This dissertation focuses on the relevant stability, which is transient stability. After that, a short review of the important methods to analyze transient stability is

illustrated which includes: numerical methods, and direct methods which are based on equal area criterion. In addition, power system models are presented for both SMIB and multi machine power systems. In this dissertation, the multi-machine power system model with respect to the COI is used to verify the proposed method.

In Chapter 3, numerical methods are discussed in details. These methods include: Euler method, Runge-Kutta second- and forth-order methods, and implicit integration method. Also, a method of how to simulate a power system dynamics using matrices is discussed.

Chapter 3

3 Transient Stability Using Numerical Methods

3.1 Overview

The differential equations to be solved in power system stability analysis are nonlinear ordinary differential equation with known initial values and can be represented by,

$$\frac{dx}{dt} = f(x, t) \quad (3.1)$$

where \mathbf{x} is the state vector of n dependent variables and t is the independent variable (time). The main goal of numerical integration techniques is to solve for \mathbf{x} . In this chapter, different numerical integration methods are presented, and a way to simulate a power system with the model in equation 3.1 is illustrated.

3.2 Numerical Integration Methods

In the following sections, the most commonly used techniques to perform numerical integration are presented.

3.2.1 Euler Method

Consider the first-order differential equation,

$$\frac{dx}{dt} = f(x, t) \quad (3.2)$$

with $x = x_0$ at $t = t_0$. Figure 3.1 shows the principle of applying the Euler method.

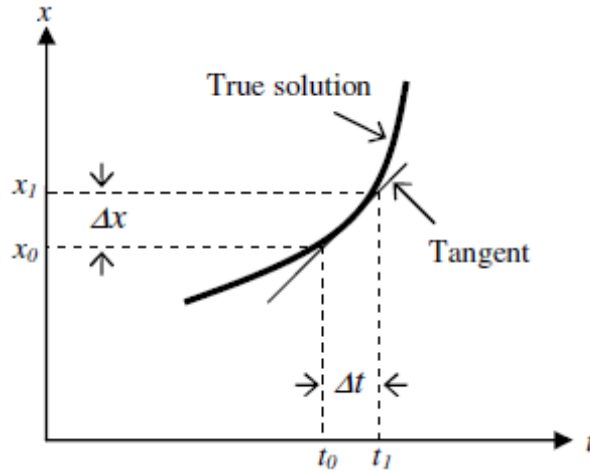


Figure 3.1: Euler's method illustration

At $x = x_0$, $t = t_0$, the curve representing the true solution can be approximated by its tangent having a slope

$$\left. \frac{dx}{dt} \right|_{x=x_0} = f(x_0, t_0) \quad (3.3)$$

Therefore, the value of x at $t = t_1 = t_0 + \Delta t$ is given by

$$x_1 = x_0 + \Delta x = x_0 + \left. \frac{dx}{dt} \right|_{x=x_0} \cdot \Delta t \quad (3.4)$$

After using the Euler technique for determining $x = x_1$ corresponding to $t = t_1$, another short time step Δt can be taken and x_2 corresponding to $t_2 = t_1 + \Delta t$ can be determined as follows:

$$x_2 = x_1 + \left. \frac{dx}{dt} \right|_{x=x_1} \cdot \Delta t \quad (3.5)$$

The method is also referred to as a *first-order* method because it considers the first derivative in its Taylor series expanded version.

3.2.2 Runge-Kutta (R-K) Methods

3.2.2.1 Second-order R-K Method

The second-order R-K formula for the value of x at $t = t_0 + \Delta t$ is

$$x_1 = x_0 + \Delta x = x_0 + \frac{k_1 + k_2}{2} \quad (3.6)$$

where

$$k_1 = f(x_0, t_0) \Delta t$$

$$k_2 = f(x_0 + k_1, t_0 + \Delta t) \Delta t$$

A general formula giving the value of x for the $(n+1)^{st}$ step is

$$x_{n+1} = x_n + \frac{k_1 + k_2}{2} \quad (3.7)$$

where

$$k_1 = f(x_n, t_n) \Delta t$$

$$k_2 = f(x_n + k_1, t_n + \Delta t) \Delta t$$

The method is called second-order R-K because it is equivalent to considering up to the second derivative terms of the Taylor series expansion.

3.2.2.2 Fourth-order R-K Method

The general formula giving the value of x for the $(n+1)^{st}$ step is

$$x_{n+1} = x_n + \frac{1}{6}(k_1 + 2k_2 + 2k_3 + k_4) \quad (3.8)$$

where

$$k_1 = f(x_n, t_n) \Delta t$$

$$k_2 = f\left(x_n + \frac{k_1}{2}, t_n + \frac{\Delta t}{2}\right)\Delta t$$

$$k_3 = f\left(x_n + \frac{k_2}{2}, t_n + \frac{\Delta t}{2}\right)\Delta t$$

$$k_4 = f(x_n + k_3, t_n + \Delta t)\Delta t$$

The physical interpretation of the above solution is as follows:

k_1 = (slope at the beginning of time step) Δt

k_2 = (first approximation to slope at mid step) Δt

k_3 = (second approximation to slope at mid step) Δt

k_4 = (slope at the end of step) Δt

$$\Delta x = \frac{1}{6}(k_1 + k_2 + k_3 + k_4)$$

This method is called fourth-order R-K because it is equivalent to considering up to the fourth derivative terms of the Taylor series expansion.

3.2.3 Implicit Integration Methods

Consider the differential equation in (3.2). The solution for x at $t = t_1 = t_0 + \Delta t$ may be expressed in integral form as

$$x_1 = x_0 + \int_{t_0}^{t_1} f(x, \tau) d\tau \quad (3.9)$$

Implicit integration methods use interpolation functions for the expression under the integral. The most common implicit integration method is *trapezoidal* rule. The area under the integral of (3.9) is approximated by trapezoids.

The trapezoidal rule for (3.9) is given by

$$x_1 = x_0 + \frac{\Delta t}{2} [f(x_0, t_0) + f(x_1, t_1)] \quad (3.10)$$

A general formula giving the value of x at $t = t_{n+1}$ is

$$x_{n+1} = x_n + \frac{\Delta t}{2} [f(x_n, t_n) + f(x_{n+1}, t_{n+1})] \quad (3.11)$$

The trapezoidal rule is a second-order method and it is numerically *A-stable*, which means that the stiffness of the system being analyzed affects accuracy but not numerical stability. Implicit integration methods of higher order have been proposed in the literature on numerical methods; however, they have not been widely used for power system applications especially that they are more difficult to program and less numerically stable than the trapezoidal rule.

When numerical integration methods are used, the system's equations have to be arranged as first-order differential equations.

3.3 Simulation of Power System Dynamic Response

3.3.1 Overall System Equations

Equations for each of the generating units and other dynamic devices may be expressed in the following form:

$$\dot{\mathbf{x}}_d = \mathbf{f}_d(\mathbf{x}_d, \mathbf{V}_d) \quad (3.12)$$

$$\mathbf{I}_d = \mathbf{g}_d(\mathbf{x}_d, \mathbf{V}_d) \quad (3.13)$$

where

\mathbf{x}_d state vector of individual device

\mathbf{I}_d complex components of current injection from the device into the network

\mathbf{V}_d complex components of bus voltage

Equations (3.12) and (3.13) can be represented using the general form comprising a set of first-order differential equations of Equation (3.14) and a set of algebraic equations of Equation (3.15).

$$\dot{\mathbf{x}} = \mathbf{f}(\mathbf{x}, \mathbf{V}) \quad (3.14)$$

$$\mathbf{I}(\mathbf{x}, \mathbf{V}) = \mathbf{Y}_N \mathbf{V} \quad (3.15)$$

where

\mathbf{x} state vector of the system

\mathbf{V} bus voltage vector

\mathbf{I} current injection vector

\mathbf{Y}_N Y-matrix

3.3.2 Solution of Overall System Equations Using Implicit Integration Methods

The solution of \mathbf{x} at $t = t_{n+1} = t_n + \Delta t$ is given by applying the trapezoidal rule to solve (3.14),

$$\mathbf{x}_{n+1} = \mathbf{x}_n + \frac{\Delta t}{2} [\mathbf{f}(\mathbf{x}_{n+1}, \mathbf{V}_{n+1}) + \mathbf{f}(\mathbf{x}_n, \mathbf{V}_n)] \quad (3.16)$$

From (3.15), the solution of \mathbf{V} at $t = t_{n+1}$ is

$$\mathbf{I}(\mathbf{x}_{n+1}, \mathbf{V}_{n+1}) = \mathbf{Y}_N \mathbf{V}_{n+1} \quad (3.17)$$

The vectors \mathbf{x}_{n+1} and \mathbf{V}_{n+1} are unknown. Let

$$\mathbf{F}(\mathbf{x}_{n+1}, \mathbf{V}_{n+1}) = \mathbf{x}_{n+1} - \mathbf{x}_n - \frac{\Delta t}{2} [\mathbf{f}(\mathbf{x}_{n+1}, \mathbf{V}_{n+1}) + \mathbf{f}(\mathbf{x}_n, \mathbf{V}_n)] \quad (3.18)$$

and,

$$\mathbf{G}(\mathbf{x}_{n+1}, \mathbf{V}_{n+1}) = \mathbf{Y}_N \mathbf{V}_{n+1} - \mathbf{I}(\mathbf{x}_{n+1}, \mathbf{V}_{n+1}) \quad (3.19)$$

at solution,

$$\mathbf{F}(\mathbf{x}_{n+1}, \mathbf{V}_{n+1}) = 0 \quad (3.20)$$

$$\mathbf{G}(\mathbf{x}_{n+1}, \mathbf{V}_{n+1}) = 0 \quad (3.21)$$

Applying the Newton's method to solve (3.20) and (3.21) iteratively, we get,

$$\begin{bmatrix} \mathbf{x}_{n+1}^{k+1} \\ \mathbf{V}_{n+1}^{k+1} \end{bmatrix} = \begin{bmatrix} \mathbf{x}_{n+1}^k \\ \mathbf{V}_{n+1}^k \end{bmatrix} + \begin{bmatrix} \Delta \mathbf{x}_{n+1}^k \\ \Delta \mathbf{V}_{n+1}^k \end{bmatrix} \quad (3.22)$$

Equation (3.23) is solved to obtain $\Delta \mathbf{x}_{n+1}^k$ and $\Delta \mathbf{V}_{n+1}^k$.

$$\begin{bmatrix} -\mathbf{F}(\mathbf{x}_{n+1}^k, \mathbf{V}_{n+1}^k) \\ -\mathbf{G}(\mathbf{x}_{n+1}^k, \mathbf{V}_{n+1}^k) \end{bmatrix} = \begin{bmatrix} \frac{\partial \mathbf{F}}{\partial \mathbf{x}} & \frac{\partial \mathbf{F}}{\partial \mathbf{V}} \\ \frac{\partial \mathbf{G}}{\partial \mathbf{x}} & \frac{\partial \mathbf{G}}{\partial \mathbf{V}} \end{bmatrix} \begin{bmatrix} \Delta \mathbf{x}_{n+1}^k \\ \Delta \mathbf{V}_{n+1}^k \end{bmatrix} \quad (3.23)$$

The Jacobian in (3.23) has the following structure:

$$\mathbf{J} = \begin{bmatrix} \frac{\partial \mathbf{F}}{\partial \mathbf{x}} & \frac{\partial \mathbf{F}}{\partial \mathbf{V}} \\ \frac{\partial \mathbf{G}}{\partial \mathbf{x}} & \frac{\partial \mathbf{G}}{\partial \mathbf{V}} \end{bmatrix} = \begin{bmatrix} \mathbf{A}_D & \mathbf{B}_D \\ \mathbf{C}_D & (\mathbf{Y}_N - \mathbf{Y}_D) \end{bmatrix} \quad (3.24)$$

where

$$\mathbf{A}_D = \begin{bmatrix} \mathbf{A}_{d1} & 0 & \cdots & 0 \\ 0 & \mathbf{A}_{d2} & \cdots & 0 \\ \vdots & \vdots & \ddots & \vdots \\ 0 & 0 & \cdots & \mathbf{A}_{dm} \end{bmatrix} \quad \mathbf{B}_D = \begin{bmatrix} \mathbf{B}_{d1} \\ \mathbf{B}_{d2} \\ \vdots \\ \mathbf{B}_{dm} \end{bmatrix}$$

$$\mathbf{Y}_D = \begin{bmatrix} \mathbf{Y}_{d1} & 0 & \cdots & 0 \\ 0 & \mathbf{Y}_{d2} & \cdots & 0 \\ \vdots & \vdots & \ddots & \vdots \\ 0 & 0 & \cdots & \mathbf{Y}_{dm} \end{bmatrix} \quad \mathbf{C}_D = [\mathbf{C}_{d1} \quad \mathbf{C}_{d2} \quad \cdots \quad \mathbf{C}_{dm}]$$

A solution to (3.20) and (3.21) can be expressed by

$$(\mathbf{Y}_N + \mathbf{Y}_D - \mathbf{C}_D \mathbf{A}_D^{-1} \mathbf{B}_D) \Delta \mathbf{V}_{n+1}^k = -\mathbf{G}_{n+1}^k + \mathbf{C}_D \mathbf{A}_D^{-1} \mathbf{F}_{n+1}^k \quad (3.25)$$

3.4 Summary

In this chapter, four different numerical integration techniques are presented. The first method is Euler method which is represented by (3.4) and (3.5). The second and third methods presented are the second- and forth-order R-K methods which are represented by (3.7) and (3.8), respectively. The forth method presented is the implicit integration methods, and as an example of these methods, trapezoidal rule is illustrated which is represented by (3.11). Finally, a way of how to simulate a power system dynamic response is discussed and a solution to system dynamics is presented.

In Chapter 4, the second main method of transient stability analysis (direct methods) is discussed and various direct methods based on transient energy function (TEF) are presented. We shall use both step-by-step integration of Chapter 3 and TEF of Chapter 4 to describe the dissertation methodology in Chapter 5.

Chapter 4

4 Transient Stability Analysis Using Direct Methods

4.1 Overview

In transient stability, the critical clearing time of circuit breakers to clear a fault is of vital importance when the system is subjected to large disturbances. In real-world application, the critical clearing time can be interpreted in terms of meaningful quantities such as maximum power transfer in the prefault state. The energy-based methods are a special case of the more general Lyapunov's second method or the direct method. The direct methods determine stability without explicitly solving the system differential equations. Energy function methods have proven to be good ways to determine transient stability in a more reliable way than numerical methods. Energy function methods are considered the future of dynamic security assessment [7].

In this chapter, detailed discussion of direct methods assessment of transient stability will be presented.

4.2 Lyapunov's Method [7]

In 1892, A. M. Lyapunov proposed that stability of the equilibrium point of a nonlinear dynamic system of dimension n of

$$\dot{\mathbf{x}} = f(\mathbf{x}), f(\mathbf{0}) = 0 \quad (4.1)$$

can be ascertained without numerical integration. Lyapunov's theorem states that if there exists a scalar function $V(x)$ for (4.1) that is positive-definite around the equilibrium point "0" and the derivative $\dot{V}(x) < 0$, then the equilibrium is asymptotically stable. $\dot{V}(x)$ can be obtained as in (4.2).

$$\dot{V}(x) = \nabla V^T \cdot f(x) \quad (4.2)$$

$V(x)$ is actually a generalization of the concept of the energy of a system. Application of the energy function method to power system stability began with the early work of Magnusson [8] and Aylett [9]. Although many different Lyapunov functions have been tried since then, the first integral of motion, which is the sum of kinetic and potential energies, may have provided the best result. In power literature, Lyapunov's method has become the so-called Transient Energy Function (TEF) method.

4.3 Transient Energy Function (TEF) Formulation

4.3.1 Main Idea

As previously explained, the transient energy approach can be described by a ball rolling on the inner surface of a bowl as depicted in Figure 2.9. Initially the ball is resting which is equivalent to a power system in its steady-state equilibrium. When an external force is applied to the ball, the ball moves away from the equilibrium point. Equivalently, in a power system, a fault occurs on the system which causes the generator's rotors to accelerate and gain some kinetic energy causing the system to move away from the SEP. If the ball converts all its kinetic energy into potential energy before reaching the rim, then it will roll back and settle down at the SEP eventually. In power systems, after the fault is cleared, the kinetic energy gained during the fault will be converted into potential energy if the system is capable enough to absorb that kinetic energy. Otherwise, the kinetic energy will increase causing the system's machines to lose synchronism and become unstable.

4.3.2 Mathematical Development

From basic mechanics, the sum of potential energy (PE) and kinetic energy (KE) for a conservative system is constant. Thus using well-known formulas for KE and PE, we have an expression for the total energy of the system in terms of the state $\delta = (\delta, \dot{\delta})$,

$$V(\delta) = \frac{1}{2} M \dot{\delta}^2 + \int_{\delta^0}^{\delta} P(u) du \quad (4.3)$$

It can be noted that at equilibrium point (i.e., with $\delta = \delta^0$ and $\dot{\delta} = 0$), both the KE and PE are zero. Now, for the power system after time $t \geq T$, that is after the fault is cleared, the system energy is described by

$$V(\delta(t)) = \frac{1}{2} M \dot{\delta}_T^2 + \int_{\delta^0}^{\delta_T} P(u) du \quad (4.4)$$

The potential energy curve is the key factor in determining the transient stability. In Figure 4.1, the potential energy curve is illustrated.

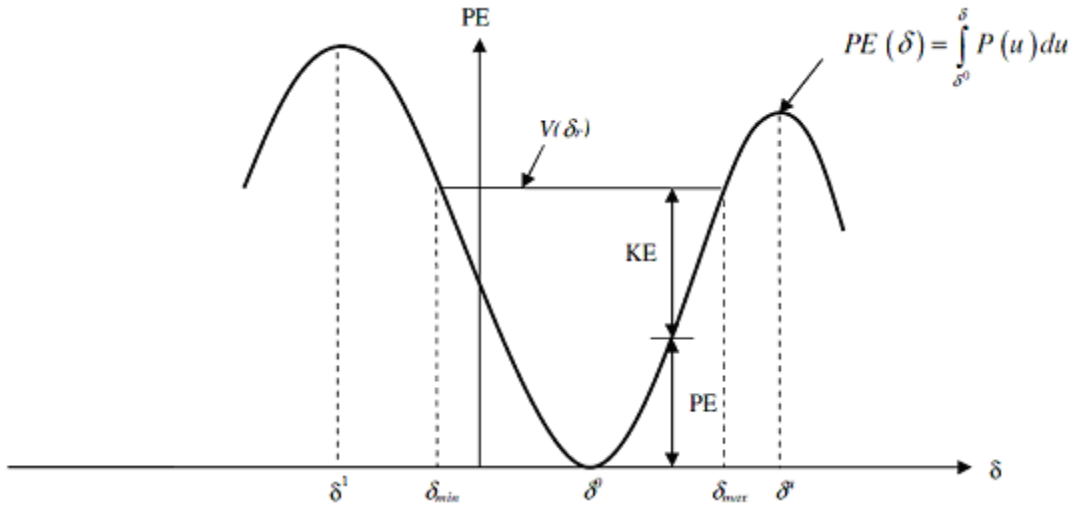


Figure 4.1: Potential energy plot. Redrawn from [14]

From Figure 4.1, the PE curve has a local minimum at $\delta = \delta^0$ and has two neighboring local maxima at δ^1 and δ^2 . Also, the plot shows that if the rotor angle reaches δ_{max} , the system

becomes unstable, that is, if the fault is not cleared before the rotor angle becomes δ_{max} , the trajectory will diverge toward the UEP δ^u . For any $T > T_{critical}$, $\dot{\delta}(t)$ is always positive and $\delta(t)$ increases monotonically with t .

Assume the usual case of a SMIB system, with the generator delivering power. From (4.3) and the definition of PE_{max} , $V(\delta_T) < PE_{max}$ implies that

$$\frac{1}{2}M\dot{\delta}_T^2 + \int_{\delta^0}^{\delta_T} P(u) du < \int_{\delta^0}^{\delta^u} P(u) du \quad (4.5)$$

The condition of stability is hence,

$$P_m(\delta_T - \delta^0) < \int_{\delta_T}^{\delta^u} P(u) du \quad (4.6)$$

4.3.3 Mathematical Development of TEF of Multi-Machine Power System

4.3.3.1 Synchronous Reference Frame Development [18]

Consider the system model represented by (2.17) and (2.18). The TEF V for the synchronous reference frame has the form,

$$V = \sum_{i=1}^{n-1} \sum_{j=i+1}^n \left[\frac{1}{2M_T} M_i M_j (\omega_i - \omega_j)^2 - \frac{1}{M_T} (P_i M_j - P_j M_i) (\delta_{ij} - \delta_{ij}^0) - C_{ij} (\cos \delta_{ij} - \cos \delta_{ij}^0) + \int_{\delta_i^0 + \delta_j^0 - 2\delta_o^s}^{\delta_i + \delta_j - 2\delta_o} D_{ij} \cos \delta_{ij} d(\delta_i + \delta_j - 2\delta_o) \right] \quad (4.7)$$

where,

M_i moment of inertia of machine i

ω_i generator's i rotor speed

δ_i generator's i rotor angle

δ_i^0 generator's i SEP

$$\delta_{ij} = \delta_i - \delta_j$$

$$\delta_o = \frac{1}{M_T} \sum_{i=1}^n M_i \delta_i$$

P_i, C_{ij}, D_{ij} defined by (2.18)

Equation (4.7) can be used to calculate the total energy of the system after solving for δ_i 's numerically. It consists of four terms: the first term represents the total change in kinetic energy, the second term represents the total change in potential energy, the third term represents the total change in magnetic stored energy, and the fourth term represents the total change in dissipated energy.

4.3.3.2 Center of Inertia Reference Frame [19]

Consider the system model represented by (2.19) – (2.28). The TEF V can be obtained by finding the $n(n-1)/2$ relative acceleration equations, multiplying each of these by the corresponding relative velocity and integrating the sum of the resulting equations from a fixed lower limit of the SEP (denoted by δ^0) to a variable upper limit. Equation (4.8) describes the energy V as a function of angular displacement δ and velocity ω .

$$V = \sum_{i=1}^{n-1} \sum_{j=i+1}^n \left[\frac{1}{2M_T} M_i M_j (\omega_i - \omega_j)^2 - \frac{1}{M_T} (P_i M_j - P_j M_i) (\delta_{ij} - \delta_{ij}^0) \right. \\ \left. - C_{ij} (\cos \delta_{ij} - \cos \delta_{ij}^0) + \int_{\delta_i^0 + \delta_j^0 - 2\delta_o^s}^{\delta_i + \delta_j - 2\delta_o} D_{ij} \cos \delta_{ij} d(\delta_i + \delta_j - 2\delta_o) \right] \quad (4.8)$$

Equation (4.8) can be written differently as,

$$V = 1/2 \sum_{i=1}^n M_i \tilde{\omega}_i^2 - \sum_{i=1}^n P_i (\theta_i - \theta_i^0) \\ - \sum_{i=1}^{n-1} \sum_{j=i+1}^n \left[C_{ij} (\cos \theta_{ij} - \cos \theta_{ij}^0) - \int_{\theta_i^0 + \theta_j^0}^{\theta_i + \theta_j} D_{ij} \cos \theta_{ij} d(\theta_i + \theta_j) \right] \quad (4.9)$$

where,

$M_i =$ moment of inertia of machine i

$\tilde{\omega}_i =$ generator's i rotor speed relative to COI

$\theta_i =$ generator's i rotor angle relative to COI

$\theta_i^0 =$ generator's i SEP relative to COI

$\theta_{ij} = \theta_i - \theta_j$

P_i, C_{ij}, D_{ij} defined by (2.18)

The terms of the TEF can be physically interpreted in the following way:

- $V_{KE} = 1/2 \sum_{i=1}^n M_i \tilde{\omega}_i^2 = 1/2 \sum_{i=1}^n M_i \omega_i^2 - 1/2 M_T \omega_o^2$

Total change in rotor KE relative to COI is equal to total change in rotor KE minus change in KE_{COI} .

- $V_{PE} = \sum_{i=1}^n P_i (\theta_i - \theta_i^0) = \sum_{i=1}^n P_i (\delta_i - \delta_i^0) - \sum_{i=1}^n P_i (\delta_o - \delta_o^0)$

Given that $\delta_o \triangleq 1/M_T \sum_{i=1}^n M_i \delta_i$, change in rotor PE relative to COI is equal to the

change in rotor potential energy minus change in COI potential energy.

- $C_{ij} (\cos \theta_{ij} - \cos \theta_{ij}^0)$ is the change in magnetic stored energy of branch ij .

- $\int_{\theta_i^0 + \theta_j^0}^{\theta_i + \theta_j} D_{ij} \cos \theta_{ij} d(\theta_i + \theta_j)$ is the change in dissipated energy of branch ij .

From the above discussion, it is clear that the change in energy associated with motion of the system COI is subtracted from the total system energy in order to obtain the TEF.

4.4 Multi-machine Transient Stability Measure Using TEF

The multi-machine equal area stability measure is an extension to the well-known Equal Area Criterion (EAC) method, but without considering the SMIB assumption. This stability measure is different from the EAC because it releases some of the assumptions made in the EAC such as, the conductance term could be included in the analysis, and it is used for multi-machine power system analysis without aggregating the system.

In the following sections, a detailed explanation of the use of Transient Energy Function (TEF) to determine stability using the following: TEF for synchronous reference frame, TEF for COI reference frame, and extended equal area criterion (EEAC).

4.4.1 Individual Machine Energy Function for Synchronous Reference Frame [18]

The multi-machine equal area based stability measure is constructed by finding the accelerating and decelerating energy of a particular machine in the power system. To evaluate the accelerating energy, the system is evaluated using the during fault configuration. However, to find the decelerating energy (absorbing energy), the post fault configuration is used. Additionally, to perform the EAC for a multi-machine system, the critical machine has to be identified. To identify the critical machine (or the most Severely Disturbed Unit SDU), the initial faulted acceleration $d\omega_i/dt$ is computed for all machines in the system. The SDU can be considered to be the one having the largest faulted acceleration [20]. According to the energy function of (4.7), the potential energy for machine i is:

$$\begin{aligned}
 V_{PEi}(t) = & \frac{1}{M_T} \sum_{i=1}^N (P_i M_j - P_j M_i) (\delta_{ij}(t) - \delta_{ij}^0(t)) \\
 & + \sum_{\substack{j=1 \\ j \neq i}}^N C_{ij} (\cos \delta_{ij}(t) - \cos \delta_{ij}^0) \\
 & - D_{ij} \frac{\delta_i(t) + \delta_j(t) - \delta_i^0 - \delta_j^0}{\delta_i(t) - \delta_j(t) - \delta_i^0 + \delta_j^0} [\sin \delta_{ij}(t) - \sin \delta_{ij}^0]
 \end{aligned} \tag{4.10}$$

If machine i is chosen to be the critical generator, the accelerating and decelerating energy of machine i can be used as a stability measure. The accelerating energy at the clearing time t_c is

$$A_a(t_c) = V_{PEi}(t_c) \quad (4.11)$$

where $V_{PEi}(t)$ depends on the faulted network.

The decelerating energy is

$$A_d(t, t_c) = V_{PEi}(t) - V_{PEi}(t_c) \quad (4.12)$$

where $V_{PEi}(t_c)$ depends on the post fault network configuration.

For a given fault-clearing time t_c , the system is considered to be stable if $A_a < A_d$. For a stable system, the SDU reaches the peak angle before the system trajectory reaches the controlling UEP.

Equation (4.10) can be subtracted from the KE of generator i ,

$$V_{KEi} = \frac{1}{2M_T} \sum_{\substack{j=1 \\ j \neq i}}^N M_i M_j (\omega_i - \omega_j)^2 \quad (4.13)$$

which results the total energy of generator i . This function is shown to be a Lyapunov function when the conductance term is ignored.

4.4.2 Individual Machine Energy Function for COI Reference Frame

Consider the system model of Equation 2.19. Assume that the effect of damping is neglected in the system since the energy function is used for first swing stability. The following derivation is followed from [17]. By multiplying the i th post fault swing equation by $\dot{\theta}_i$ and rearranging, we obtain the expression

$$\left[M_i \dot{\tilde{\omega}}_i - P_i + P_{ei} + \frac{M_i}{M_T} P_{COI} \right] \dot{\theta}_i = 0, \quad i = 1, \dots, n \quad (4.14)$$

Integrating (4.14) with respect to time, using t_0 as a lower limit, where $\dot{\tilde{\omega}}(t_0) = 0$ and $\theta(t_0) = \theta^0$ is the SEP, yields

$$\begin{aligned} V_i = & \frac{1}{2} M_i \tilde{\omega}_i^2 - P_i (\theta_i - \theta_i^0) + \sum_{\substack{j=1 \\ j \neq i}}^n C_{ij} \int_{\theta_i^0}^{\theta_i} \sin \theta_{ij} d\theta_i \\ & + \sum_{\substack{j=1 \\ j \neq i}}^n D_{ij} \int_{\theta_i^0}^{\theta_i} \cos \theta_{ij} d\theta_i + \frac{M_i}{M_T} \int_{\theta_i^0}^{\theta_i} P_{COI} d\theta_i \end{aligned} \quad (4.15)$$

Equation (4.15) is evaluated using the post fault network configuration. The first term in (4.15) represents the KE of machine i with respect to the system COI. The remaining terms are considered to be the PE. Thus, (4.15) can be expressed as,

$$V_i = V_{KEi} + V_{PEi} \quad (4.16)$$

For a given disturbance, transient energy injected into the system during the fault causing the total energy V_i to increase which causes machine i to diverge from its equilibrium. When the fault is cleared, machine's i gained KE is converted into PE . This process continues until the initial KE is converted totally into PE causing the machine to converge toward the rest of the system. However, if the KE of machine i is not converted totally into PE , machine i loses synchronism and separates from the system.

Equation (4.16) consists of two parts: kinetic energy, and potential energy. Both energies need to be solved numerically. After the rotor angles are found numerically, the energies can be represented by

$$V_{KEi} = \frac{1}{2} M_i \tilde{\omega}_i^2 \quad (4.17)$$

$$\begin{aligned}
V_{PEi} = & P_i(\theta_i - \theta_i^0) + \sum_{\substack{j=1 \\ j \neq i}}^n C_{ij} \left[\cos(\theta_i^0 - \theta_j) - \cos(\theta_i - \theta_j) \right] \\
& + \sum_{\substack{j=1 \\ j \neq i}}^n D_{ij} \left[\sin(\theta_i - \theta_j) - \sin(\theta_i^0 - \theta_j) \right] + \frac{M_i}{M_T} \int_{\theta_i^0}^{\theta_i} P_{COR} d\theta_i
\end{aligned} \tag{4.18}$$

$$\begin{aligned}
\int_{\theta_i^0}^{\theta_i} P_{COR} d\theta_i = & \sum_{i=1}^n (\theta_i - \theta_i^0) - \sum_{i=1}^n \sum_{\substack{j=1 \\ j \neq i}}^n C_{ij} \left[\cos(\theta_i^0 - \theta_j) - \cos \theta_{ij} \right] \\
& - \sum_{i=1}^n \sum_{\substack{j=1 \\ j \neq i}}^n D_{ij} \left[\sin \theta_{ij} - \sin(\theta_i^0 - \theta_j) \right]
\end{aligned} \tag{4.19}$$

By using the total energy of the system, part of the boundary of the region of stability is determined by hypersurfaces which passes through the saddle points. These hypersurfaces are from the Potential Energy Boundary Surface (PEBS). At the PEBS, the potential energy is maximum as well as on the boundary of the region of stability. The potential energy close to the UEP is flat. The system maintain stability if the total kinetic energy is converted into potential energy before reaching the PEBS.

Using the preceding discussion, machine i remains stable if V_{PEi} is maximum. This maximum value is fairly flat and it is equal to the critical total energy $V_{cr,i}$ of machine i .

4.4.3 Equal Area Criterion for Multi-Machine System [20]

In the derivation of this method, it is assumed that only one machine is severely disturbed (SDU) and it is responsible for system instability. The other machines are less disturbed and their rotor angles variations are not significant compared to the SDU during the transient period. The SDU can be identified by observing the initial faulted acceleration of the machines.

Let i be the critical or SDU for a given disturbance. The dynamics are given by

$$\left. \begin{aligned} \frac{d\theta_i}{dt} &= \tilde{\omega}_i \\ M_i \frac{d\tilde{\omega}_i}{dt} &= P_{Ai} \end{aligned} \right\} \quad (4.20)$$

where

$$P_{Ai} = a_i - \sum_{\substack{j=1 \\ j \neq i}}^n (b_{ij} \sin \theta_i + d_{ij} \cos \theta_i) \quad (4.21)$$

$$a_i = P_i - \frac{M_i}{M_T} P_T + 2 \frac{M_i}{M_T} \sum_{\substack{k=1 \\ k \neq i}}^{n-1} \sum_{\substack{j=k+1 \\ j \neq i}}^n D_{kj} \cos \theta_{kj} \quad (4.22)$$

$$b_{ij} = C_{ij} \cos \theta_j + D_{ij} \left(1 - 2 \frac{M_i}{M_T} \right) \sin \theta_j \quad (4.23)$$

$$d_{ij} = -C_{ij} \sin \theta_j + D_{ij} \left(1 - 2 \frac{M_i}{M_T} \right) \cos \theta_j \quad (4.24)$$

By eliminating the independent variable time t in (4.20), the differential relationship between $\tilde{\omega}_i$ and θ_i can be written as,

$$M_i \tilde{\omega}_i d\tilde{\omega}_i = P_{Ai} d\theta_i \quad (4.25)$$

Let us consider the system is critically stable ($t = t_c = t_{cr}$) where t_c and t_{cr} represent clearing and critical clearing times, respectively. For such a system, the post fault trajectory passes near the vicinity of an unstable equilibrium point (UEP) called the controlling UEP. The controlling UEP is the solution of equation to the sum of the squared change in angular speed represented by (4.26) at which $\theta_i > 90^\circ$ and the absolute angle of the rest of the machines is less than 90° .

$$F(\theta) = \sum_{k=1}^n \left(P_k - P_{ek} - \frac{M_k}{M_T} P_{COI} \right)^2 = 0 \quad (4.26)$$

Let (4.25) be integrated from the prefault operating point to the post fault controlling UEP,

$$\int_{\omega_i^0=0}^{\omega_i^u=0} M_i \tilde{\omega}_i d\tilde{\omega}_i = \int_{\theta_i^0}^{\theta_i^u} P_{Ai} d\theta_i = 0 \quad (4.27)$$

Note that the change in angular velocity is 0 for all equilibrium points. Now, given that the network changes its configuration at fault clearing (t_c), the right-hand equation of (4.27) can be reconstructed into two parts,

$$\int_{\theta_i^0}^{\theta_i^c} P_{Ai}^f d\theta_i = - \int_{\theta_i^c}^{\theta_i^u} P_{Ai}^p d\theta_i \quad (4.28)$$

The superscripts f , p , and c represent the faulted, post faulted, and clearing conditions, respectively. The left-hand side of (4.28) is called the accelerating area (energy) A_a and after substitution in the main model of (2.19), we get,

$$A_a = \int_{\theta_i^0}^{\theta_i^c} P_{Ai}^f d\theta_i = \int_{\theta_i^0}^{\theta_i^c} \left(P_i^f - P_{ei}^f - \frac{M_i}{M_T} P_{COI}^f \right) d\theta_i \quad (4.29)$$

Equation (4.29) is the equivalent of the so-called integral of accelerating power (P_{Ai}) and it can be solved numerically. Also, it can be represented by the following:

$$A_a = \int_{\theta_i^0}^{\theta_i^c} P_{Ai}^f d\theta_i = \int_{\theta_i^0}^{\theta_i^c} \left\{ a_i^f - \sum_{\substack{j=1 \\ j \neq i}}^n (b_{ij}^f \sin \theta_i + d_{ij}^f \cos \theta_i) \right\} d\theta_i \quad (4.30)$$

Since a_i^f , b_i^f and d_i^f are independent of θ_i but depend on angles of other machines in the system, a correction factor (the average of sinusoid) is added to convert the integral of Equation 4.30 into summation. Therefore, the accelerating energy becomes,

$$A_a = a_i^f (\theta_i^c - \theta_i^0) + \sum_{\substack{j=1 \\ j \neq i}}^n \left\{ b_{ij}^f (\cos \theta_i^c - \cos \theta_i^0) - d_{ij}^f (\sin \theta_i^c - \sin \theta_i^0) \right\} \quad (4.31)$$

where in (4.31)

$$a_i^f = P_i^f - \frac{M_i}{M_T} P_T^f + 2 \frac{M_i}{M_T} \sum_{k=1}^{n-1} \sum_{\substack{j=k+1 \\ j \neq i}}^n D_{kj}^f \frac{(\cos \theta_{kj}^c + \cos \theta_{kj}^0)}{2} \quad (4.32)$$

$$b_{ij}^f = C_{ij}^f \frac{(\cos \theta_j^c + \cos \theta_j^0)}{2} + D_{ij}^f \left(1 - 2 \frac{M_i}{M_T} \right) \frac{(\sin \theta_j^c + \sin \theta_j^0)}{2} \quad (4.33)$$

$$d_{ij}^f = -C_{ij}^f \frac{(\sin \theta_j^c + \sin \theta_j^0)}{2} + D_{ij}^f \left(1 - 2 \frac{M_i}{M_T} \right) \frac{(\cos \theta_j^c + \cos \theta_j^0)}{2} \quad (4.34)$$

Using the same principle, the decelerating area A_d (energy) for the post fault system configuration can be written with just changing the subscripts of f , c , and 0 to be p , u , and c , respectively which represents post fault, UEP, and clearing states. Thus, the decelerating area can be written as,

$$A_d = a_i^p (\theta_i^u - \theta_i^c) + \sum_{\substack{j=1 \\ j \neq i}}^n \left\{ b_{ij}^p (\cos \theta_i^u - \cos \theta_i^c) - d_{ij}^p (\sin \theta_i^u - \sin \theta_i^c) \right\} \quad (4.35)$$

where

$$a_i^p = P_i^p - \frac{M_i}{M_T} P_T^p + 2 \frac{M_i}{M_T} \sum_{k=1}^{n-1} \sum_{\substack{j=k+1 \\ j \neq i}}^n D_{kj}^p \frac{(\cos \theta_{kj}^u + \cos \theta_{kj}^c)}{2} \quad (4.36)$$

$$b_{ij}^p = C_{ij}^p \frac{(\cos \theta_j^u + \cos \theta_j^c)}{2} + D_{ij}^p \left(1 - 2 \frac{M_i}{M_T} \right) \frac{(\sin \theta_j^u + \sin \theta_j^c)}{2} \quad (4.37)$$

$$d_{ij}^p = -C_{ij}^p \frac{(\sin \theta_j^u + \sin \theta_j^c)}{2} + D_{ij}^p \left(1 - 2 \frac{M_i}{M_T} \right) \frac{(\cos \theta_j^u + \cos \theta_j^c)}{2} \quad (4.38)$$

For the case of SDU, the critical clearing time occurs when the accelerating area equals to the decelerating area ($A_a = A_d$); the SDU reaches the zero speed deviation when the fault is cleared exactly on the critical clearing time. However, if the SDU cannot reach the zero speed

deviation when its angle reaches the value θ_i^u , the system considered to be unstable. This happens when $t_c > t_{cr}$. For a given fault clearing time t_c , the system is considered to be stable if $A_a < A_d$.

4.5 Proof of Concept Proposed Method

We previously published a proof of concept to our proposed method in [1] – [3]. The proposed proof of concept is based on the single-machine energy function explained in sections 4.4.1 and 4.4.2. Since the focus of this thesis is on the COI, the method is explained for the COI only. At first, the system is separated into two groups: the severely disturbed group, and the less disturbed group. Each of the groups has to consist of at least two machines. Let SDG be the number of severely disturbed machines, where $2 \leq SDG < n$. In order to determine the SDG , a tolerance is set by the user such that,

$$SDG = \left\{ i : \max_{1 \leq i \leq n} |\alpha_i| - |\alpha_i| \leq \text{tolerance} \right\} \quad (4.39)$$

where

$$\alpha_i = P_i - P_{ei} - \frac{M_i}{M_T} P_{COI} \quad (4.40)$$

After the SDG is determined, the kinetic energy of the clearing instant of the generators at SDG is calculated using (4.17). The calculated kinetic energies are added together as follows:

$$V_{KE,SDG} = \frac{1}{2} \sum_{i=1}^{\text{length}(SDG)} M_{SDG(i)} \omega_{SDG(i)}^2 \quad (4.41)$$

where

$SDG(i)$ means the machine number of the SDG , that is, i works as an index to the SDG set.

After determining the kinetic energies of the SDG , the potential energies of each machine in the system are calculated using the post-fault configuration using (4.18) and (4.19). Depending

on the length of the set SDG , the same number of machines is used to sum the smallest resulting potential energies. To calculate the potential energy, θ_i^0 and θ_i in (4.18) and (4.19) are replaced by θ_i^s and θ_i^c , respectively. That is,

$$V_{PE,\overline{SDG}} = \sum_{i=1}^{\text{length}(SDG)} V_{PEi}(\theta_i^s, \theta_i^c) \quad (4.42)$$

after sorting the potential energies from the smallest to the largest. The two values are compared and based on the comparison a decision on stability can be made. If $V_{PE,\overline{SDG}} > V_{KE,SDG}$, then the system is considered stable. Otherwise, the system is unstable. If $V_{PE,\overline{SDG}} = V_{KE,SDG}$, then the system is critically stable.

4.6 Summary

In this chapter, detailed discussion of direct methods is provided. A brief discussion of Lyapunov's method is presented. Lyapunov's method introduces the energy function of a power system that can be used in stability studies. Then, transient energy function (TEF) is discussed and mathematical formulation is provided. The more specific case of the multi-machine energy function is developed for both the synchronous reference frame and the COI reference frame. Also, the extended equal area criterion for the severely disturbed machine is discussed and the mathematical formulation is developed. Finally, the proof of concept method is explained briefly for the COI reference frame.

In Chapter 5, the specific problem and all the complications that make this problem important to be solved are discussed. Also, the objective of this research to achieve the needed results is talked about. Then the proposed method and the mathematical formulas are introduced and discussed in details.

Chapter 5

5 Problem Statement, Objective, and Methodology

The previous sections have given an overview into the power system stability problems, and transient instability. This section will discuss the difficulties in detecting transient stability in real time, and the approach taken in this research to analyze the dynamic response of a power system that is perturbed by an external force and to how to use this response to detect transient stability status. Also, a method is proposed to calculate the Critical Clearing Time (CCT) for a faulted power system in the next sections.

5.1 Problem Statement

Power system transient stability involves subjecting the system to a severe transient disturbance such as a fault on transmission facilities, loss of generation, or loss of a large load. The system response to such disturbances involves large excursions of generator rotor angles, power flows, bus voltages and other system variables [5]. For some portions of the North American power grids, such as the Western Electricity Coordinating Council (WECC), transient stability has always been an important consideration [40], while for other portions it is of growing concern due partially to the widespread integration of wind generation.

Transient stability analyses form a critical part of assessing the system for planning and operation purposes in Normal state. It is, however, widely known that different industry-grade transient stability simulation tools can give substantially different results for similar system models [41]. As the system is moving in time, there are many “*small*” changes occurring from change in load to unexpected contingency which underlines the need for a more sophisticated,

adaptive and intelligent method that can determine how close/far a system is from transient instability had any fault or contingency occurs.

Power system may experience one of the following five states [49]:

1. Normal State: In this state, the system's variables (voltage, frequency, temperature, and power flow) are within the normal range and with no load interruption. The system is normally built to operate in this state.
2. Alert State: In this state, all the system's variables are also within the acceptable range except that the variables are close to their limits. In this case, the system may move into the Emergency state following a disturbance.
3. Emergency State: In this state, some system variables are outside the acceptable range and the system is ready to fall into the Extremis state. Some loads may lose power and possible islanding may occur. In this case, the system may be disintegrated.
4. Extremis State: In this state, partial or system wide blackout could occur.
5. Restorative State: In this state, the system is in the process of being restored by reconnecting parts of the system and resynchronizing generators in a certain sequence in order to achieve a return to Normal state.

Figure 5.1 shows a detailed description of the “Dy-Liacco diagram”. It is referred to by Dy-Liacco because of its original creator, Dy Liacco who laid down the conceptual foundations of power system security and for defining the different operation mode [50].

Since transient stability requires solving the system's differential equations, many accurate parameters are required. Transient simulators generally require very detailed modeling, which may not always be available in many utilities. Due to this fact, another way of handling the detailed modeling has to be employed.

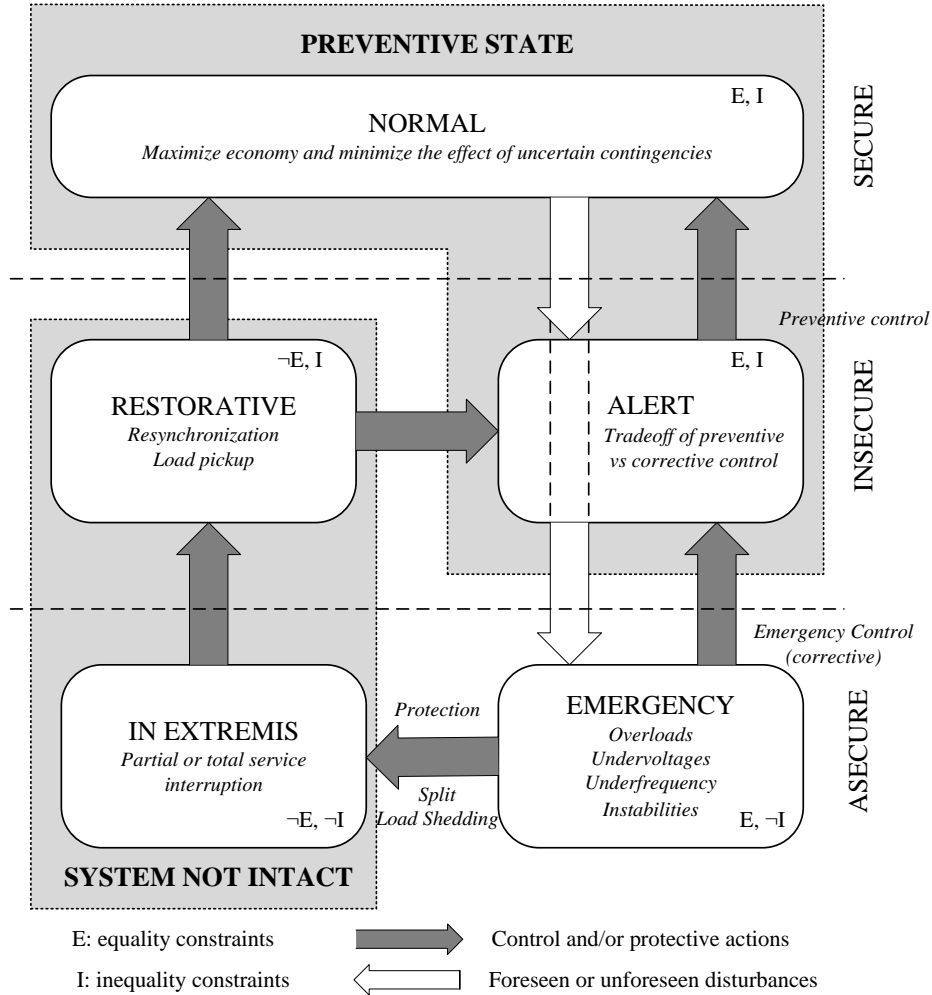


Figure 5.1: Power System Operational States [50]

Additionally, pre-fault load condition can have a high impact on transient stability. Figure 5.2 shows a generator operating at load P_{m1} prior to a three-phase fault. The fault is cleared when the acceleration area 1-2-3-4 is smaller than the available deceleration area 4-5-8. The system is stable with stability margin 6-7-8. Increasing the pre-fault load by 50% to $P_{m2} = 1.5P_{m1}$ increases the acceleration power $P_{acc} = P_m - P_{E'}(\delta') = P_m$ by one and a half times so that the change in the power angle $\Delta\delta'$ also increases by a factor of 1.5. Consequently, as each side of the accelerating area rectangle 1-2-3-4 has increased 1.5 times, the acceleration area 1-2-3-4 is now much larger than the available deceleration area 4-5-8 and the system is unstable.

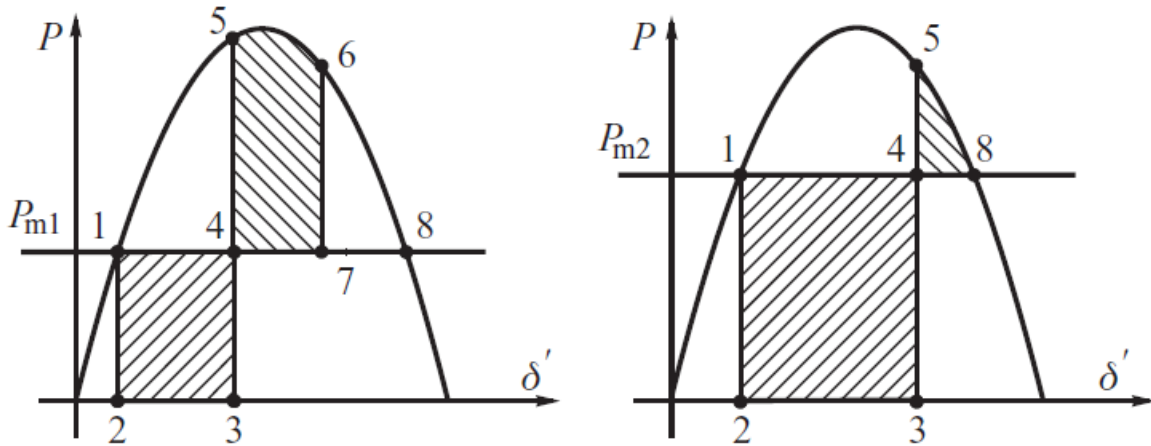


Figure 5.2: Effect of Prefault Loading Condition on CCT [42]

The prefault load is an important factor with regard to determining the critical clearing time and generator stability. The higher the loading on a generator, the lower the critical clearing time.

5.2 Objective

The main objective of this research is to provide a method that can determine large-scale power system transient stability not only for planning purposes but also for operation of power systems in Normal state. The method focuses on using online dynamic data (rotor angles and speeds) for the accessible generators in the event of a disturbance occurrence on the system in any location at an instant of time to determine whether the system will return back to the Normal state or not. That is, the research uses online dynamic data to determine transient stability for any disturbance on the system.

5.3 Methodology

As mentioned in the previous sections, the main objective of this research is to detect transient instability by means of providing applicable information. Some of the relevant information that influences transient stability is the prefault load condition (transient stability

margin) and critical machine(s) for a faulted case which is dependent on the machines' dynamics and electrical connection from the fault location to the available machines. The methodology to achieve this objective consists of four phases:

1. **Modeling and Simulation:** Modeling of test system and simulating it to capture the power system dynamic responses for various fault conditions.
2. **Identification of Critical Machine(s):** In this phase, extraction of the system relevant variables around the instance of a disturbance that includes some pre-disturbance, during disturbance, and post-disturbance variables.
3. **Online Transient Stability Assessment:** This phase is the final phase that will determine the transient stability in the event of system perturbation.
4. **Critical Clearing Time Calculation:** This phase uses the results of the previous phases to calculate the CCT.

5.3.1 Modeling and Simulation of the Test System (Phase I)

This phase of the methodology is only used for verification of the proposed method and it is not needed for application on a real system. In this phase, the dynamic response of the system is captured after a disturbance. The system response consists of various variables which include bus voltage magnitudes and angles, real and reactive powers, and generator rotor angles and change in speed. Dynamic response of the system can be captured by any of the following two methods:

1. **Using the equivalent system models and dynamic simulation tools:** To use this method, an accurate equivalent model needs to be created. There are many dynamic simulation toolboxes, and in this research, the MATLAB-based Power System Analysis Toolbox (PSAT) is used to perform the dynamic simulation. The generators

rotor angles and speeds are captured before the fault and at the instant the fault is removed in order to use them for determining critical machines (SDG) in Phase II.

2. Collecting data from the field by using Phasor Measurement Units (PMUs): PMU's are currently available in many places throughout the US Power Grid. These units can be used to capture and record system variables with time stamp synchronized to GPS time clock.

This research will use the first method as the second method is not possible. To test the methodology, the IEEE 39 Bus New England equivalent system is used to capture the necessary dynamic response in order to detect transient stability. Flow chart that shows all the steps of Phase I is as shown in Figure 5.3.

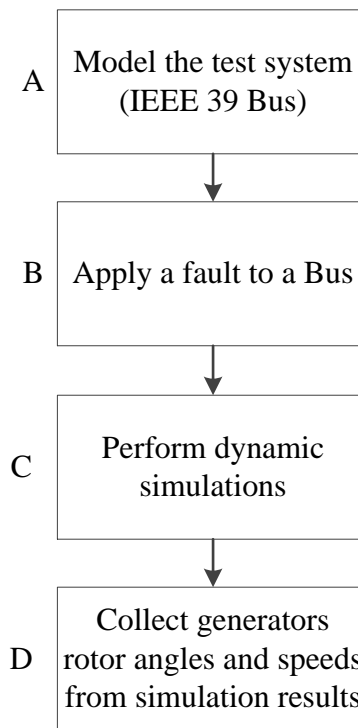


Figure 5.3: Phase I – Modeling and Simulation

When the first method is used, Phase I of the methodology consists of four steps:

Step A: In this step the test system is built in PSAT based on the equivalent model data that are available in public domain. These data consists of generator equivalent models, transmission line equivalent models, and various load models. Once the system model is built, static and dynamic simulation for base case are performed to ensure that the system model is steady-state stable.

Step B: In this step, a 3-phase fault is applied on one of the Buses available in the model. The faulted Bus can be a generator Bus, load Bus or a transmission line Bus. In this step, the time at which the fault is occurred and when the fault is cleared are required to be entered or automated for CCT search purpose.

Step C: In this step, dynamic simulation of the power system is performed using PSAT. All the raw dynamic variables are captured in this step.

Step D: In this step, system's relevant variables, i.e. generators rotor angles and speed variation are captured. These variables are three points: pre-fault generators rotor angles, fault clearing instant generators rotor angles, and fault clearing instant rotor speeds. However, Phase II contains some steps that requires every rotor angles and speeds samples of the fault duration to determine the SDG.

5.3.2 Identification of Critical Machine(s) (Phase II)

In Phase II of the methodology, the critical machines of a certain disturbance are detected. A critical machine can be defined by a machine that contributes to system separation in the event of an external force applied onto the power system. This phase consists of six steps that are shown in the flow chart shown in Figure 5.4.

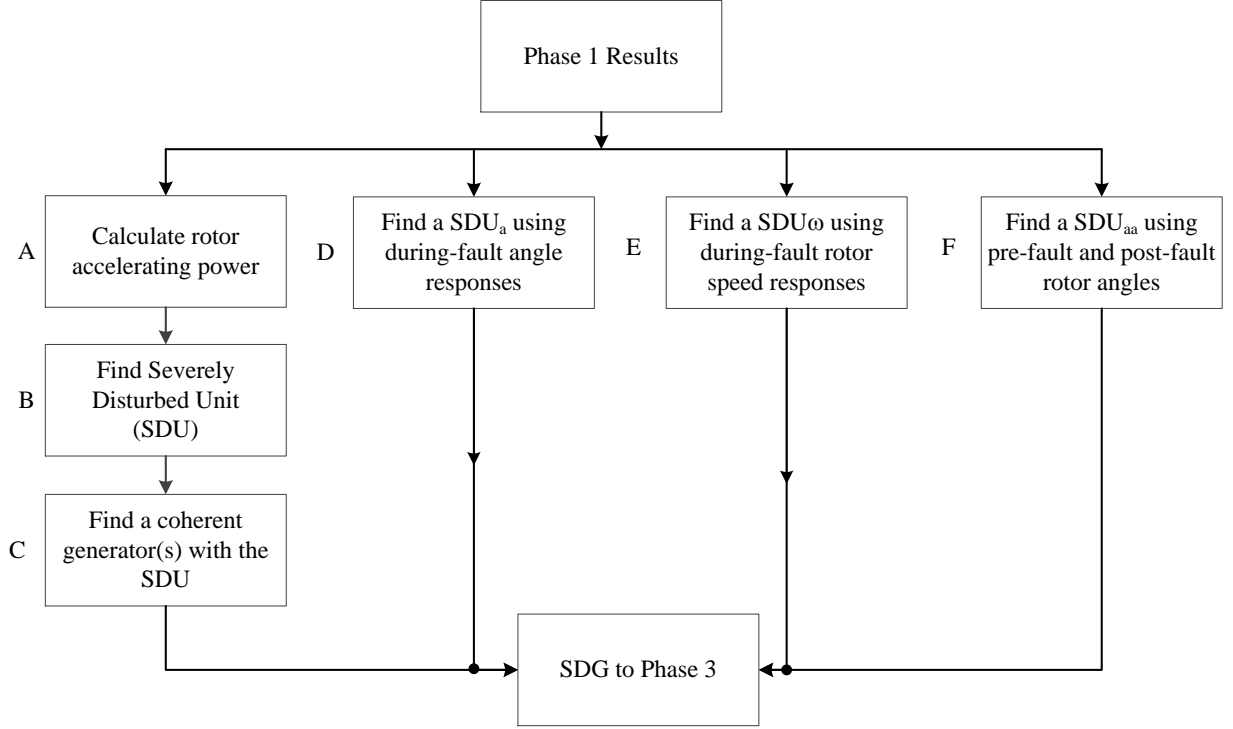


Figure 5.4: Phase II – Identification of Critical Machine(s)

Phase II of the methodology consists of six steps:

Step A: Calculate rotor accelerating power: In this step, the captured dynamic response of each machine is used to calculate the acceleration at which the rotor speed changed. The accelerating power can be calculated using,

$$P_{ai}(t) = M_i \frac{\tilde{\omega}_i(t + \Delta t) - \tilde{\omega}_i(t)}{\Delta t} \quad (5.1)$$

where,

$\tilde{\omega}_i(t)$ is rotor speed of machine i at time t

Δt is the integration step size in time-domain simulation

M_i is the inertia constant of machine i

An alternate way that can be used in this step to use the following equation [18],

$$P_{ai}(t) = \left(P_i - P_{ei} - \frac{M_i}{M_T} P_{COI} \right) M_i^{-1} \quad (5.2)$$

where the variables are as defined in (2.19) – (2.28).

Step B: Find the Severely Disturbed Unit (SDU): Using the accelerating power, the generator with the highest initial accelerating power is considered to be the SDU.

Step C: Find coherent generators with SDU: In this step, the coherent generators with the SDU are determined. If the fault causes the system to be transient instable, initially, the SDU loses synchronism and subsequently other Severely Disturbed Units may join the critical machine to form a larger group of unstable machines. Generally, those machines that are physically coherent with the critical machine are the ones that follow that particular machine. Hence this is an important feature to use in order to construct the SDG. To perform this step, the following steps are needed [48]:

1. The during-fault rotor speed deviation response needs to be captured for all machines.

That is, the rotor speed deviation for all machine are captured from t_{0+} to t_{cl} .

2. The speed deviation $\tilde{\omega}_{ik}$ of each machine with respect to the synchronous rated speed ω_s is defined as:

$$\tilde{\omega}_{ik} = \tilde{\omega}_{ik}(t) - \omega_s \quad \text{for } i = 1, n \text{ and } k = 1, N \quad (5.3)$$

where n is the number of generators and N is the number of observation points within the observation time.

3. The average of rotor speed deviations of each machine, $\bar{\omega}_i$, is calculated using the following equation

$$\bar{\omega}_i = \frac{\Delta t}{T_{obs}} \sum_{k=1}^N \tilde{\omega}_{ik} \quad (5.4)$$

4. The values of $\bar{\omega}_i$ are sorted in ascending order.
5. The successive deviations for each $\bar{\omega}_i$ are calculated using the following equation,

$$\bar{\omega}_{i,i+1} = \bar{\omega}_i - \bar{\omega}_{i+1} \quad \text{for } i = 1, \dots, n-1 \quad (5.5)$$

6. A coherency quality index q and also a ξ tolerance admitted between the speed deviations to form groups are determined. In this research, the quality index is assumed and the tolerance is solved for by using the following equation,

$$\xi = q\bar{\omega}_{ij}^{\min} + (1-q)\bar{\omega}_{ij}^{\max} \quad (5.6)$$

The quality index can be understood by the following example,

- If $q = 1$, then there is a low tolerance and that $n - 1$ groups are formed
- If $q = 0$, then there is a high tolerance and that all machines belong to the same cluster.

Therefore, the quality index is assumed depending on the size of the power system.

7. Using the coherency criterion which is represented by,

$$|\omega_i(t) - \omega_j(t)| \leq \xi \quad \text{for } 0 \leq t \leq T_{obs} \quad (5.7)$$

8. Add the found generators to the SDG, which, by this step, contains the SDU and all other generators found in this step.

Step D: Find a SDU using during-fault rotor angle response: In this step, the root-squared error is used to find the generator with the largest rate of change in the rotor angle. To calculate the average of root-squared error, the following equation is used,

$$\varepsilon_{ij}^{\theta} = \frac{\Delta t}{T_{obs}} \sqrt{\sum_{k=1}^N (\theta_{ik} - \theta_{jk})^2} \quad (5.8)$$

where θ_{ik} is the rotor angle of machine i , N is the number of observed points, Δt is the integration step size, and T_{obs} is the observed time. In the proposed method, T_{obs} is equal to the fault duration. To find the critical machine using (5.8), the following steps are developed:

1. Calculate the root-mean squared error for all possible combinations of rotor angles for during-fault state.
2. Sort the average error in ascending order.
3. Use the highest error to add the two corresponding machines to a queue.
4. Determine the generator that has the highest change in rotor angle of the two generators in the queue.
5. Add the found machine to the SDG. If it is already in the SDG, then do not add it and go to Step E.

Step E: Find a SDU using during-fault rotor speed deviation response: In this step, the root-squared error is used to find the generator with the largest rate of change in the rotor speed deviation. To calculate the average of root-squared error, the following equation is used,

$$\varepsilon_{ij}^{\omega} = \frac{\Delta t}{T_{obs}} \sqrt{\sum_{k=1}^N (\tilde{\omega}_{ik} - \tilde{\omega}_{jk})^2} \quad (5.9)$$

where $\tilde{\omega}_{ik}$ is the rotor angle of machine i , N is the number of observed points, Δt is the integration step size, and T_{obs} is the observed time. In the proposed method, T_{obs} is equal to the fault duration. To find the critical machine using (5.8), the following steps are developed:

1. Calculate the root-mean squared error for all possible combinations of rotor speed deviation for during-fault state.
2. Sort the average error in ascending order.
3. Use the highest error to add the two corresponding machines to a queue.

4. Determine the generator that has the highest change in rotor speed deviation of the two generators in the queue.
5. Add the found machine to the SDG. If it is already in the SDG, then do not add it and go to Step F.

Step F: Find a SDU using the difference between post-fault and pre-fault: In this step, a single parameter for each machine is calculated. This parameter determines the degree of change in generators rotor angles. The following equation is used for this purpose:

$$\Delta\theta_i = |\theta_i^{cl} - \theta_i^{pre}| \quad (5.10)$$

where θ_i^{cl} is the rotor angle of machine i at the clearing instant, and θ_i^{pre} is the rotor angle of machine i before the fault occurrence. Using the measure in (5.10), find the generator with the highest change in rotor angle and add it to the SDG. If it is already in the set, do not add this generator and go to the next step.

5.3.3 Online Transient Stability Assessment (Phase III)

In Phase III of the methodology, transient stability decision is made based on the measurements and calculations made in Phases I, and II. In addition, the change in kinetic and potential energies are calculated. This phase consists of six steps that are shown in the flow chart shown in Figure 5.5.

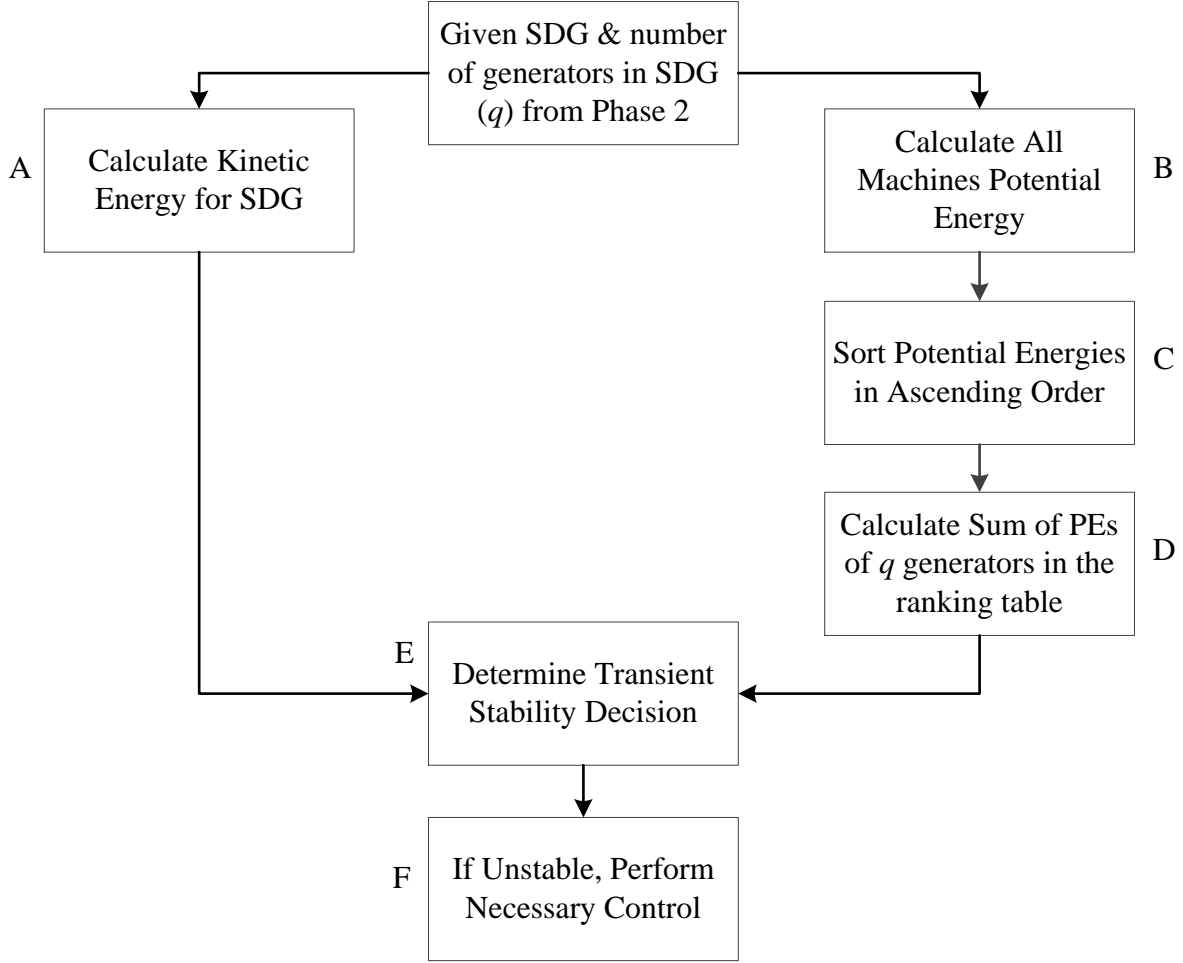


Figure 5.5: Phase III – Online Transient Stability Assessment

Phase III of the methodology consists of five steps:

Step A: Calculate the Kinetic Energy for all the generators in the SDG. The Kinetic Energy of a single-machine of a multi-machine power system is defined in [17] by,

$$V_{KEi} = \frac{1}{2} M_i \tilde{\omega}_i^2 \quad (5.11)$$

The summation of each machine's Kinetic Energy represents the total kinetic energy of the SDG which is defined as,

$$V_{KE} = \sum_{SDG} V_{KEi} \quad (5.12)$$

Step B: Calculate the Potential Energy of all machines by using the single-machine of a multi-machine power system equation defined in [17] by,

$$\begin{aligned}
 V_{PEi} = & P_i(\theta_i - \theta_i^0) + \sum_{\substack{j=1 \\ j \neq i}}^n C_{ij} \left[\cos(\theta_i^0 - \theta_j) - \cos(\theta_i - \theta_j) \right] \\
 & + \sum_{\substack{j=1 \\ j \neq i}}^n D_{ij} \left[\sin(\theta_i - \theta_j) - \sin(\theta_i^0 - \theta_j) \right] + \frac{M_i}{M_T} \int_{\theta_i^0}^{\theta_i} P_{COI} d\theta_i
 \end{aligned} \tag{5.13}$$

In (5.13), θ_i^0 is the steady-state SEP of unit i relative to COI.

Step C: Sort all generator's Potential Energies in ascending order and select the lowest energies that corresponds to the same number of generators in SDG. That is, for example, there are x generators in the SDG, then the first x sorted potential energies are selected. This set is denoted by \overline{SDG} ,

Step D: Calculate the sum of the Potential Energies in the \overline{SDG} . The summation of the Potential Energy in the \overline{SDG} can be calculated by,

$$V_{PE} = \sum_{\overline{SDG}} V_{PEi} \tag{5.14}$$

Step E: Make transient stability decision. The two energy values are compared and based on the comparison a decision on stability can be made. If $V_{PE} > V_{KE}$, then the system is considered stable. Otherwise, the system is unstable. If $V_{PE} = V_{KE}$, then the system is critically stable.

Step F: If the system is transient unstable, then some automated or human-interfaced action needs to be performed in order to maintain the system from disintegrating which causes voltage collapse and loss of power.

5.3.4 Critical Clearing Time Calculations (Phase IV)

Phase IV of the methodology is an optional one and can be used as a screening tool or for the proposed method verification. This phase consists of ten steps that are shown in the flow chart shown in Figure 5.6. Phase IV algorithm is as follows:

Step A: Data Initialization – In this step, the modeled system is entered and all the necessary variables are initialized. These variables include the time step increment multiplier, the error tolerance, and the fault location.

Step B: Run Power Flow – In this step the initial power flow equations are solved and all the initial generators voltages and rotor angles are calculated.

Step C: Run Step-by-Step Integration – Numerical methods are used in this step. The system's dynamic equations are solved from the instant the fault occurs until the fault is cleared at t_{cl}^+ .

Step D: Save Rotor Speeds and Angles, and Y-matrix – In this step, the generators' rotor angles and angular are obtained from the results of the step-by-step integration. Also, the admittance matrix (Y_{Bus}) of the post-fault configuration is obtained.

Step E: Determine SDG – In this step, the SDG is constructed using the same procedure in 5.3.2.

Step F: Find Reduced Y Using Kron Reduction – This step uses Kron reduction to find the reduced matrix from $m \times m$ to $n \times n$, where m is the number of the Buses in the system and n is the number of machines in the system.

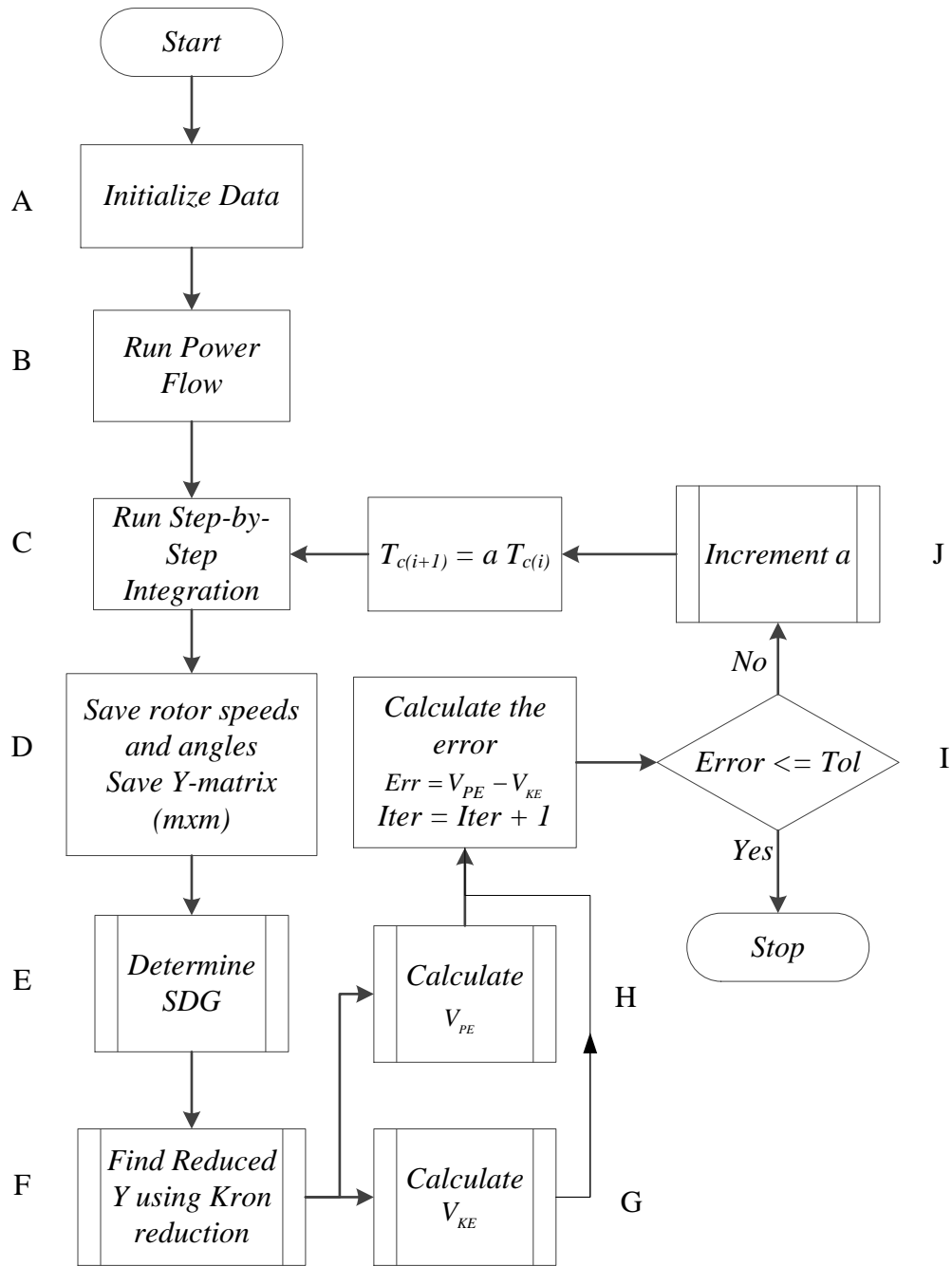


Figure 5.6: Phase IV – Critical Clearing Time Calculations

Step G: Calculate V_{KE} – In this step, the Kinetic Energies of the machines in the SDG are calculated and the summation of these energies is calculated as explained in Step A in 5.3.3.

Step H: Calculate V_{PE} – In this step, the potential energies of all machines are calculated and sorted in ascending order. Depending on the number of machines in the SDG, say x machines, the smallest x potential energies are summed up as explained in Steps B – D in 5.3.3.

Step I: Calculate the error and compare it to tolerance – The error equation used in this algorithm is simply the difference between the kinetic and potential energies calculated in steps G and H. If the error is within the set tolerance, the exit; a CCT is found. Otherwise, go to next step.

Step J: Increment the fault clearing time t_{cl} – In this step, the clearing time is incremented by using a factor a then steps C – I are repeated until a convergent solution is found.

5.4 Summary

In this chapter, the problem statement and the issues that make transient stability assessment complicated to solve in operation are discussed. Then the objective of this research is talked about and what features needed in order to solve online transient stability problem. Finally, the proposed methodology is discussed in step-by-step manner.

In Chapter 6, the IEEE 39 Bus equivalent power system is introduced and all its parameters are presented. The IEEE 39 Bus system is used for testing and verifying the performance of the proposed method.

Chapter 6

6 Test System

6.1 IEEE 39-Bus Test System

The IEEE 39 Bus (New England) power system is an equivalent power system of subsystems of the New England area and Canada. It consists of 39 Buses of which 10 Buses are generator Buses, 12 transformers, 10 generators, 34 transmission lines, and 19 loads. The system is shown in Figure 6.1. This test system will be modeled to use for validating the proposed method.

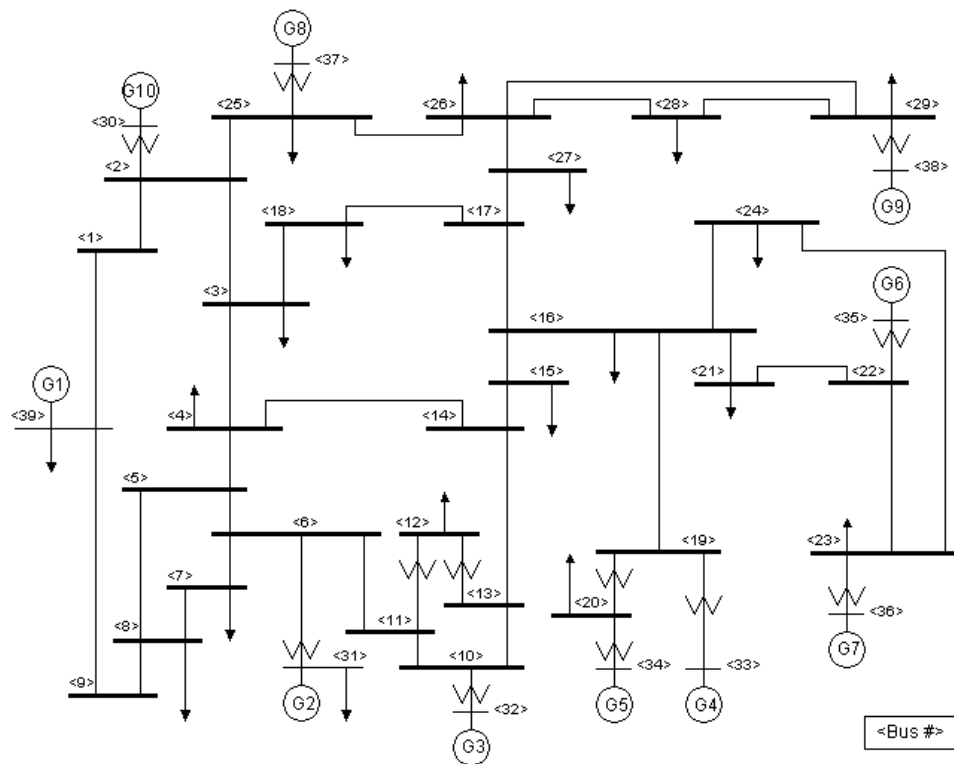


Figure 6.1: IEEE 39-Bus System

6.1.1 Transmission Lines

The IEEE 39 Bus system contains 34 transmission lines. Each transmission line has different length with different resistance, reactance, and suceptance per unit length depending on the material. However, since the length of transmission line does not affect the analysis in this thesis, only the per unit parameters are presented in Table 6.1.

Table 6.1: Transmission Line Data

Line	Resistance PU	Reactance PU	Suceptance PU	Line	Resistance PU	Reactance PU	Suceptance PU
1 to 2	0.0035	0.0411	0.6987	13 to 14	0.0009	0.0101	0.1723
1 to 39	0.001	0.025	0.75	14 to 15	0.0018	0.0217	0.366
2 to 3	0.0013	0.0151	0.2572	15 to 16	0.0009	0.0094	0.171
2 to 25	0.007	0.0086	0.146	16 to 17	0.0007	0.0089	0.1342
3 to 4	0.0013	0.0213	0.2214	16 to 19	0.0016	0.0195	0.304
3 to 18	0.0011	0.0133	0.2138	16 to 21	0.0008	0.0135	0.2548
4 to 5	0.0008	0.0128	0.1342	16 to 24	0.0003	0.0059	0.068
4 to 14	0.0008	0.0129	0.1382	17 to 18	0.0007	0.0082	0.1319
5 to 6	0.0002	0.0026	0.0434	17 to 27	0.0013	0.0173	0.3216
5 to 8	0.0008	0.0112	0.1476	21 to 22	0.0008	0.014	0.2565
6 to 7	0.0006	0.0092	0.113	22 to 23	0.0006	0.0096	0.1846
6 to 11	0.0007	0.0082	0.1389	23 to 24	0.0022	0.035	0.361
7 to 8	0.0004	0.0046	0.078	25 to 26	0.0032	0.0323	0.513
8 to 9	0.0023	0.0363	0.3804	26 to 27	0.0014	0.0147	0.2396
9 to 39	0.001	0.025	1.2	26 to 28	0.0043	0.0474	0.7802
10 to 11	0.0004	0.0043	0.0729	26 to 29	0.0057	0.0625	1.029
10 to 13	0.0004	0.0043	0.0729	28 to 29	0.0014	0.0151	0.249

The above data are in per unit system at base voltage of 345 kV and 100 MVA . The resistance, impedance and suceptance are given for the total length of transmission lines.

6.1.2 Transformers

The transformers data consists of R_T (Resistance) and X_T (Reactance) which are the equivalent of the primary and secondary windings of the transformer. Table 6.2 provides the transformers parameters.

Table 6.2: Transformers Data

Line Data				Transformer Tap	
From Bus	To Bus	R_T	X_T	Magnitude	Angle
12	11	0.0016	0.0435	1.006	0
12	13	0.0016	0.0435	1.006	0
6	31	0	0.025	1.07	0
10	32	0	0.02	1.07	0
19	33	0.0007	0.0142	1.07	0
20	34	0.0009	0.018	1.009	0
22	35	0	0.0143	1.025	0
23	36	0.0005	0.0272	1	0
25	37	0.0006	0.0232	1.025	0
2	30	0	0.0181	1.025	0
29	38	0.0008	0.0156	1.025	0
19	20	0.0007	0.0138	1.06	0

All the above data are in per unit based on 20 kV for the primary windings and 345 kV for the secondary.

6.1.3 Generators

There are 10 generators in the system. The 10 generators are connected to Bus 30 through Bus 39. Bus 31 is considered a slack Bus, while the remaining 9 are called PV Buses. The 29 remaining Buses are all called PQ Buses.

Table 6.3 gives the initial load flow conditions of the 10 generators Buses. All the values are based on 100 MVA and the machines rated terminal voltages.

Table 6.3: Generators' Initial Load Flow

Bus	Generator	Rated Voltage kV	Voltage PU	Active Power PU
30	10	20	1.0475	2.5
31	2	20	0.982	Slack Generator
32	3	20	0.9831	6.5
33	4	20	0.9972	6.32
34	5	20	1.0123	5.08
35	6	20	1.0493	6.5
36	7	20	1.0635	5.6
37	8	20	1.0278	5.4
38	9	20	1.0265	8.3
39	1	345	1.03	10

Table 6.4 gives the generators' rated voltage, inertia, resistance, leakage reactance, transient and sub-transient reactance's, and time constants.

Table 6.4: Generators Details

GEN	R_a	X_l	X_d	X_q	X'_d	X'_q	X''_d	X''_q	T'_{d0}	T'_{q0}	T''_{d0}	T''_{q0}	H(s)
1	0	0.0030	0.2000	0.0190	0.0060	0.0080	0.0006	0.0006	7.0000	0.7000	0.0330	0.0563	500
2	0	0.0350	0.2950	0.2820	0.0697	0.1700	0.0369	0.0369	6.5600	1.5000	0.0660	0.0660	30.3
3	0	0.0304	0.2495	0.2370	0.0531	0.0876	0.0320	0.0320	5.7000	1.5000	0.0570	0.0570	35.8
4	0	0.0295	0.2620	0.2580	0.0436	0.1660	0.0310	0.0310	5.5900	1.5000	0.0570	0.0570	28.6
5	0	0.0540	0.6700	0.6200	0.1320	0.1660	0.0568	0.0568	5.4000	0.4400	0.0540	0.0540	26
6	0	0.0224	0.2540	0.2410	0.0500	0.0814	0.0236	0.0236	7.3000	0.4000	0.0730	0.0730	34.8
7	0	0.0322	0.2950	0.2920	0.0490	0.1860	0.0340	0.0340	5.6600	1.5000	0.0560	0.0560	26.4
8	0	0.0280	0.2900	0.2800	0.0570	0.0911	0.0300	0.0300	6.7000	0.4100	0.0670	0.0670	24.3
9	0	0.0298	0.2106	0.2050	0.0570	0.0587	0.0314	0.0314	4.7900	1.9600	0.0470	0.0470	34.5
10	0	0.0125	0.1000	0.0690	0.0310	0.0180	0.0132	0.0132	10.2000	0.3000	0.1000	0.1000	42

6.1.4 Loads

The loads of this system are represented by fixed impedance for the purpose of this thesis. The following table shows the data of the 19 loads of the system.

Table 6.5: Loads Data

Bus	Rated Voltage kV	Load MW	Load MVAR	Bus	Rated Voltage kV	Load MW	Load MVAR
3	345	322	2.4	23	345	247.5	84.6
4	345	500	184	24	345	308.6	-92.2
7	345	233.8	84	25	345	224	47.2
8	345	522	176	26	345	139	17
12	345	7.5	88	27	345	281	75.5
15	345	320	153	28	345	206	27.6
16	345	329	32.3	29	345	283.5	26.9
18	345	158	30	31	20	9.2	4.6
20	345	628	103	39	345	1104	250
21	345	274	115				

6.2 Summary

In this chapter, the IEEE 39 Bus power system is introduced and all its parameters are provided. As previously stated, the system consists of 39 Buses, 12 transformers, 10 generators, 34 transmission lines, and 19 loads. The transmission lines parameters are given in the standard per unit as well as the transformers and generators. For the purpose of this thesis, the loads are represented by fixed impedances. This system will be used to test and simulate previous methods and the proposed method of transient stability.

In Chapter 7, PSAT for Matlab is used to model the IEEE 39 Bus system which then is used to simulate the proposed methodology, step-by-step integration, and two other direct methods that are referenced earlier chapters of this dissertation.

Chapter 7

7 Simulation Results

In this chapter, various methods are used to compare the proposed method to traditional methods of step-by-step integration and direct methods.

7.1 Modeling and Simulation of IEEE 39 Bus System (Phase I)

In order to verify the effectiveness of the proposed methodology, the IEEE 39 bus equivalent test system was built in Matlab-based toolbox PSAT (Power System Analysis Toolbox). A detailed model is used to build the system according to the data tabulated in Chapter 6. After modeling the test system, load flow solution is solved for and the results are verified. A description of the Matlab model file and associated load flow solution are summarized in Appendix A.

In Phase I of the methodology, it is needed to collect the generators' rotor angles and rotor speeds. Both variables were obtained with respect to the Center-of-Inertia reference frame. Generally, a 3-phase to ground fault is applied to a Bus. A demonstration of the collected data is shown next.

A fault is applied on Bus 25 at 0.1 seconds and is cleared at 0.2 seconds mark (for a stable case). The rotor speed for all the generators is shown in Figure 7.1 and rotor angle for all the generators is shown in Figure 7.2.

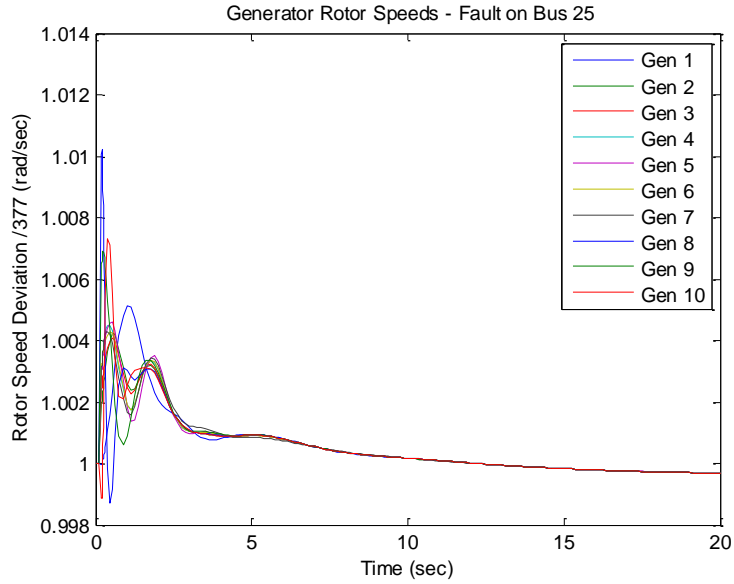


Figure 7.1: Generator rotor speeds for a fault on Bus 25

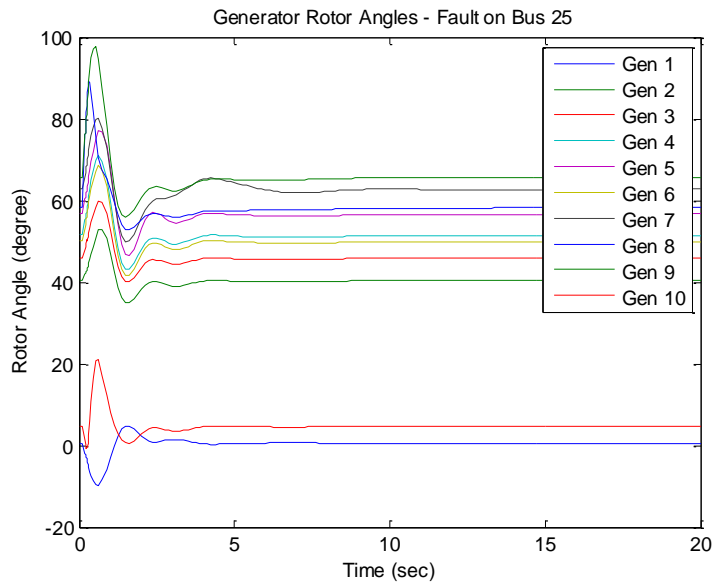


Figure 7.2: Generator rotor angles for a fault on Bus 25

The above two figures show a sample of step-by-step integration using Euler method. This is a transient stable case because the generators get disturbed but retain synchronism after the fault is cleared. Notice that this is not the sample collected using the proposed method because the step-by-step integration is used up to the clearing instant (0.2 seconds in this case).

Next, the same fault is applied but the data are collected up to the clearing time. Figure 7.3 and Figure 7.4 show the rotor speeds and angles for all the generators for the proposed methodology.

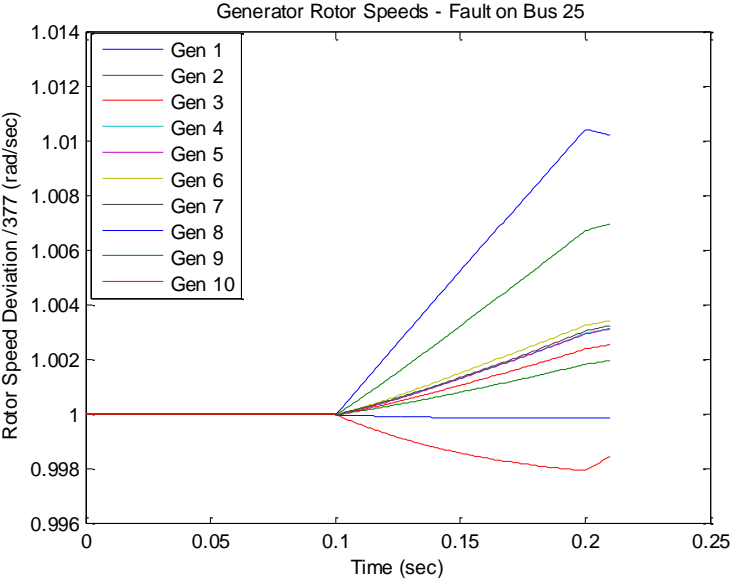


Figure 7.3: Generator rotor speeds for a fault on Bus 25 for Phase I

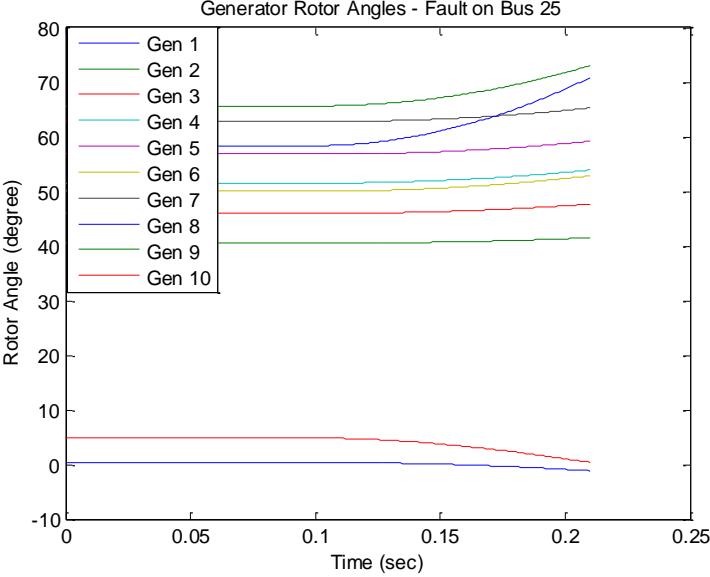


Figure 7.4: Generator rotor angles for a fault on Bus 25 for Phase I

From Figure 7.3 and Figure 7.4, it can be seen that the sample taken is not sufficient to determine transient stability by using traditional methods.

Another example, a fault on Bus 35 is applied at 0.1 sec and then it is cleared at 0.33 sec.

In this case, the system is transient unstable as shown in the figures below.

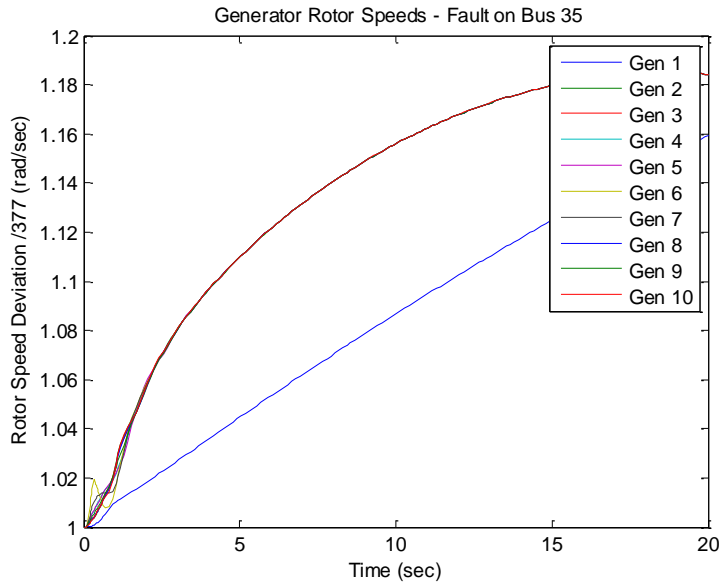


Figure 7.5: Generator rotor speeds for a fault on Bus 35

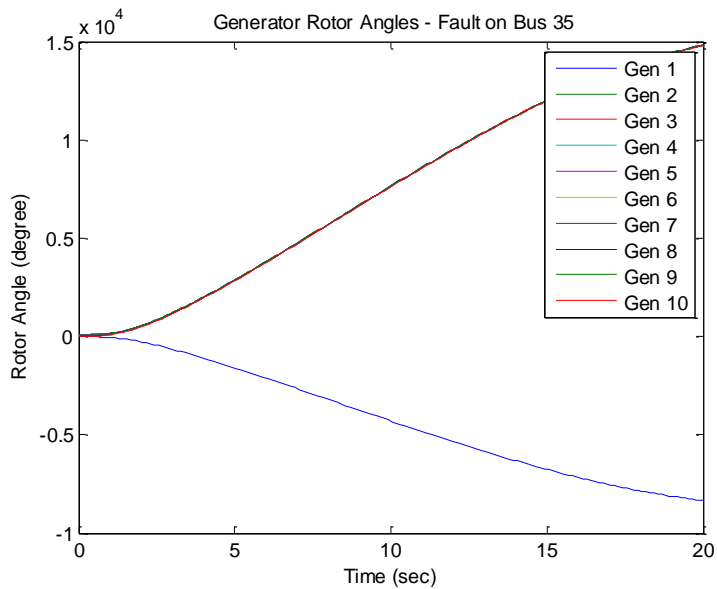


Figure 7.6: Generator rotor angles for a fault on Bus 35

Figure 7.5 and Figure 7.6 show the traditional step-by-step integration plots that are needed to determine transient stability. It can be seen from the figures that the generators loses

synchronism after the fault is cleared. Now, the same fault is applied and Phase I methodology is used. The following plots are obtained.

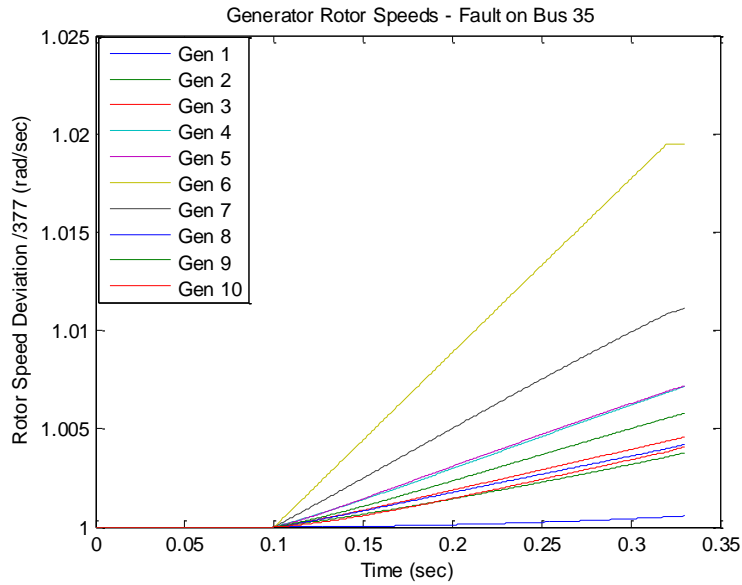


Figure 7.7: Generator rotor speeds for a fault on Bus 35 for Phase I

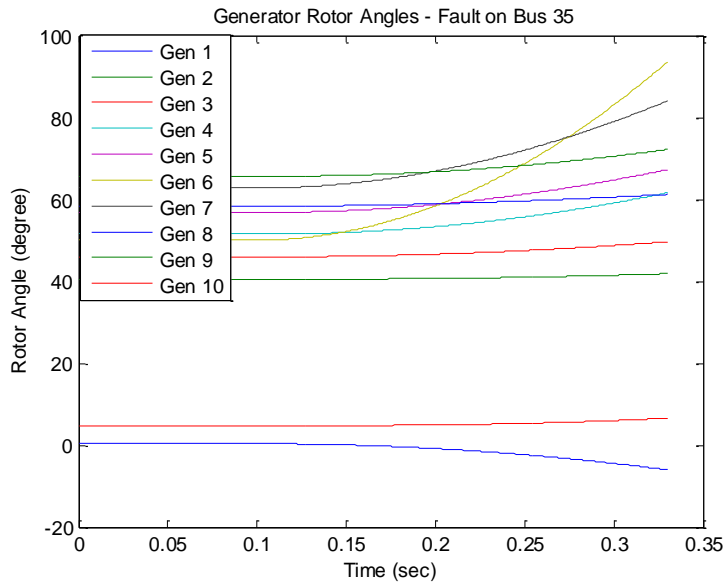


Figure 7.8: Generator rotor angles for a fault on Bus 35 for Phase I

It can be seen that it is not feasible to determine whether the system is transient stable or unstable if Figure 7.7 and Figure 7.8 are used. However, the proposed methodology only needs

the samples collected from the moment of the fault occurrence (0.1 sec in the two examples) up to a sample after the fault clearing time (0.201 sec in the first example and 0.331 sec in the second example.)

7.2 Identification of Critical Machine(s) (Phase II)

In this part of the report, the proposed methodology to identify critical machines and build the Severely Disturbed Group (SDG) is shown. Each step of Phase II is demonstrated in a separate subsection. For continuity, the two examples in 7.1 are used throughout this section.

7.2.1 Determination of the Severely Disturbed Unit (SDU) Using Accelerating Power

In this section, the results from Phase I are used to calculate the accelerating power by using (5.1). Using the first example by applying a fault on Bus 25 and clearing the fault after 0.1 sec (stable case), the accelerating power for each generator is calculated and tabulated in Table 7.1.

Table 7.1: Accelerating Power for fault on Bus 25 cleared in 0.10 sec

		Accelerating Power $\times 10^{-3} (rad / sec^3)$								
Gen #	G1	G2	G3	G4	G5	G6	G7	G8	G9	G10
P_{ai}	1.31	4.28	5.66	6.54	5.29	7.13	6.18	13.28	13.89	-0.92

From Table 7.1, it can be seen that Generator 9 is the SDU. This does not indicate that Generator 9 is the only disturbed machine as in [20]. In fact, Generator 8 appears to be swinging in a similar fashion as Generator 9. However, in the proposed methodology, only one unit is used in this step that is sent to the next step to determine any other generator that may swing similar to the SDU. It can also be noted that Generator 10 is decelerating. The causes of this deceleration are the dynamic of this generator with respect to the rest of the system and the electric closeness of this generator to the fault location. Therefore, from this step, only Generator 9 is added to the SDG set that is built using Phase 2 of the proposed methodology.

Now, a fault is applied on Bus 25 but it is cleared after 0.23 sec (unstable case). Table 7.2 summarizes the resulting Accelerating Power of each generator in the test system.

Table 7.2: Accelerating Power for fault on Bus 25 cleared in 0.23 sec

		Accelerating Power $\times 10^{-3} (rad / sec^3)$									
Gen #	G1	G2	G3	G4	G5	G6	G7	G8	G9	G10	
P_{ai}	3.86	4.44	5.81	6.53	5.44	7.33	6.12	13.27	13.85	-0.01	

It can be noted from Table 7.2 that Generator 9 is the SDU. Also, the same observation can be seen that generator 8 appears to be close to generator 9 dynamically. In addition, if the two tables are compared, one can see the evolution of the accelerating power that it is increasing as the clearing time increases.

Next is to use the second example by applying a fault on Bus 35 and clearing the fault after 0.1 sec (stable case), the accelerating power for each generator is calculated and summarized in Table 7.3.

Table 7.3: Accelerating Power for fault on Bus 35 cleared in 0.1 sec

		Accelerating Power $\times 10^{-3} (rad / sec^3)$									
Gen #	G1	G2	G3	G4	G5	G6	G7	G8	G9	G10	
P_{ai}	6.15	3.20	4.24	5.70	4.91	16.32	7.58	3.19	5.84	3.81	

From Table 7.3, Generator 6 is the SDU while Generator 7 is the second ranked generator in the Accelerating power. Now, by using the second example, and applying a fault on Bus 35 and clearing the fault after 0.23 sec (unstable case), the accelerating power for each generator is calculated and tabulated in Table 7.4.

Table 7.4: Accelerating Power for fault on Bus 35 cleared in 0.23 sec

		Accelerating Power $\times 10^{-3} (rad / sec^3)$									
Gen #	G1	G2	G3	G4	G5	G6	G7	G8	G9	G10	
P_{ai}	8.45	3.29	4.30	5.55	4.91	16.35	7.42	3.09	5.72	4.08	

From Table 7.4, it can be seen that Generator 6 is the SDU. From the numbers in the table, it appears that generator 6 separate itself from the rest of the system. Unlike the first example in which Generator 10 decelerate, all the generators accelerate which is expected as this case is transient unstable case. In addition, the accelerating power evolution can be observed which shows that as the clearing time increases, the accelerating power increases which indicates that the accelerated generator is moving closer to instability with a higher rate.

7.2.2 Finding Coherent Generators with the SDU

In this section, the proposed methodology in Phase II to identify coherent generator (Step C) is demonstrated. In order to perform this step, the quality factor q needs to be set before applying the algorithm. As per the recommendations in [48], multiple experiments were performed and the angular speed for all the generators are observed. Based on the experiments performed on the IEEE 39 Bus Test System and the size of it, a quality factor of 0.9 is found to be the most applicable and reliable to this test system. Notice that the authors of [48] recommended a quality factor between 0.85 and 0.95.

The first example in 7.2.1 is used, which is applying a fault on Bus 25 and clearing it after 0.1 sec. According to the results from Table 7.1, Generator 9 is the SDU. Now, applying the algorithm described in Step C of Phase II, there is no coherent generator with Generator 9. This step confirms that there is only one generator that is trying to separate itself from the rest of the system, given that this case is a stable case.

The second example is applying a fault on Bus 25 and clearing it after 0.23 sec (unstable case). Based on the result from Table 7.2, Generator 9 is the SDU. By applying the algorithm to find coherent generators with Generator 9, there is no other generator that is coherent with Generator 9.

The third example is applying a fault on Bus 35 and clearing it after 0.1 sec (stable case). Based on the result from Table 7.3, Generator 6 is the SDU. When the algorithm of finding coherent generators is used, the algorithm finds no other generator coherent with Generator 6. Likewise, when the fourth example is used, that is by applying a fault on Bus 35 and clearing it after 0.23 sec, there is no coherent generator with Generator 6 (the SDU.)

An additional example that shows a coherent generator with the SDU from the previous step is applying a fault on Bus 9 and clearing it after 0.25 sec (stable case). Once the fault is applied, generator 2 is found to be the SDU. By applying the coherency algorithm with a quality factor of 0.9, generator 9 is found to be coherent with the SDU (generator 2) as shown in Figure 7.9.

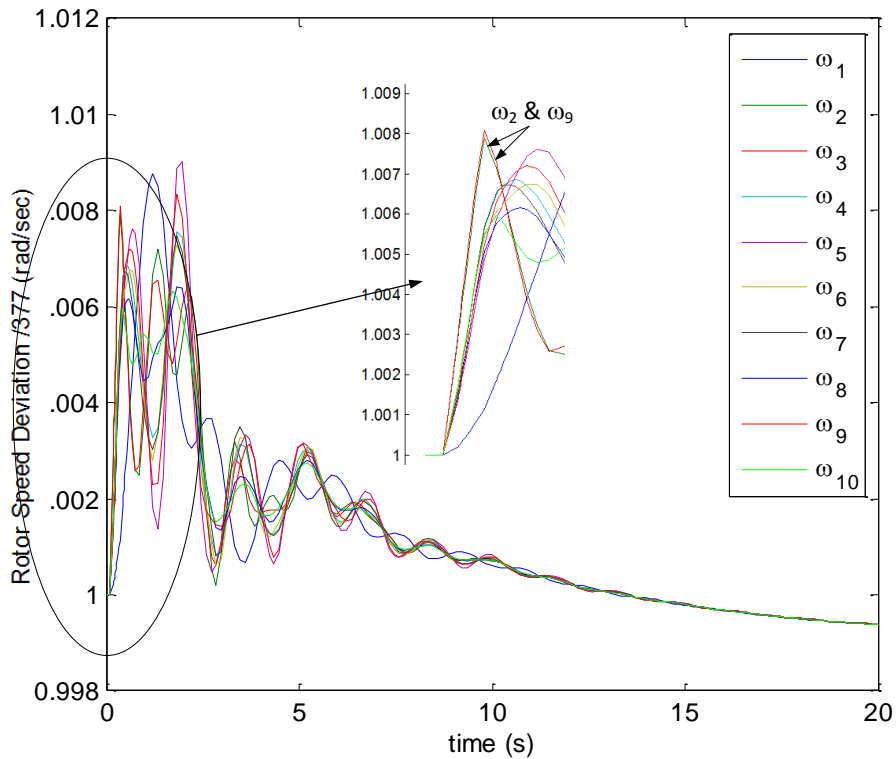


Figure 7.9: Generator rotor speeds for a fault on Bus 9

From the above results, the coherency measure is consistent for similar faults, i.e. faults on the same bus, with different clearing times. It was proven in [48] that the coherency algorithm used in the proposed methodology can identify coherent groups within a power system.

7.2.3 Finding SDU Using During-Fault Rotor Angles

In this section, Step D of Phase II of the proposed methodology is demonstrated. In order to demonstrate this method, tables and histogram plots are used.

The first example in 7.2.1 is used, which is applying a fault on Bus 25 and clearing it after 0.1 sec (stable case). Now, if the algorithm discussed in Step D of Phase II is used by applying (5.8), the following table is captured from the simulation.

Table 7.5: During-Fault Rotor Angles Distance Measure (Bus 25 $t_c = 0.10$ sec)

Index	1	2	3	4	5	6	7	8	9	10
Units i,j	1,2	1,3	1,4	1,5	1,6	1,7	1,8	1,9	1,10	2,3
ϵ_{ij}^θ	0.073	0.082	0.093	0.102	0.090	0.113	0.109	0.120	0.008	0.010
Index	11	12	13	14	15	16	17	18	19	20
Units i,j	2,4	2,5	2,6	2,7	2,8	2,9	2,10	3,4	3,5	3,6
ϵ_{ij}^θ	0.021	0.030	0.018	0.040	0.037	0.048	0.065	0.011	0.020	0.008
Index	21	22	23	24	25	26	27	28	29	30
Units i,j	3,7	3,8	3,9	3,10	4,5	4,6	4,7	4,8	4,9	4,10
ϵ_{ij}^θ	0.031	0.027	0.038	0.075	0.009	0.003	0.020	0.017	0.027	0.086
Index	31	32	33	34	35	36	37	38	39	40
Units i,j	5,6	5,7	5,8	5,9	5,10	6,7	6,8	6,9	6,10	7,8
ϵ_{ij}^θ	0.012	0.011	0.008	0.018	0.095	0.023	0.019	0.030	0.083	0.005
Index	41	42	43	44	45					
Units i,j	7,9	7,10	8,9	8,10	9,10					
ϵ_{ij}^θ	0.007	0.105	0.011	0.102	0.113					

To explain the results in Table 7.5, it can be seen that the value indexed by 8 is the largest. To show that in a better form, the histogram in Figure 7.10 is obtained.

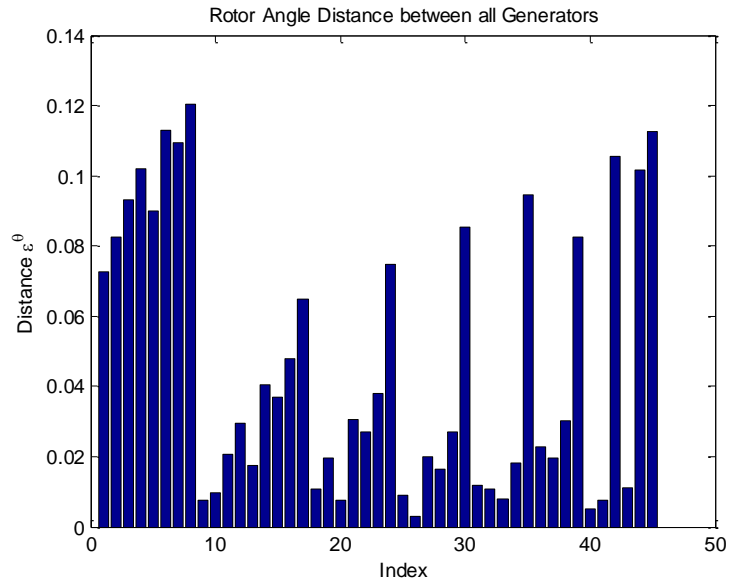


Figure 7.10: Rotor angle distance for fault on Bus 25 cleared in 0.1 sec

This means that either unit 1 or 9 are severely disturbed because one of their rotors has moved the most from the pre-fault state. To identify the generator that in fact belongs to the SDG, the generator with the largest angle is used. In this case, generator 9 is the SDU which is already found (in this example) in Steps A and B of Phase II.

Next, the same fault is applied with a clearing time of 0.23 sec (unstable case). The following table and plot are obtained.

Table 7.6: During-Fault Rotor Angles Distance Measure (Bus 25 $t_c = 0.23$ sec)

Index	1	2	3	4	5	6	7	8	9	10
Units i,j	1,2	1,3	1,4	1,5	1,6	1,7	1,8	1,9	1,10	2,3
ϵ_{ij}^θ	0.053	0.060	0.069	0.074	0.067	0.082	0.093	0.094	0.004	0.007
Index	11	12	13	14	15	16	17	18	19	20
Units i,j	2,4	2,5	2,6	2,7	2,8	2,9	2,10	3,4	3,5	3,6
ϵ_{ij}^θ	0.017	0.022	0.014	0.030	0.041	0.041	0.048	0.010	0.015	0.007
Index	21	22	23	24	25	26	27	28	29	30
Units i,j	3,7	3,8	3,9	3,10	4,5	4,6	4,7	4,8	4,9	4,10
ϵ_{ij}^θ	0.023	0.034	0.034	0.056	0.005	0.003	0.013	0.025	0.025	0.065
Index	31	32	33	34	35	36	37	38	39	40
Units i,j	5,6	5,7	5,8	5,9	5,10	6,7	6,8	6,9	6,10	7,8
ϵ_{ij}^θ	0.008	0.008	0.021	0.020	0.070	0.016	0.027	0.027	0.062	0.015
Index	41	42	43	44	45					
Units i,j	7,9	7,10	8,9	8,10	9,10					
ϵ_{ij}^θ	0.012	0.078	0.006	0.089	0.090					

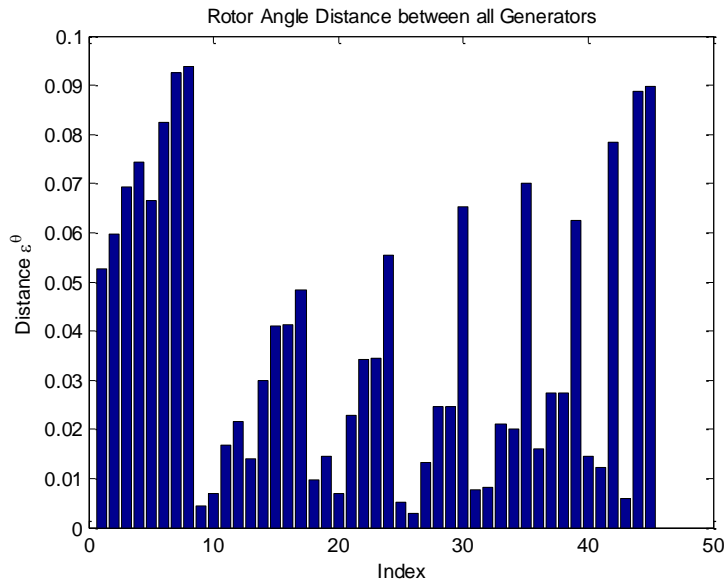


Figure 7.11: Rotor angle distance for fault on Bus 25 cleared in 0.23 sec

From Table 7.6 and Figure 7.11, the set of machines under index 8 is the one of interest.

Based on the table, either generator 1 or 9 is the SDU. If the change in angle is used, generator 9 is the SDU which confirms what is found in Steps A and B of Phase II.

Now, the third example is used by applying a fault on Bus 35 and clearing the fault in 0.1 sec (stable case). Upon applying (5.8), the following table and plot are obtained.

Table 7.7: During-Fault Rotor Angles Distance Measure (Bus 35 $t_c = 0.10$ sec)

Index	1	2	3	4	5	6	7	8	9	10
Units i,j	1,2	1,3	1,4	1,5	1,6	1,7	1,8	1,9	1,10	2,3
ϵ_{ij}^θ	0.072	0.082	0.093	0.102	0.093	0.114	0.104	0.117	0.009	0.010
Index	11	12	13	14	15	16	17	18	19	20
Units i,j	2,4	2,5	2,6	2,7	2,8	2,9	2,10	3,4	3,5	3,6
ϵ_{ij}^θ	0.021	0.030	0.022	0.042	0.032	0.045	0.063	0.011	0.020	0.012
Index	21	22	23	24	25	26	27	28	29	30
Units i,j	3,7	3,8	3,9	3,10	4,5	4,6	4,7	4,8	4,9	4,10
ϵ_{ij}^θ	0.032	0.022	0.035	0.073	0.009	0.003	0.021	0.011	0.025	0.084
Index	31	32	33	34	35	36	37	38	39	40
Units i,j	5,6	5,7	5,8	5,9	5,10	6,7	6,8	6,9	6,10	7,8
ϵ_{ij}^θ	0.009	0.012	0.002	0.015	0.093	0.020	0.011	0.024	0.085	0.010
Index	41	42	43	44	45					
Units i,j	7,9	7,10	8,9	8,10	9,10					
ϵ_{ij}^θ	0.004	0.105	0.013	0.095	0.108					

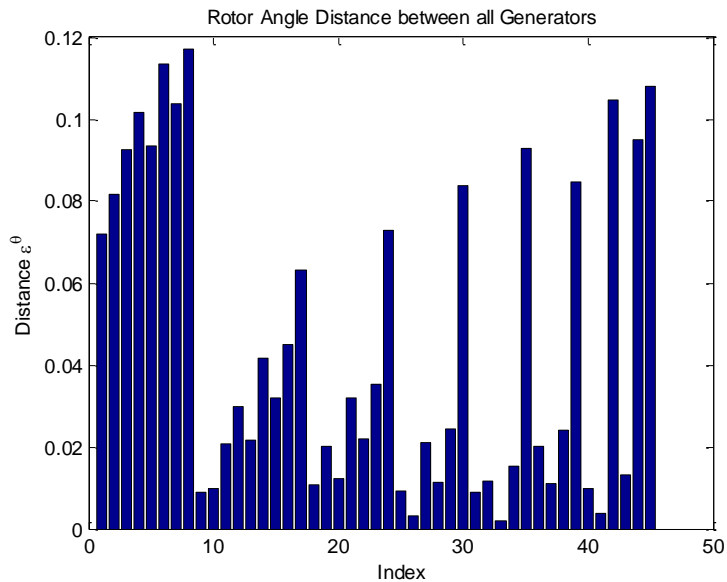


Figure 7.12: Rotor angle distance for fault on Bus 35 cleared in 0.10 sec

Based on the results from Table 7.7 and Figure 7.12, either generator 1 or 9 contributes to system separation. When the angles comparison is made, then generator 9 is the SDU. This is another machine that is not found in steps A – C of Phase II.

Next, the same fault is applied but with a clearing time of 0.23 sec (unstable case). The following table and plot are obtained.

Table 7.8: During-Fault Rotor Angles Distance Measure (Bus 35 $t_c = 0.23$ sec)

Index	1	2	3	4	5	6	7	8	9	10
Units i,j	1,2	1,3	1,4	1,5	1,6	1,7	1,8	1,9	1,10	2,3
ε_{ij}^θ	0.0505	0.0574	0.0674	0.0731	0.0789	0.0845	0.0722	0.0823	0.0091	0.0069
Index	11	12	13	14	15	16	17	18	19	20
Units i,j	2,4	2,5	2,6	2,7	2,8	2,9	2,10	3,4	3,5	3,6
ε_{ij}^θ	0.017	0.0226	0.03	0.0341	0.0217	0.0318	0.0418	0.0103	0.0158	0.0238
Index	21	22	23	24	25	26	27	28	29	30
Units i,j	3,7	3,8	3,9	3,10	4,5	4,6	4,7	4,8	4,9	4,10
ε_{ij}^θ	0.0273	0.0148	0.0249	0.0487	0.0057	0.0144	0.0171	0.0057	0.0151	0.0587
Index	31	32	33	34	35	36	37	38	39	40
Units i,j	5,6	5,7	5,8	5,9	5,10	6,7	6,8	6,9	6,10	7,8
ε_{ij}^θ	0.0115	0.0116	0.0024	0.0094	0.0643	0.0099	0.0139	0.0127	0.0699	0.0132
Index	41	42	43	44	45					
Units i,j	7,9	7,10	8,9	8,10	9,10					
ε_{ij}^θ	0.0048	0.0756	0.0101	0.0636	0.0736					

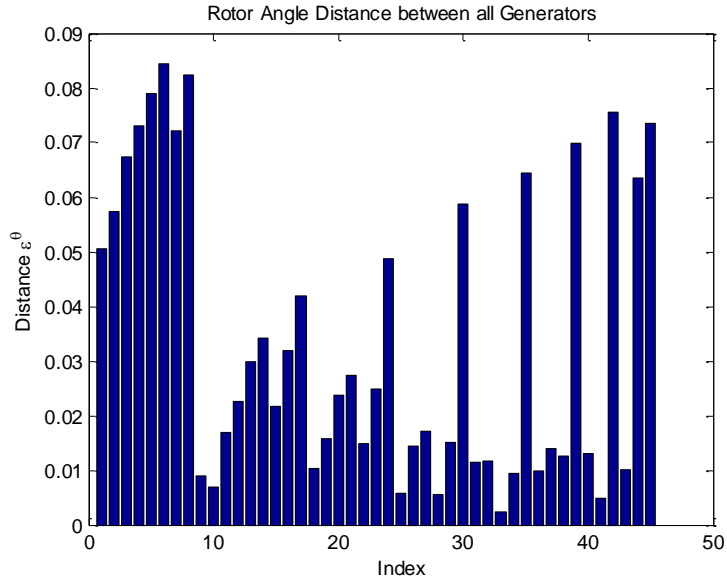


Figure 7.13: Rotor angle distance for fault on Bus 35 cleared in 0.23 sec

Based on Table 7.8 and Figure 7.13, the generators Indexed 6 are the possible units that contribute to system separation and transient instability. In this case, generator 7 is found to be the unit of interest because its rotor angle has changed more than generator 1.

From the results of the examples introduced in this section, it can be seen that (5.8) is a good measure to find machines that may be critical and may contribute to system’s separation. Notice that generator 1 is a common generator in the examples mentioned in this section. Generator 1 is the largest machine in the system and it is the last machine to reach instability due to its size and power.

7.2.4 Finding SDU Using During-Fault Rotor Speed

In this section, Step E of Phase II of the proposed methodology is demonstrated. In order to demonstrate this method, tables and histogram plots are used.

The first example in 7.2.1 is used, which is applying a fault on Bus 25 and clearing it after 0.1 sec (stable case). Now, if the algorithm discussed in Step E of Phase II is used by applying (5.9), the following table and plot are captured from the simulation.

Table 7.9: During-Fault Rotor Speeds Distance Measure (Bus 25 $t_c = 0.10$ sec)

Index	1	2	3	4	5	6	7	8	9	10
Units i,j	1,2	1,3	1,4	1,5	1,6	1,7	1,8	1,9	1,10	2,3
ϵ_{ij}^{ω}	1.6E-04	1.8E-04	2.6E-04	2.3E-04	2.3E-04	2.6E-04	6.1E-04	4.5E-04	3.0E-05	1.9E-05
Index	11	12	13	14	15	16	17	18	19	20
Units i,j	2,4	2,5	2,6	2,7	2,8	2,9	2,10	3,4	3,5	3,6
ϵ_{ij}^{ω}	1.0E-04	7.0E-05	7.2E-05	1.1E-04	4.6E-04	3.0E-04	1.9E-04	8.1E-05	5.1E-05	5.3E-05
Index	21	22	23	24	25	26	27	28	29	30
Units i,j	3,7	3,8	3,9	3,10	4,5	4,6	4,7	4,8	4,9	4,10
ϵ_{ij}^{ω}	8.7E-05	4.4E-04	2.8E-04	2.1E-04	2.9E-05	2.8E-05	6.5E-06	3.6E-04	2.0E-04	2.9E-04
Index	31	32	33	34	35	36	37	38	39	40
Units i,j	5,6	5,7	5,8	5,9	5,10	6,7	6,8	6,9	6,10	7,8
ϵ_{ij}^{ω}	1.4E-06	3.6E-05	3.9E-04	2.3E-04	2.6E-04	3.4E-05	3.9E-04	2.2E-04	2.6E-04	3.5E-04
Index	41	42	43	44	45					
Units i,j	7,9	7,10	8,9	8,10	9,10					
ϵ_{ij}^{ω}	1.9E-04	2.9E-04	1.6E-04	6.4E-04	4.8E-04					

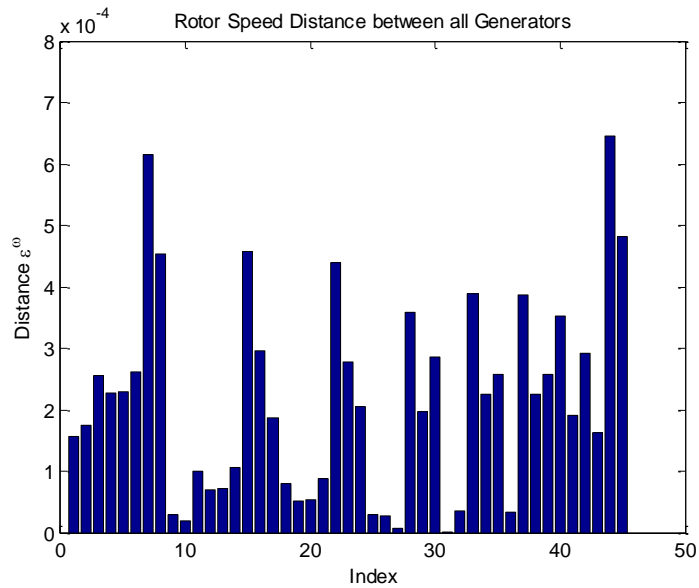


Figure 7.14: Rotor speed distance for fault on Bus 25 cleared in 0.1 sec

According to the results in Table 7.9 and Figure 7.14, it can be seen that the value indexed by 44 is the largest. This means that either unit 8 or 10 are severely disturbed because one of their rotors has speeded up the most from the pre-fault state causing it to move with a faster rate. To identify the generator that in fact belongs to the SDG, the generator with the

largest change in speed is used. In this case, generator 8 is the SDU which is not found (in this example) in Steps A and B of Phase II.

Next, the same fault is applied with a clearing time of 0.23 sec (unstable case). The following table and plot are obtained.

Table 7.10: During-Fault Rotor Speeds Distance Measure (Bus 25 $t_c = 0.23$ sec)

Index	1	2	3	4	5	6	7	8	9	10
Units i,j	1,2	1,3	1,4	1,5	1,6	1,7	1,8	1,9	1,10	2,3
ϵ_{ij}^{ω}	2.3E-04	2.6E-04	3.7E-04	3.4E-04	3.4E-04	3.8E-04	9.1E-04	6.7E-04	2.7E-05	2.7E-05
Index	11	12	13	14	15	16	17	18	19	20
Units i,j	2,4	2,5	2,6	2,7	2,8	2,9	2,10	3,4	3,5	3,6
ϵ_{ij}^{ω}	1.4E-04	1.0E-04	1.1E-04	1.5E-04	6.8E-04	4.3E-04	2.6E-04	1.1E-04	7.8E-05	8.0E-05
Index	21	22	23	24	25	26	27	28	29	30
Units i,j	3,7	3,8	3,9	3,10	4,5	4,6	4,7	4,8	4,9	4,10
ϵ_{ij}^{ω}	1.2E-04	6.5E-04	4.1E-04	2.9E-04	3.7E-05	3.4E-05	7.2E-06	5.3E-04	2.9E-04	4.0E-04
Index	31	32	33	34	35	36	37	38	39	40
Units i,j	5,6	5,7	5,8	5,9	5,10	6,7	6,8	6,9	6,10	7,8
ϵ_{ij}^{ω}	2.3E-06	4.4E-05	5.7E-04	3.3E-04	3.6E-04	4.1E-05	5.7E-04	3.3E-04	3.7E-04	5.3E-04
Index	41	42	43	44	45					
Units i,j	7,9	7,10	8,9	8,10	9,10					
ϵ_{ij}^{ω}	2.8E-04	4.1E-04	2.4E-04	9.3E-04	6.9E-04					

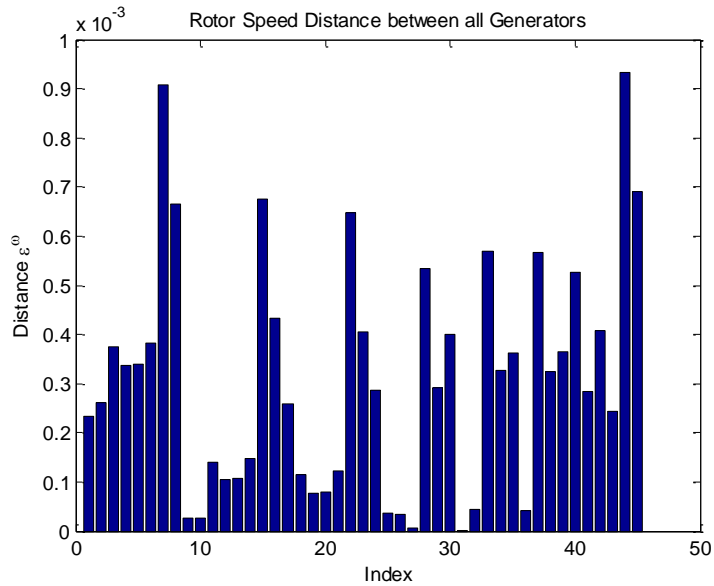


Figure 7.15: Rotor speed distance for fault on Bus 25 cleared in 0.23 sec

From Table 7.10 and Figure 7.15, the set of machines under index 44 is the one of interest. Based on the table, either generator 8 or 10 is the SDU. If the change in speed is used, generator 8 is the SDU which confirms the finding in the first example.

Now, the third example is used by applying a fault on Bus 35 and clearing the fault in 0.1 sec (stable case). Upon applying (5.9), the following table and plot are obtained.

Table 7.11: During-Fault Rotor Speed Distance Measure (Bus 35 $t_c = 0.10$ sec)

Index	1	2	3	4	5	6	7	8	9	10
Units i,j	1,2	1,3	1,4	1,5	1,6	1,7	1,8	1,9	1,10	2,3
ϵ_{ij}^{ω}	1.1E-04	1.2E-04	2.1E-04	2.0E-04	5.2E-04	3.1E-04	1.4E-04	1.8E-04	8.8E-05	1.5E-05
Index	11	12	13	14	15	16	17	18	19	20
Units i,j	2,4	2,5	2,6	2,7	2,8	2,9	2,10	3,4	3,5	3,6
ϵ_{ij}^{ω}	1.1E-04	9.5E-05	4.1E-04	2.1E-04	3.0E-05	7.3E-05	1.7E-05	9.2E-05	8.0E-05	4.0E-04
Index	21	22	23	24	25	26	27	28	29	30
Units i,j	3,7	3,8	3,9	3,10	4,5	4,6	4,7	4,8	4,9	4,10
ϵ_{ij}^{ω}	1.9E-04	1.6E-05	5.8E-05	3.2E-05	1.2E-05	3.0E-04	9.9E-05	7.7E-05	3.4E-05	1.2E-04
Index	31	32	33	34	35	36	37	38	39	40
Units i,j	5,6	5,7	5,8	5,9	5,10	6,7	6,8	6,9	6,10	7,8
ϵ_{ij}^{ω}	3.2E-04	1.1E-04	6.4E-05	2.1E-05	1.1E-04	2.0E-04	3.8E-04	3.4E-04	4.3E-04	1.8E-04
Index	41	42	43	44	45					
Units i,j	7,9	7,10	8,9	8,10	9,10					
ϵ_{ij}^{ω}	1.3E-04	2.2E-04	4.3E-05	4.8E-05	9.0E-05					

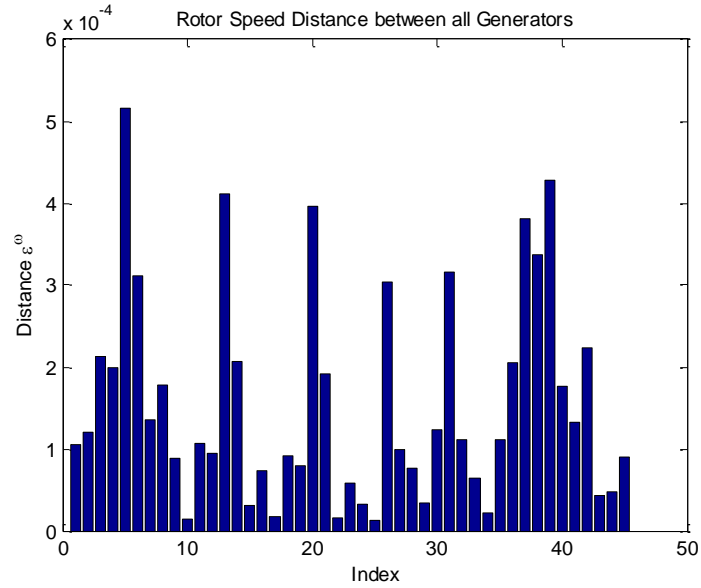


Figure 7.16: Rotor speed distance for fault on Bus 35 cleared in 0.10 sec

Based on the results from Table 7.11 and Figure 7.16, either generator 1 or 6 contributes to system separation. When the rotor speed comparison is used, then generator 6 is the SDU. This machine is already found in steps A – C of Phase II.

Next, the same fault is applied but with a clearing time of 0.23 sec (unstable case). The following table and plot are obtained.

Table 7.12: During-Fault Rotor Speeds Distance Measure (Bus 35 $t_c = 0.23$ sec)

Index	1	2	3	4	5	6	7	8	9	10
Units i,j	1,2	1,3	1,4	1,5	1,6	1,7	1,8	1,9	1,10	2,3
ϵ_{ij}^{ω}	1.6E-04	1.8E-04	3.0E-04	2.9E-04	7.6E-04	4.5E-04	1.9E-04	2.6E-04	1.3E-04	2.0E-05
Index	11	12	13	14	15	16	17	18	19	20
Units i,j	2,4	2,5	2,6	2,7	2,8	2,9	2,10	3,4	3,5	3,6
ϵ_{ij}^{ω}	1.5E-04	1.4E-04	6.1E-04	3.0E-04	3.7E-05	1.0E-04	2.2E-05	1.3E-04	1.2E-04	5.9E-04
Index	21	22	23	24	25	26	27	28	29	30
Units i,j	3,7	3,8	3,9	3,10	4,5	4,6	4,7	4,8	4,9	4,10
ϵ_{ij}^{ω}	2.8E-04	1.6E-05	8.0E-05	4.2E-05	1.3E-05	4.6E-04	1.5E-04	1.1E-04	4.9E-05	1.7E-04
Index	31	32	33	34	35	36	37	38	39	40
Units i,j	5,6	5,7	5,8	5,9	5,10	6,7	6,8	6,9	6,10	7,8
ϵ_{ij}^{ω}	4.7E-04	1.6E-04	1.0E-04	3.6E-05	1.6E-04	3.1E-04	5.7E-04	5.1E-04	6.3E-04	2.6E-04
Index	41	42	43	44	45					
Units i,j	7,9	7,10	8,9	8,10	9,10					
ϵ_{ij}^{ω}	2.0E-04	3.2E-04	6.4E-05	5.8E-05	1.2E-04					

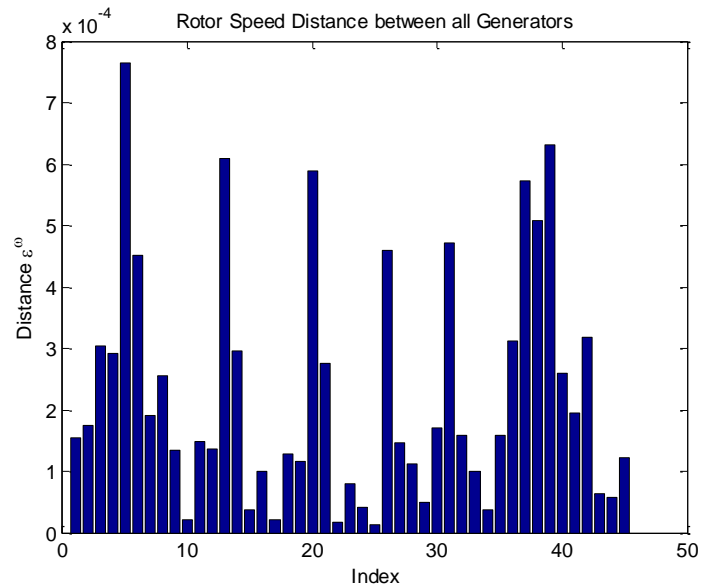


Figure 7.17: Rotor speed distance for fault on Bus 35 cleared in 0.23 sec

Based on Table 7.12 and Figure 7.17, the generators Indexed 6 are the possible units that contribute to system separation and transient instability. In this case, generator 6 is found to be the unit of interest because its rotor speed has changed more than generator 1.

From the results of the examples introduced in this section, it can be seen that step E of Phase II can be used to identify critical machines that can contribute to system's separation.

7.2.5 Finding SDU Using Change in Rotor Angle

In this section, the pre-fault and post-fault angles are used to determine another (or the same) SDU. This can be done by using the algorithm in Step F in Phase II of the proposed methodology. Once again, to show how this algorithm determines the SDU, the examples used in the previous sections are used.

First, a fault on Bus 25 is applied and it is cleared in 0.1 sec (stable case). The rotor angles for all the generators with respect to COI are captured and tabulated in Table 7.13.

Table 7.13: Rotor Angle Change Measure (Bus 25 $t_c = 0.10$ sec)

Gen #	G1	G2	G3	G4	G5	G6	G7	G8	G9	G10
$\theta_i^{pre} (deg)$	0.361	40.505	45.976	51.516	56.822	50.027	62.774	58.367	65.641	4.840
$\theta_i^{cl} (deg)$	-1.280	41.800	47.627	54.685	59.440	52.671	66.069	68.273	72.503	2.626
$\Delta\theta_i (deg)$	1.641	1.295	1.652	3.170	2.619	2.644	3.295	9.906	6.863	2.214

From the above table, unit 8 appears to be moved the most which confirms the findings in step A of Phase II. In step A, Generator 9 is found to be the SDU; however, generator 8 has similar nature with a very high accelerating power. Therefore, Generator 8 can be added to the SDG.

Next, the same fault is applied on bus 25 but the clearing time is changed to 0.23 sec (unstable case). To examine the results by using this criterion, the following table is obtained.

Table 7.14: Rotor Angle Change Measure (Bus 25 $t_c = 0.23$ sec)

Gen #	G1	G2	G3	G4	G5	G6	G7	G8	G9	G10
$\theta_i^{pre} (deg)$	0.361	40.505	45.976	51.516	56.822	50.027	62.774	58.367	65.641	4.840
$\theta_i^{cl} (deg)$	-8.147	47.248	54.507	67.594	70.424	63.779	79.350	109.363	100.778	-5.561
$\Delta\theta_i (deg)$	8.508	6.743	8.531	16.079	13.602	13.752	16.576	50.996	35.137	10.401

Table 7.14 confirms that Unit 8 is also critical because it is nearing the instability boundary at the clearing instant. It also verifies the finding in Steps A of this phase, that is, Generator 9 is the SDU with Generator 8 nearing that. Therefore, based on these results, we can safely add generator 8 to the SDG set.

We next examine the other fault applied on Bus 35 and cleared in 0.1 sec (stable case). The following table is obtained.

Table 7.15: Rotor Angle Change Measure (Bus 35 $t_c = 0.10$ sec)

Gen #	G1	G2	G3	G4	G5	G6	G7	G8	G9	G10
θ_i^{pre} (deg)	0.361	40.505	45.976	51.516	56.822	50.027	62.774	58.367	65.641	4.840
θ_i^{cl} (deg)	-1.033	41.088	46.838	54.114	59.184	58.324	67.232	59.526	67.602	5.099
$\Delta\theta_i$ (deg)	1.395	0.583	0.863	2.598	2.362	8.297	4.458	1.159	1.962	0.259

According to the results in Table 7.15, Generator 6 is the SDU. This generator has already been found in steps A – C of Phase II which confirms that this is a good measure to determine the critical machines.

Finally, the same fault on Bus 35 is applied, but with a clearing time of 0.23 sec (unstable case). After running this criterion, the following results are captured and tabulated in Table 7.16.

Table 7.16: Rotor Angle Change Measure (Bus 35 $t_c = 0.23$ sec)

Gen #	G1	G2	G3	G4	G5	G6	G7	G8	G9	G10
θ_i^{pre} (deg)	0.361	40.505	45.976	51.516	56.822	50.027	62.774	58.367	65.641	4.840
θ_i^{cl} (deg)	-6.762	43.559	50.387	64.473	68.890	92.922	85.352	63.917	75.387	6.428
$\Delta\theta_i$ (deg)	7.123	3.054	4.411	12.957	12.068	42.895	22.578	5.550	9.747	1.588

From the above table, Generator 6 is found to be the SDU. This result is consistent with the findings of the previous steps.

Based on the four examples discussed in this section, it can be noticed that rotor angles differences can be used to determine some critical machines in the event of a sever disturbance on the system. Also, this step can be used as a confirmation step as the other measures in Phase

II may have already found all the critical machines. However, in a larger power system (more than 39 Buses and 10 machines systems), this step is important as there may be more than two groups in the system.

7.3 Online Transient Stability Assessment (Phase III)

After determining the critical machines represented by the SDG set, the data can be passed to Phase III of the proposed methodology. In this section, Phase III is tested for various faults on the system and the results are compared with the benchmark method (step-by-step integration). Also, the performance of the proposed methodology is discussed to show its suitability for online transient stability assessment.

Before testing this phase, a confirmation step is implemented to show the number of generators with the smallest potential energies that need to be included to be compared with the SDG kinetic energy. As per the discussion in section 5.3.3, the *SDG* is a set that contains the critical machines (say q generators) while the \overline{SDG} contains the generators with the smallest potential energy, i.e. the q generators with the smallest potential energy. To investigate this aspect, the following results table is obtained.

Table 7.17: Potential Energy per Group of Machines Investigation Result

Bus Fault	Disc. Line	Clearing Time (sec)	SDG	KE	Potential Energy per Group of Machines									
					1 Machine		2 Machines		3 Machines		4 Machines		5 Machines	
					\overline{SDG}	PE	\overline{SDG}	PE	\overline{SDG}	PE	\overline{SDG}	PE	\overline{SDG}	PE
3	3-4	0.21	1,3,9	4.92	9	0.29	9,3	2.12	9,3,1	4.92	9,3,1,10	11.27	9,3,1,10,7	19.58
		0.23		5.89	9	0.28	9,3	2.02	9,3,1	4.65	9,3,1,10	10.79	9,3,1,10,7	18.75
6	6-11	0.23	1,2,3,9	8.51	9	0.34	9,2	2.78	9,2,3	5.47	9,2,3,1	8.52	9,2,3,1,7	19.17
		0.24		8.68	9	0.23	9,2	2.60	9,2,3	5.10	9,2,3,1	8.05	9,2,3,1,7	18.23
9	9-39	0.29	2,9	2.16	2	0.38	2,9	2.17	2,9,3	4.24	2,9,3,1	13.32	2,9,3,1,7	26.53
		0.3		2.29	2	0.32	2,9	2.02	2,9,3	4.01	2,9,3,1	12.90	2,9,3,1,7	26.01
12	11-12	0.13	3	0.68	10	0.68	10,3	1.40	10,3,3	2.47	10,3,3,1	5.92	10,3,3,1,7	19.02
		0.25		2.38	3	0.16	3,10	0.86	3,10,3	1.58	3,10,3,1	4.65	3,10,3,1,7	16.90
17	17-27	0.11	4,7,9	2.84	9	0.17	9,7	1.20	9,7,4	2.85	9,7,4,10	10.06	9,7,4,10,8	19.48
		0.15		5.25	9	0.14	9,7	1.11	9,7,4	2.67	9,7,4,10	9.83	9,7,4,10,8	19.15
19	16-19	0.14	4,9,10	2.90	10	0.16	10,5	1.17	10,5,9	2.90	10,5,9,4	6.22	10,5,9,4,8	15.30
		0.17		4.26	10	0.12	10,5	1.03	10,5,9	2.43	10,5,9,4	5.48	10,5,9,4,8	14.41
23	23-24	0.13	7,10	1.83	10	0.51	10,9	1.83	10,9,7	3.25	10,9,7,5	12.15	10,9,7,5,8	21.30
		0.18		3.61	10	0.22	10,9	1.30	10,9,7	2.42	10,9,7,5	11.22	10,9,7,5,8	20.31
26	25-26	0.1	7,9,10	2.31	10	0.07	10,9	1.76	10,9,8	2.31	10,9,8,7	7.25	10,9,8,7,5	19.24
		0.13		2.83	10	-0.12	10,9	1.44	10,9,8	2.01	10,9,8,7	6.37	10,9,8,7,5	17.41
30	2-30	0.16	9	0.38	9	0.38	9,10	1.61	9,10,1	3.68	9,10,1,7	8.07	9,10,1,7,5	17.36
		0.18		0.89	9	1.02	9,10	2.03	9,10,1	3.82	9,10,1,7	7.76	9,10,1,7,5	17.28
32	10-32	0.2	3,9	1.35	9	0.42	9,3	1.35	9,3,10	3.15	9,3,10,7	7.09	9,3,10,7,8	16.61
		0.21		1.51	9	0.35	9,3	1.26	9,3,10	2.77	9,3,10,7	6.58	9,3,10,7,8	15.84
36	23-36	0.18	7,10	3.41	10	1.65	10,3	3.41	10,3,9	6.16	10,3,9,7	14.62	10,3,9,7,8	23.86
		0.21		4.65	10	-0.21	10,3	1.09	10,3,9	3.82	10,3,9,7	12.42	10,3,9,7,8	21.63
38	29-38	0.08	9	1.14	10	1.15	10,9	2.29	10,9,6	4.20	10,9,6,7	7.08	10,9,6,7,8	18.69
		0.14		3.50	10	0.91	10,9	1.93	10,9,6	3.04	10,9,6,7	5.86	10,9,6,7,8	17.46

In Table 7.17, the first column represents the faulted bus, the second column represents the disconnected line to clear the fault, the third column represents the clearing time in seconds, the fourth column represents the SDG set found by Phase II of the proposed methodology, the fifth column represents the kinetic energy of the SDG, the sixth column represents the machine with the smallest potential energy of the post-fault system, the seventh column represents its corresponding potential energy, the remaining columns represent the machines with the smallest two, three, four or five potential energies with their corresponding total potential energies. The strategy used to construct the table, the CCT found by using the proposed method (first row for each clearing time per faulted bus) and numerical methods (the second row for each clearing

time per faulted bus) are used as a pivot since it is the only known variable. Then, Phase III is applied for different number of machines in the \overline{SDG} . According to the results summarized in the table above, it can be confirmed that a one-to-one comparison can be made, i.e. depending on how many machines in the SDG, one can use the least potential energies for the same number of machines in the SDG. For example, if one takes the case of faulted Bus 17, it can be seen that when the fault is cleared in 0.11 seconds, the SDG consists of generators 4, 7, and 9. Therefore, there are three generators in the SDG. If one takes only the smallest potential energy of one generator, which happened to be generator 9, and compared it with the SDG kinetic energy, the algorithm becomes extremely conservative. If one takes the least two potential energies (generators 9 and 7) and compare the total of the two potential energies with SDG kinetic energy, the algorithm is still very conservative but not as conservative as when one potential energy is used. However, if one uses the least three potential energies (generators 9, 7 and 4) and compare the total potential energy with the SDG kinetic energy, the algorithm is still conservative but the results are very close to the actual critical clearing time of 0.15 seconds. If one uses the least four or five potential energies, the algorithm makes the wrong decision which is the type of error the method needs to avoid. Also, another trial with a different clearing time (0.15 seconds), which is the CCT by using step-by-step integration, is performed. If one uses the least potential energies of one or two generators, the results are very conservative. In the contrary, if one uses three generators, the decision is still conservative but it is the best possible decision for the proposed method since using four or five generators cause the algorithm to produce a false positive error. Notice that the smallest potential energies for this case correspond to the same generators in the SDG but this is not always the case, e.g. faulted Bus 26 case.

Next, the proposed Phase III methodology is tested. The first test performed on this stage is to apply various faults and release the faults by removing them from the faulted bus/line, and then determine the transient stability. The result of each test is compared to the results from step-by-step integration. The decision can be either transient stable or transient unstable. Some of the tested stable cases are summarized in Table 7.18 below.

Table 7.18: TSA Results (Stable Cases Pre- = Post-Fault)

Test #	Faulted Bus	Clearing Time (sec)	SDG	Energy Function		Numerical Method	Proposed Method
				V_{KE}	V_{PE}		
1	1	0.15	9	0.3768	1.4769	Stable	Stable
2	1	0.25	9	1.0942	2.3872	Stable	Stable
3	4	0.1	1,3,9	1.1163	5.0321	Stable	Stable
4	4	0.26	1,3,9	7.442	8.8183	Stable	Stable
5	6	0.16	1,2,3,9	4.6366	15.0945	Stable	Stable
6	6	0.22	1,2,3,9	8.7103	8.9163	Stable	Stable
7	9	0.17	2,9	0.8378	5.1623	Stable	Stable
8	9	0.40	2,9	3.6923	3.3727	Stable	Unstable
9	13	0.15	3,9	1.1274	1.2479	Stable	Stable
10	13	0.20	3,9	4.4286	2.1616	Stable	Unstable
11	16	0.15	4,6,9	5.9657	6.6734	Stable	Stable
12	16	0.18	4,6,7	9.3216	7.6521	Stable	Unstable
13	19	0.19	4,9	1.1361	1.1596	Stable	Stable
14	19	0.20	4,9	1.4015	1.2154	Stable	Unstable
15	22	0.19	6,7	1.0612	1.1661	Stable	Stable
16	22	0.25	6,7	4.0651	1.5855	Stable	Unstable
17	25	0.10	8,9	1.758	5.2638	Stable	Stable
18	25	0.22	8,9	8.3829	8.5091	Stable	Stable
19	30	0.18	9	0.8854	0.0361	Stable	Unstable
20	30	0.22	9	1.2937	0.0535	Stable	Unstable
21	32	0.10	3,9	1.0668	1.0923	Stable	Stable
22	32	0.22	3,9	3.9146	1.4541	Stable	Unstable
23	35	0.10	6,9	1.127	1.1813	Stable	Stable
24	35	0.22	6,9	1.4283	1.2012	Stable	Unstable
25	38	0.05	9	0.4631	0.4645	Stable	Stable
26	38	0.15	9	1.7881	0.5619	Stable	Unstable

From the above table, the proposed method works as good as numerical methods to assess transient stability. To explain the table, the first column represents an index to the tested case, the second column represents the faulted Bus, the third column represents the clearing time after which the fault is removed from the system, the fourth column represents the resulting SDG from Phase II, the fifth column represents the SDG kinetic energy calculated by (5.12), the sixth

column represents the smallest potential energy calculated by (5.14), the seventh column is the benchmark assessment (Forward Euler’s Integration method) and the last column is the proposed methodology’s assessment. Out of the 26 examples in Table 7.18, the proposed methodology determined transient stability correctly in 17 examples (65% accuracy). In the remaining 9 cases, the proposed method determined that the system is unstable when in reality it is otherwise. This result is due to the nature of direct methods and TEF methods which generally produces conservative results. For example, Tests 11 and 12 in the table above show a fault on Bus 16 with two different clearing times. In Test 11, the fault is cleared after 0.15 sec with the step-by-step integration assessment of transient stable case which confirms the result of the proposed methodology. In Test 12, the fault is cleared after 0.18 sec with the step-by-step integration assessment of transient stable case. However, the proposed methodology determined that the fault cause the system to become transient unstable.

Next, unstable cases are used to verify the accuracy of the proposed methodology in identifying transient unstable cases. Table 7.19 summarizes some of the simulated cases which cause the system to be transient unstable.

Table 7.19: TSA Results (Unstable Cases Pre- = Post-Fault)

Test #	Faulted Bus	Clearing Time (sec)	SDG	Energy Function		Numerical Method	Proposed Method
				V_{KE}	V_{PE}		
1	1	0.35	9	1.5624	0.102	Unstable	Unstable
2	4	0.29	1,3,9	8.7131	4.1161	Unstable	Unstable
3	6	0.25	1,2,3,9	10.9702	7.6921	Unstable	Unstable
4	9	0.36	2,9	3.1922	3.0279	Unstable	Unstable
5	13	0.28	3,9	8.5514	3.269	Unstable	Unstable
6	16	0.2	4,6,9	11.492	8.3951	Unstable	Unstable
7	19	0.21	4,9	3.7297	2.1474	Unstable	Unstable
8	22	0.24	6,7	3.3424	2.5387	Unstable	Unstable
9	25	0.23	8,9	9.1567	8.8779	Unstable	Unstable
10	30	0.32	9	2.5957	0.1177	Unstable	Unstable
11	32	0.25	3,9	4.7432	1.8181	Unstable	Unstable
12	35	0.24	6,9,7	3.5828	2.0544	Unstable	Unstable
13	38	0.16	9	2.576	2.1452	Unstable	Unstable

From Table 7.19, the proposed methodology can determine transient instability accurately. According to the table above, the proposed methodology is suitable for transient stability assessment. However, the above two tables cannot qualify its suitability for online transient stability assessment (OTSA) purposes.

To further investigate the suitability of the proposed method, the same test cases summarized in the previous two tables are used but instead of just removing the fault from the system, a transmission line is removed which changes the system's topology. Reference [3] shows some examples of how the admittance matrix is affected by the change in system's topology.

At first, some stable cases are simulated and the results are tabulated in Table 7.20.

Table 7.20: TSA Results (Stable Cases Pre- ≠ Post-Fault)

Test #	Faulted Bus	Disconnected Line	Clearing Time (sec)	SDG	Energy Function		Numerical Method	Proposed Method
					V_{KE}	V_{PE}		
1	1	1-39	0.3	9	1.0523	1.1818	Stable	Stable
2	1	1-39	0.33	9	1.5624	1.4275	Stable	Unstable
3	4	3-4	0.2	1,3,9	3.3007	5.2381	Stable	Stable
4	6	6-11	0.2	1,2,3,9	7.7996	8.8001	Stable	Stable
5	9	9-39	0.29	2,9	2.164	2.1736	Stable	Stable
6	13	10-13	0.21	3,9	2.196	4.8723	Stable	Stable
7	16	16-17	0.1	4,6,9	1.1024	1.1235	Stable	Stable
8	19	16-19	0.18	4,9,10	4.4984	1.5544	Stable	Unstable
9	22	22-23	0.17	6,7	5.2135	1.7392	Stable	Unstable
10	25	25-26	0.14	8,9	3.4276	4.8329	Stable	Stable
11	30	2-30	0.28	9	0.2693	0.3565	Stable	Stable
12	32	10-32	0.23	3,9	1.7162	1.6963	Stable	Unstable
13	35	22-35	0.22	6,9	3.9146	1.0284	Stable	Unstable
14	38	29-38	0.1	9	1.7881	0.3615	Stable	Unstable

From Table 7.20, the proposed method gave conservative decisions to determine transient stability. In the table, the third column represents the disconnected transmission line which is assumed to be the faulted line. Notice that the simulated faults are close-in faults, i.e. the fault is on the line but it is very close to the Bus for which the fault source impedance is negligible. The proposed method is able to determine transient stability correctly in 8 cases out of the 14

presented cases producing about 60% accuracy. In the remaining cases, the proposed method failed to determine that the system was in fact transient stable but that is because the conservative nature of TEF methods. For example, Test 12 in the table above show a fault on Bus 32 which is cleared by disconnecting the line between Bus 10 and Bus 32 after 0.23 seconds. In this test, the system is transient stable according to the benchmark method of step-by-step integration. However, the proposed method determined that the system was transient unstable.

Next, some unstable cases are simulated to determine the accuracy of the proposed method. The results are tabulated in Table 7.21.

Table 7.21: TSA Results (Unstable Cases Pre- ≠ Post-Fault)

Test #	Faulted Bus	Disconnected Line	Clearing Time (sec)	SDG	Energy Function		Numerical Method	Proposed Method
					KE	PE		
1	4	3-4	0.28	1,3,9	6.1381	3.8026	Unstable	Unstable
2	6	6-11	0.24	1,2,3,9	8.5437	6.4635	Unstable	Unstable
3	9	9-39	0.33	2,9	2.7347	2.5771	Unstable	Unstable
4	13	10-13	0.25	3,9	6.8506	2.7656	Unstable	Unstable
5	16	16-17	0.2	4,6,7	11.492	5.5152	Unstable	Unstable
6	19	16-19	0.2	4,9,10	5.5383	1.9177	Unstable	Unstable
7	22	22-23	0.2	6,7	7.1996	2.0441	Unstable	Unstable
8	25	25-26	0.2	8,9	6.9404	5.9857	Unstable	Unstable
9	30	2-30	0.3	9	0.8708	0.4028	Unstable	Unstable
10	32	10-32	0.25	3,9	2.7432	1.8271	Unstable	Unstable
11	35	22-35	0.25	6,7,9	4.215	2.1384	Unstable	Unstable
12	38	29-38	0.14	9	3.5036	0.1528	Unstable	Unstable

From the table above, it can be seen that the proposed method produced 100% accurate transient instability decision. Although the proposed method is not very accurate in determining transient stable cases, it is more important to determine the possibility of transient instability than transient stability.

To determine the suitability for online transient stability assessment purposes, some cases are simulated and the proposed methodology is used from Phase I to Phase III and the simulation time is captured. It then is simulated by ignoring Phase I by assuming that the needed information from Phase I are given, i.e. in real systems, PMUs can be used to capture the needed

information in Phase I. The following table summarizes the captured simulation times for all the cases with and without Phase I simulation. Notice that the simulation times are based on a Core i7-2670QM CPU @ 2.20GHz computer.

Table 7.22: Average Simulation Time of Proposed Method

Test #	Faulted Bus	Clearing Time (sec)	Total Simulation Time (sec)	Decision Time (sec)
1	1	0.15	2.351	0.084
2	1	0.25	5.834	0.09
3	4	0.1	2.491	0.087
4	4	0.26	6.241	0.092
5	6	0.16	2.582	0.089
6	6	0.22	4.74	0.09
7	9	0.17	3.738	0.085
8	9	0.4	7.524	0.089
9	13	0.15	2.342	0.089
10	13	0.2	4.0851	0.087
11	16	0.15	2.445	0.09
12	16	0.18	3.987	0.085
13	19	0.09	2.606	0.089
14	19	0.1	2.71	0.084
15	22	0.09	2.609	0.088
16	22	0.15	2.445	0.09
17	25	0.1	2.712	0.082
18	25	0.22	4.72	0.09
19	30	0.18	3.977	0.089
20	30	0.22	4.497	0.09
21	32	0.1	2.587	0.088
22	32	0.19	3.9146	0.087
23	35	0.1	2.598	0.101
24	35	0.11	2.711	0.087
25	38	0.05	1.983	0.092
26	38	0.1	2.561	0.09

To explain Table 7.22, the last two columns represent the average simulation time of the proposed methodology with Phase I included and excluded, respectively. From the results, it can be seen that the average simulation time is about 3.5 sec if Phase I is included while it is about 88 ms to assess transient stability online (Phase I is excluded). According to the results, one can argue that this method is not suitable for online purposes; however, this simulation time is performed on a personal computer and it uses Matlab which are two sources that create a lot of inefficiency. The method can be faster than this if it was to be used on specialized equipment

such as a microprocessor protective relay which also uses specialized programs and codes. Also, the current code is not optimized as it is not the scope of this research.

In the next section, the proposed methodology is used to search for the CCT.

7.4 Critical Clearing Time Calculation (Phase IV)

In this section, the CCT is calculated by applying the algorithm introduced in section 5.3.4. The proposed methodology's result is then compared to two different direct methods and to the benchmark method (step-by-step integration).

To understand the search algorithm used and the corresponding CCT, a fault is applied on bus 10 and cleared by removing the line between bus 10 and 13. The following figure is obtained by running the search algorithm beyond the CCT and difference between the potential and kinetic energies is captured for the corresponding fault clearing time. Notice that a clearing time is not a critical clearing time.

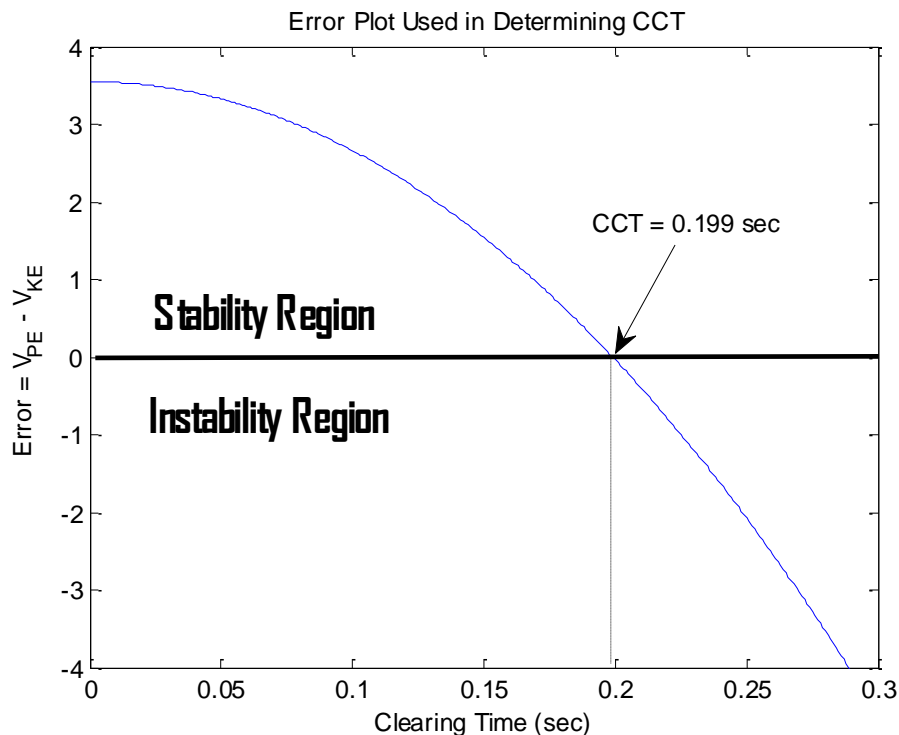


Figure 7.18: The difference between PE and KE for different clearing times

Based on the plot in Figure 7.18, the CCT for a fault on Bus 10 that is cleared by removing the line between Buses 10 and 13 is 0.199 seconds. It can be noted when the potential energy of the relevant group is greater than the kinetic energy of the SDG, the system is transient stable (denoted by Stability Region in the above figure). Also, when the kinetic energy of the SDG is greater than the relevant potential energy, i.e. the error is negative then the system is unstable (denoted by Instability Region in the above figure). When the error is approximately zero, the system is critical stable. This point is the CCT.

Now, according to the preceding, some faults are applied to the system on different buses and the fault is removed, and then the algorithm starts searching for the CCT. The results of the simulation are summarized in Table 7.23.

Table 7.23: CCT Calculation Comparison (pre-fault = post-fault)

Faulted Bus	Critical Clearing Time (sec)			
	Direct Method (EAC) [20]	Direct Method (Total Energy) [5]	Numerical Method	Proposed Method
2	0.17	0.25	0.33	0.26
3	0.18	0.32	0.34	0.30
5	0.21	0.23	0.25	0.24
6	0.22	0.24	0.24	0.24
8	0.19	0.20	0.21	0.20
9	0.18	0.31	0.36	0.26
11	0.23	0.23	0.26	0.23
12	0.17	0.20	0.25	0.13
14	0.21	0.23	0.27	0.26
15	0.16	0.25	0.28	0.28
17	0.18	0.23	0.27	0.26
18	0.18	0.12	0.13	0.12
19	0.20	0.20	0.20	0.20
20	0.27	0.20	0.23	0.20
21	0.18	0.22	0.24	0.22
23	0.21	0.21	0.23	0.14
26	0.16	0.19	0.21	0.12
28	0.15	0.17	0.17	0.15
29	0.15	0.15	0.17	0.12
30	0.16	0.25	0.31	0.17
32	0.23	0.22	0.25	0.22
33	0.21	0.20	0.26	0.20
36	0.20	0.23	0.25	0.20
38	0.14	0.14	0.15	0.11
39	0.22	0.40	0.63	0.60

From the table above, it can be observed that the proposed methodology can be used as a screening tool for planning and operation. Notice that the direct methods that are used in this table are the methods introduced in [5] and [20]. The authors of these references used Davidon-Fletcher-Powell to determine the UEP and suggested that any suitable search algorithm can be used to minimize an objective function. Therefore, in this research, Nelder-Mead simplex algorithm is utilized to determine the UEP as it was found to produce smaller error during the search for the equilibrium points. Although the results of the proposed methodology are not as accurate as numerical methods, it still gives conservative results. Also, it can be noted from the table that the direct methods that are used in this research failed in two examples (Faulted Bus 18 and 20 for the method of [20]). In addition, the proposed method is fairly more accurate than the direct method used in this research.

Alternatively, the same faults above are applied on different buses, but to clear the faults, a transmission line is disconnected. The following table summarizes the results of the simulated cases.

Table 7.24: CCT Calculation Comparison (pre-fault \neq post-fault)

Faulted Bus	Disconnected Line	Critical Clearing Time (sec)			
		Direct Method (EAC) [20]	Direct Method (Total Energy) [5]	Numerical Method	Proposed Method
2	1-2	0.17	0.24	0.25	0.24
3	3-4	0.15	0.18	0.23	0.21
5	5-6	0.21	0.24	0.25	0.20
6	6-11	0.23	0.23	0.24	0.20
8	8-9	0.20	0.21	0.21	0.15
9	9-39	0.39	0.37	0.36	0.29
11	6-11	0.23	0.22	0.23	0.22
12	11-12	0.08	0.23	0.25	0.13
14	13-14	0.22	0.20	0.25	0.25
15	15-16	0.16	0.19	0.24	0.22
17	17-27	0.15	0.15	0.15	0.11
18	17-18	0.17	0.14	0.13	0.12
19	16-19	0.17	0.17	0.17	0.14
20	19-20	0.18	0.15	0.14	0.13
21	16-21	0.20	0.20	0.20	0.16
23	23-24	0.13	0.18	0.18	0.13
26	25-26	0.11	0.13	0.13	0.10
28	26-28	0.11	0.13	0.14	0.11
29	28-29	0.19	0.12	0.12	0.09
30	2-30	0.20	0.18	0.18	0.16
32	10-32	0.21	0.20	0.21	0.20
33	19-33	0.07	0.24	0.24	0.19
36	23-36	0.14	0.21	0.21	0.18
38	29-38	0.12	0.13	0.14	0.08
39	1-39	0.08	0.37	0.52	0.50

From the results of Table 7.24, the proposed method calculated the CCT conservatively accurately when compared to the benchmark of step-by-step integration. For example, if one takes the case where Bus 15 is faulted, it can be seen that the proposed method calculated CCT is 0.22 sec while it is 0.24 sec by using numerical method, and 0.16 sec and 0.19 by using the chosen direct methods. This shows that the proposed method is more accurate than the chosen direct methods. In addition, if one takes the case where Bus 18 is the faulted Bus, it can be seen that the direct methods of [20] and [5] failed to calculate a conservative CCT while the proposed method found a close CCT to the actual one. This likely occurred because the first chosen direct method considers only one machine to be critical (referred to as the SDM in [20]) and the second chosen direct method of [5] may not have found the actual UEP while the proposed method finds

all the critical machines and does not require finding the UEP as the UEP corresponds to the CCT rotor angles.

Next, the simulation time needed for the three methods to find a CCT is tabulated in Table 7.25.

Table 7.25: Average Simulation Time for Calculating CCT

Faulted Bus	Simulation Time (sec)			
	Direct Method (EAC) [20]	Direct Method (Total Energy) [5]	Numerical Method	Proposed Method
2	17.439	88.582	141.468	39.834
3	88.013	48.962	130.573	22.104
5	47.829	68.692	142.158	45.693
6	49.255	65.285	134.758	46.001
8	61.071	78.837	114.185	41.646
9	139.025	102.948	140.028	61.191
11	45.186	84.286	140.782	36.318
12	41.756	73.726	128.853	176.515
14	39.872	50.275	111.582	40.484
15	13.743	52.572	152.958	40.746
17	58.380	79.386	178.820	40.524
18	94.397	87.475	118.728	21.802
19	334.800	58.386	139.754	21.630
20	38.829	45.386	110.738	32.298
21	38.236	53.582	150.957	34.722
23	25.983	58.683	126.925	25.487
26	31.613	63.778	167.967	174.482
28	22.183	73.683	178.245	34.563
29	36.439	51.573	139.820	42.573
30	37.580	28.837	149.748	97.186
32	128.779	69.486	147.957	42.802
33	371.393	83.867	148.857	46.460
36	48.371	73.445	152.018	56.150
38	48.940	85.374	130.783	160.929
39	79.970	55.859	115.958	290.507

From the Table 7.25, the average simulation time for the Direct Methods used is about 73 seconds while it is 60 seconds for the proposed methodology and 138 seconds for step-by-step integration. Notice that the step-by-step integration requires an ending time to stop the simulation and 20 seconds is typically used. In this research, for the comparison purpose, a time step of 1 ms and an ending time of 4 seconds are used. The 4 seconds duration is not sufficient to determine transient stability by using step-by-step integration.

7.5 Results Discussion

Although the findings of this dissertation describe that the hybrid method utilizes the advantages of the numerical and direct methods, it does not exactly follow the framework of direct methods. The well-defined Direct Methods use either an individual energy function of one machine or the global energy function for all the machines of a system. These methods use the Lyapunov Stability theory to make a transient stability decision of a certain fault by calculating the kinetic and potential energies for one or all the machines. To calculate the kinetic energy, these methods require the faulted admittance matrix while they require the post-fault admittance matrix to calculate the potential energy. Also, to calculate the potential energy of the post-fault topology, it is needed to determine the relevant UEP and SEP by using one of the many proposed methods in literature.

However, the proposed method uses the results of integrating the faulted system to calculate the kinetic energy. It also uses the post-fault admittance matrix to calculate the potential energy without the need to calculate any UEP or SEP. Therefore, the formulation of the potential and kinetic energies from Direct Methods is used. The potential energy of the proposed method is not equivalent to the potential energy that is used in any direct method. Although there is no theoretical proof that the proposed method can be used on any multi-machine power system regardless of its size, there is enough logic and simulation results behind it. The proposed method fundamentally uses the energy conversion phenomena. That is, if there is enough of the smallest potential energy that can absorb the produced maximum kinetic energy, then the system is capable to return to stable steady-state equilibrium.

In addition, the proposed method is compared to two other direct methods. The first method is introduced in [20] by Haque which uses the energy function of the severely disturbed

machine. When the proposed method is compared to that method, it can be seen that the proposed method is far more superior than Haque's method as it is not always the case that only one machine is critical. The proposed method overcame that problem by introducing a method that can determine the possible critical machines along with other machines that may contribute to system's separation. Also, another direct method that is discussed in [5] by Kundor that uses the energy function of all the machines is compared to the proposed method. It can be noticed that this method produces more accurate results with the exception of three cases. This method requires the UEP which is also a time-consuming to calculate and make accurate decision unlike the proposed method. The proposed method is intended to be used for online purposes for which we can give some accuracy up as long as the results are still conservative. Processing time is the most important factor after the conservative result to use the method for online purposes.

Given the above discussion, it is my belief that the proposed method can be extended to be used on different power systems with different sizes and capability. With the advantageous processing speed of the proposed method, it can also be used to calculate the stability margin for online purposes given that a more specialized microprocessor computer, such as a microprocessor-based relay, is used. Also, the method has an advantage that it can be parallel processed.

7.6 Summary

In this chapter, the IEEE 39 Bus power system is used to simulate the proposed method. PSAT package is used to model the system in Matlab. After the necessary model adjustments are made, the power system is used to simulate various faults and the proposed hybrid methodology is used to determine transient stability for the corresponding fault. The proposed methodology suitability for online assessment is presented. It then is compared with numerical methods and

one of the direct methods. In addition, the proposed method is used to calculate the CCT which is also compared to the benchmark (step-by-step integration) and the direct method in [20].

Concluding remarks and suggestion for future work for this dissertation are presented in Chapter 8.

Chapter 8

8 Concluding Remarks and Future Work

8.1 Concluding Remarks

The research demonstrated in this dissertation provides an alternative and effective hybrid method to assess transient stability of a multi-machine power system. The proposed methodology is based on transient energy function methods and step-by-step integration. The step-by-step integration is used to simulate the generator's rotor angles and speeds during-fault profiles. This result is then used to apply transient energy function in order to determine transient stability. The proposed methodology uses the energy conversion phenomena for any object. The method uses the single-machine smallest post-fault potential and largest fault clearing kinetic energies which are compared with each other. If the potential energy is greater than the kinetic energy, then the system is considered transient stable. However, since the system may have more than one machine that is severely disturbed, we proposed a method to identify the critical group of machines. This corresponds to Phase II of the proposed methodology. In this phase, we use five different measures. The first measure is the accelerating power which can determine the severely disturbed unit effectively. We then use the coherency to find any generator that may be swinging with the severely disturbed unit. After that, the during-fault rotors angles and speeds profiles are used to find another machine or confirm the found machines in previous steps. Also, the pre-fault and post-fault rotors angles are used to find if there is a severely disturbed unit that may not belong to the most disturbed group of machines. The resulting of this phase is a set of the so-called Severely Disturbed Group (SDG) of machines. This set is used in Phase III to calculate the kinetic and potential energies in order to determine transient stability.

The proposed method is applied on the IEEE 39 Bus power system for multiple fault cases. The method performance is verified by comparing it with the numerical methods results. Also, the method's suitability for online purposes is verified. The method produces a conservative result which is as expected for direct methods, but it is still more accurate than the tested direct method. The proposed method is an effective tool for planning purposes, which is faster than the numerical integration that is dependent on the integration step. For example, the proposed method can be used in the "what-if" scenarios which may require very long time in numerical integration is used. The proposed method is also suitable for online transient stability assessment. The method can be optimized and implemented on a microprocessor-based protective relay which uses specialized computer. This method can adapt to the changes in the network which is an advantage over traditional microprocessor-based protective relays that require being set before installation (planning).

The simulation time to calculate the critical clearing time by using the proposed method is compared with the numerical integration method as well as with a selected direct method. It is shown that the proposed method has improved speed if compared with the selected direct method. It is also shown that the proposed method is much faster than the numerical integration method. Note that the proposed methodology requires numerical integration up to the clearing instant which is an advantage over the numerical integration methods.

A historical review of stability analysis is presented in this dissertation. The stability analysis is classified into two classes: small-signal stability and transient stability. The focal point of this dissertation is transient stability analysis. Transient stability analysis methods are presented in this dissertation. There are two main methods of transient stability analysis: numerical methods and direct methods. Different numerical methods are discussed in this thesis

such as, trapezoidal rule and Euler integration. Additionally, different methods of direct methods are presented, and the advantages and disadvantages of these methods over numerical methods are discussed.

The tool to test the proposed method is a MATLAB based toolbox titled Power System Analysis Toolbox (PSAT). PSAT is used for electric power system analysis and control. PSAT is used in this dissertation because of its availability and capability of performing power flow and numerical integration in addition to its easy-to-use graphical user interface (GUI) as well as its capability of command usage.

8.2 Future Work

It is the intention of this dissertation to apply the proposed method on a real-size power system though the IEEE 39 Bus system is used. The proposed method can be implemented in a more specialized computer system to make even faster than it is. Also, real phasor measurement units (PMU) can be utilized if an access is granted by a utility company to pilot the proposed method onto its transmission system. In addition, the algorithm can be optimized by parallelizing the identification of critical machines and the online transient stability assessment phases. The critical clearing time search algorithm incrementing step is yet to be optimized.

Appendix A

A.1 PSAT Built-in Functions [51]:

Some important built-in PSAT functions are used to implement the data file, faults, and running required analyses. At first, PSAT data format is explained for the components used in this thesis.

A.1.1 Bus Data Format:

Table A.1.1 shows the Bus data format using the command `Bus . con`.

Table A.1.1: Bus Data Format (`Bus . con`)

Column	Variable	Description	Unit
1	-	Bus number	int
2	V_s	Voltage base	kV
3	V_0	Voltage amplitude initial guess	p.u.
4	θ_0	Voltage phase initial guess	rad

A.1.2 Line Data Format:

Table A.1.2 shows the line data format in PSAT using the command (`Line . con`).

Table A.1.2: Line Data Format (`Line . con`)

Column	Variable	Description	Unit
1	k	From Bus	int
2	m	To Bus	int
3	S_n	Power rating	MVA
4	V_n	Voltage rating	kV
5	f_n	Frequency rating	Hz
6	l	Line length	km
7	-	not used	-
8	r	Resistance	p.u. (Ω /km)
9	x	Reactance	p.u. (H/km)
10	b	Susceptance	p.u. (F/km)
11	-	not used	-
12	-	not used	-
13	I_{max}	Current limit	p.u.
14	P_{max}	Active power limit	p.u.
15	S_{max}	Apparent power limit	p.u.
16	u	Connection status	{0,1}

A.1.3 Transformer Data Format:

Table A.1.3 shows the transformer data format in PSAT using the command (`Line.con`).

Table A.1.3: Transformer Data Format (`Line.con`)

Column	Variable	Description	Unit
1	k	From Bus	int
2	m	To Bus	int
3	S_n	Power rating	MVA
4	V_n	Voltage rating	kV
5	f_n	Frequency rating	Hz
6	-	not used	-
7	K_T	Primary and secondary voltage ration	kV/kV
8	r	Resistance	p.u. (Ω /km)
9	x	Reactance	p.u. (H/km)
10	-	not used	-
11	a	Fixed tap ratio	p.u./p.u.
12	ϕ	Fixed phase shift	deg
13	I_{max}	Current limit	p.u.
14	P_{max}	Active power limit	p.u.
15	S_{max}	Apparent power limit	p.u.
16	u	Connection status	{0,1}

A.1.4 Slack Generator Data Format:

Table A.1.4 shows the slack generator data format in PSAT using the command (`SW.con`).

Table A.1.4: Slack Generator Data Format (`SW.con`)

Column	Variable	Description	Unit
1	-	Bus numer	int
2	S_n	Power rating	MVA
3	V_n	Voltage rating	kV
4	V_0	Voltage magnitude	p.u.
5	θ_0	Reference angle	p.u.
6	Q_{max}	Maximum reactive power	p.u.
7	Q_{min}	Minimum reactive power	p.u.
8	V_{max}	Maximum voltage	p.u.
9	V_{min}	Minimum voltage	p.u.
10	P_{g0}	Active power guess	p.u.
11	γ	Loss participation coefficient	-
12	z	Reference bus	{0,1}
13	u	Connection status	{0,1}

A.1.5 PV Generator Data Format:

Table A.1.5 shows the PV generator data format in PSAT using the command (`PV.con`).

Table A.1.5: PV Generator Data Format (`PV.con`)

Column	Variable	Description	Unit
1	-	Bus numer	int
2	S_n	Power rating	MVA
3	V_n	Voltage rating	kV
4	V_0	Voltage magnitude	p.u.
5	θ_0	Reference angle	p.u.
6	Q_{max}	Maximum reactive power	p.u.
7	Q_{min}	Minimum reactive power	p.u.
8	V_{max}	Maximum voltage	p.u.
9	V_{min}	Minimum voltage	p.u.
10	P_{g0}	Active power guess	p.u.
11	γ	Loss participation coefficient	-

A.1.6 PQ Load Data Format:

Table A.1.6 shows the PQ Load data format in PSAT using the command (`PQ.con`).

Table A.1.6: PQ Load Data Format (`PQ.con`)

Column	Variable	Description	Unit
1	-	Bus numer	int
2	S_n	Power rating	MVA
3	V_n	Voltage rating	kV
4	P_L	Active Power	p.u.
5	Q_L	Reactive Power	p.u.
6	V_{max}	Maximum Voltage	p.u.
7	V_{min}	Minimum Voltage	p.u.
8	z	Allow conversion to impedance	{0,1}
9	u	Connection status	{0,1}

A.1.7 Fault Data Format:

Table A.1.7 shows the fault data format in PSAT using the command (`Fault.con`).

Table A.1.7: Fault Data Format (`Fault.con`)

Column	Variable	Description	Unit
1	-	Bus number	int
2	S_n	Power rating	MVA
3	V_n	Voltage rating	kV
4	f_n	Frequency rating	Hz
5	t_f	Fault time	S
6	t_c	Clearance time	s
7	r_f	Fault resistance	p.u.
8	x_f	Fault reactance	p.u.

A.1.8 Breaker Data Format:

Table A.1.8 shows the fault data format in PSAT using the command (`Breaker.con`).

Table A.1.8: Breaker Data Format (`Breaker.con`)

Column	Variable	Description	Unit
1	-	Line number	int
2	-	Bus number	int
3	S_n	Power rating	MVA
4	V_n	Voltage rating	kV
5	f_n	Frequency rating	Hz
6	U	Status	Boolean
7	t_1	First intervention time	s
8	t_2	Second intervention time	S
9	r	Line resistance	p.u.
10	x	Line reactance	p.u.
11	b	Line susceptance	p.u.
12	a	Line fixed tap ratio	p.u./p.u.
13	ϕ	Line fixed phase shift	rad

A.1.9 Synchronous Machine Data Format:

Table A.1.9 shows the synchronous machine data format in PSAT using the command (`syn.con`).

Table A.1.9: Synchronous machine data format

Column	Variable	Description	Unit
1	-	Bus number	int
2	S_n	Power rating	MVA
3	V_n	Voltage rating	kV
4	f_n	Frequency rating	Hz
5	-	Machine model	-
6	x_l	Leakage reactance	p.u.
7	r_a	Armature resistance	p.u.
8	x_d	d-axis synchronous reactance	p.u.
9	x'_d	d-axis transient reactance	p.u.
10	x''_d	d-axis subtransient reactance	p.u.
11	$T'd0$	d-axis open circuit transient time constant	s
12	$T''d0$	d-axis open circuit subtransient time constant	s
13	x_q	q-axis synchronous reactance	p.u.
14	x'_q	q-axis transient reactance	p.u.
15	x''_q	q-axis subtransient reactance	p.u.
16	$T'q0$	q-axis open circuit transient time constant	s
17	$T''q0$	q-axis open circuit subtransient time constant	s
18	$M = 2H$	Mechanical starting time	kWs/kVA
19	D	Damping coefficient	-
20	$K\omega$	Speed feedback gain	gain
21	Kp	Active power feedback gain	gain
22	γP	Active power ratio at node	[0,1]
23	γQ	Reactive power at node	[0,1]
24	TAA	d-axis additional leakage time constant	s
25	$S(1,0)$	First saturation factor	-
26	$S(1,2)$	second saturation factor	-
27	$nCOI$	Center of inertia number	int
28	u	Connection status	{0,1}

Notice that not all parameters are used when the classical model is used. Column 5 indicates the machine model and the number “2” indicates the classical model. For more details, refer to [22].

A.2 Power Flow Report:

POWER FLOW REPORT

P S A T 2.1.6

Author: Federico Milano, (c) 2002-2010
e-mail: Federico.Milano@uclm.es
website: <http://www.uclm.es/area/gsee/Web/Federico>

File: C:\Users\Hussain Al\Documents\UNO\Spring 2015\ENAS 7050 Dissertation Research\Spring Simulation\Test_02-14-2014\ieee39bus3
Date: 26-Feb-2015 00:54:27

NETWORK STATISTICS

Buses: 39
Lines: 34
Transformers: 12
Generators: 10
Loads: 30

SOLUTION STATISTICS

Number of Iterations: 4
Maximum P mismatch [p.u.] 0
Maximum Q mismatch [p.u.] 0
Power rate [MVA] 100

POWER FLOW RESULTS

Bus	V [p.u.]	phase [rad]	P gen [p.u.]	Q gen [p.u.]	P load [p.u.]	Q load [p.u.]
Bus 01	1.059	-0.14526	0	0	0	0
Bus 02	1.0789	-0.10241	0	0	0	0
Bus 03	1.0696	-0.14979	0	0	3.22	0.024
Bus 04	1.053	-0.16671	0	0	5	1.84
Bus 05	1.0566	-0.15128	0	0	0	0
Bus 06	1.0602	-0.14094	0	0	0	0
Bus 07	1.0467	-0.17517	0	0	2.338	0.84
Bus 08	1.0441	-0.18286	0	0	5.22	1.76
Bus 09	1.048	-0.17709	0	0	0	0
Bus 10	1.0727	-0.10145	0	0	0	0
Bus 11	1.0673	-0.11485	0	0	0	0
Bus 12	1.0623	-0.11435	0	0	0.085	0.88
Bus 13	1.0687	-0.11182	0	0	0	0
Bus 14	1.0629	-0.13596	0	0	0	0
Bus 15	1.0625	-0.13658	0	0	3.2	1.53
Bus 16	1.0762	-0.11149	0	0	3.29	0.323
Bus 17	1.0755	-0.12912	0	0	0	0
Bus 18	1.0721	-0.1439	0	0	1.58	0.3
Bus 19	1.1115	-0.03129	0	0	0	0
Bus 20	0.99422	-0.0488	0	0	6.28	1.03

Bus 21	1.0691	-0.07211	0	0	2.74	1.15
Bus 22	1.0788	0.00133	0	0	0	0
Bus 23	1.0699	-0.00166	0	0	2.475	0.846
Bus 24	1.0789	-0.10948	0	0	3.086	-0.922
Bus 25	1.0877	-0.0797	0	0	2.24	0.472
Bus 26	1.0873	-0.09945	0	0	1.39	0.17
Bus 27	1.0765	-0.13189	0	0	2.81	0.755
Bus 28	1.0821	-0.04162	0	0	2.06	0.276
Bus 29	1.0803	0.00394	0	0	2.835	0.269
Bus 30	1.0475	-0.06033	2.5	1.2421	0	0
Bus 31	0.982	0	5.1092	2.5614	0	0
Bus 32	0.9831	0.04016	6.5	2.7299	0	0
Bus 33	0.9972	0.06022	6.32	1.8232	0	0
Bus 34	1.0123	0.04202	5.08	1.9822	0	0
Bus 35	1.0493	0.08771	6.5	1.9311	0	0
Bus 36	1.0635	0.1326	5.6	0.02211	0	0
Bus 37	1.0278	0.03839	5.4	-0.15336	0	0
Bus 38	1.0265	0.12695	8.3	-0.02723	0	0
Bus 39	1.03	-0.17221	10	-0.41522	11.04	2.5

STATE VARIABLES

delta_Syn_1	-0.11558
omega_Syn_1	1
delta_Syn_2	0.30206
omega_Syn_2	1
delta_Syn_3	0.34126
omega_Syn_3	1
delta_Syn_4	0.31139
omega_Syn_4	1
delta_Syn_5	0.52254
omega_Syn_5	1
delta_Syn_6	0.3527
omega_Syn_6	1
delta_Syn_7	0.37039
omega_Syn_7	1
delta_Syn_8	0.32415
omega_Syn_8	1
delta_Syn_9	0.54951
omega_Syn_9	1
delta_Syn_10	0.0078
omega_Syn_10	1

OTHER ALGEBRAIC VARIABLES

vf_Syn_1	1.0292
pm_Syn_1	10
p_Syn_1	10
q_Syn_1	-0.41522
vf_Syn_2	1.219
pm_Syn_2	5.1092
p_Syn_2	5.1092
q_Syn_2	2.5614
vf_Syn_3	1.1838
pm_Syn_3	6.5
p_Syn_3	6.5

q_Syn_3	2.7299
vf_Syn_4	1.1118
pm_Syn_4	6.32
p_Syn_4	6.32
q_Syn_4	1.8232
vf_Syn_5	1.4331
pm_Syn_5	5.08
p_Syn_5	5.08
q_Syn_5	1.9822
vf_Syn_6	1.1826
pm_Syn_6	6.5
p_Syn_6	6.5
q_Syn_6	1.9311
vf_Syn_7	1.0953
pm_Syn_7	5.6
p_Syn_7	5.6
q_Syn_7	0.02211
vf_Syn_8	1.0624
pm_Syn_8	5.4
p_Syn_8	5.4
q_Syn_8	-0.15336
vf_Syn_9	1.1238
pm_Syn_9	8.3
p_Syn_9	8.3
q_Syn_9	-0.02723
vf_Syn_10	1.0868
pm_Syn_10	2.5
p_Syn_10	2.5
q_Syn_10	1.2421
delta_COI_1	0.04508
omega_COI_1	1

LINE FLOWS

From Bus	To Bus	Line	P Flow [p.u.]	Q Flow [p.u.]	P Loss [p.u.]	Q Loss [p.u.]
Bus 01	Bus 02	1	-1.2236	-0.7754	0.00513	-0.73822
Bus 01	Bus 39	2	1.2236	0.7754	0.00261	-0.75315
Bus 02	Bus 03	3	3.6577	0.28743	0.01515	-0.12081
Bus 02	Bus 25	4	-2.3864	0.78892	0.03884	-0.12363
Bus 02	Bus 30	5	-2.5	-1.1135	0	0.12855
Bus 03	Bus 04	6	0.94264	0.65883	0.00171	-0.22136
Bus 03	Bus 18	7	-0.52006	-0.27459	0.00028	-0.24175
Bus 04	Bus 05	8	-1.3542	-0.28067	0.00135	-0.12765
Bus 04	Bus 14	9	-2.7049	-0.67914	0.00554	-0.06533
Bus 05	Bus 08	10	3.1821	0.92491	0.00798	-0.05109
Bus 06	Bus 05	11	4.5415	1.0799	0.00389	0.00192
Bus 06	Bus 07	12	4.2154	1.2794	0.01045	0.03481
Bus 06	Bus 11	13	-3.6477	-0.64462	0.00849	-0.05775
Bus 07	Bus 08	14	1.8669	0.40454	0.00135	-0.06977
Bus 08	Bus 09	15	-0.18032	-0.30968	9e-005	-0.41482
Bus 09	Bus 39	16	-0.18041	0.10513	0.00056	-1.2816
Bus 10	Bus 11	17	3.6643	0.98949	0.00504	-0.02931
Bus 10	Bus 13	18	2.8357	0.71192	0.00299	-0.0514
Bus 10	Bus 32	19	-6.5	-1.7014	0	1.0285

Bus 12	Bus 11	20	-0.00289	-0.42481	0.00026	0.00712
Bus 12	Bus 13	21	-0.08211	-0.45519	0.00031	0.00845
Bus 13	Bus 14	22	2.7503	0.29968	0.00609	-0.12743
Bus 14	Bus 15	23	0.03372	-0.18669	0	-0.41329
Bus 15	Bus 16	24	-3.1663	-1.3034	0.00915	-0.09991
Bus 16	Bus 17	25	2.286	-0.16084	0.00316	-0.11511
Bus 16	Bus 19	26	-5.0249	-1.5199	0.03738	0.09173
Bus 16	Bus 21	27	-3.3066	0.67473	0.00802	-0.15782
Bus 16	Bus 24	28	-0.42	-0.52046	0.00011	-0.07687
Bus 17	Bus 18	29	2.1031	0.21271	0.00273	-0.12014
Bus 17	Bus 27	30	0.17981	-0.25843	4e-005	-0.37177
Bus 19	Bus 33	31	-6.2895	-1.2054	0.03046	0.61784
Bus 19	Bus 20	32	1.2273	-0.40629	0.0012	0.02357
Bus 20	Bus 34	33	-5.0539	-1.4599	0.02612	0.52231
Bus 21	Bus 22	34	-6.0546	-0.31745	0.02568	0.15352
Bus 22	Bus 23	35	0.41968	0.86294	0.00058	-0.20386
Bus 22	Bus 35	36	-6.5	-1.3339	0	0.59717
Bus 23	Bus 24	37	3.5302	-0.51128	0.02413	-0.03286
Bus 23	Bus 36	38	-5.5861	0.73207	0.01386	0.75418
Bus 25	Bus 26	39	0.71814	-0.35373	0.0014	-0.59259
Bus 25	Bus 37	40	-5.3834	0.79429	0.01658	0.64093
Bus 26	Bus 27	41	2.6389	0.45217	0.00866	-0.18949
Bus 26	Bus 28	42	-1.4086	-0.17178	0.00752	-0.83507
Bus 26	Bus 29	43	-1.9035	-0.21153	0.01823	-1.0088
Bus 28	Bus 29	44	-3.4761	0.38729	0.01479	-0.13157
Bus 29	Bus 38	45	-8.2477	1.0472	0.0523	1.0199
Bus 06	Bus 31	46	-5.1092	-1.7146	0	0.84683

LINE FLOWS

From Bus	To Bus	Line	P Flow	Q Flow	P Loss	Q Loss
		[p.u.]	[p.u.]	[p.u.]	[p.u.]	
Bus 02	Bus 01	1	1.2287	0.03718	0.00513	-0.73822
Bus 39	Bus 01	2	-1.221	-1.5285	0.00261	-0.75315
Bus 03	Bus 02	3	-3.6426	-0.40824	0.01515	-0.12081
Bus 25	Bus 02	4	2.4253	-0.91256	0.03884	-0.12363
Bus 30	Bus 02	5	2.5	1.2421	0	0.12855
Bus 04	Bus 03	6	-0.94092	-0.88019	0.00171	-0.22136
Bus 18	Bus 03	7	0.52034	0.03284	0.00028	-0.24175
Bus 05	Bus 04	8	1.3555	0.15302	0.00135	-0.12765
Bus 14	Bus 04	9	2.7105	0.6138	0.00554	-0.06533
Bus 08	Bus 05	10	-3.1741	-0.976	0.00798	-0.05109
Bus 05	Bus 06	11	-4.5376	-1.0779	0.00389	0.00192
Bus 07	Bus 06	12	-4.2049	-1.2445	0.01045	0.03481
Bus 11	Bus 06	13	3.6561	0.58687	0.00849	-0.05775
Bus 08	Bus 07	14	-1.8656	-0.47431	0.00135	-0.06977
Bus 09	Bus 08	15	0.18041	-0.10513	9e-005	-0.41482
Bus 39	Bus 09	16	0.18098	-1.3867	0.00056	-1.2816
Bus 11	Bus 10	17	-3.6593	-1.0188	0.00504	-0.02931
Bus 13	Bus 10	18	-2.8327	-0.76332	0.00299	-0.0514
Bus 32	Bus 10	19	6.5	2.7299	0	1.0285
Bus 11	Bus 12	20	0.00316	0.43193	0.00026	0.00712
Bus 13	Bus 12	21	0.08242	0.46364	0.00031	0.00845
Bus 14	Bus 13	22	-2.7442	-0.42711	0.00609	-0.12743
Bus 15	Bus 14	23	-0.03372	-0.2266	0	-0.41329

Bus 16	Bus 15	24	3.1754	1.2035	0.00915	-0.09991
Bus 17	Bus 16	25	-2.2829	0.04573	0.00316	-0.11511
Bus 19	Bus 16	26	5.0622	1.6117	0.03738	0.09173
Bus 21	Bus 16	27	3.3146	-0.83255	0.00802	-0.15782
Bus 24	Bus 16	28	0.42011	0.44359	0.00011	-0.07687
Bus 18	Bus 17	29	-2.1003	-0.33284	0.00273	-0.12014
Bus 27	Bus 17	30	-0.17977	-0.11334	4e-005	-0.37177
Bus 33	Bus 19	31	6.32	1.8232	0.03046	0.61784
Bus 20	Bus 19	32	-1.2261	0.42986	0.0012	0.02357
Bus 34	Bus 20	33	5.08	1.9822	0.02612	0.52231
Bus 22	Bus 21	34	6.0803	0.47096	0.02568	0.15352
Bus 23	Bus 22	35	-0.4191	-1.0668	0.00058	-0.20386
Bus 35	Bus 22	36	6.5	1.9311	0	0.59717
Bus 24	Bus 23	37	-3.5061	0.47841	0.02413	-0.03286
Bus 36	Bus 23	38	5.6	0.02211	0.01386	0.75418
Bus 26	Bus 25	39	-0.71674	-0.23886	0.0014	-0.59259
Bus 37	Bus 25	40	5.4	-0.15336	0.01658	0.64093
Bus 27	Bus 26	41	-2.6302	-0.64166	0.00866	-0.18949
Bus 28	Bus 26	42	1.4161	-0.66329	0.00752	-0.83507
Bus 29	Bus 26	43	1.9218	-0.79729	0.01823	-1.0088
Bus 29	Bus 28	44	3.4909	-0.51886	0.01479	-0.13157
Bus 38	Bus 29	45	8.3	-0.02723	0.0523	1.0199
Bus 31	Bus 06	46	5.1092	2.5614	0	0.84683

GLOBAL SUMMARY REPORT

TOTAL GENERATION

REAL POWER [p.u.] 61.3092
 REACTIVE POWER [p.u.] 11.6962

TOTAL LOAD

REAL POWER [p.u.] 60.889
 REACTIVE POWER [p.u.] 14.043

TOTAL LOSSES

REAL POWER [p.u.] 0.4202
 REACTIVE POWER [p.u.] -2.3468

Bibliography

- [1] H. H. Al Marhoon, I. Leevongwat and P. Rastgoufard, " A Fast Search Algorithm for Critical Clearing Time for Power Systems Transient Stability Analysis," *Power Systems Conference: Advanced Metering, Protection, Control, Communication, and Distributed Resources, 2014. PSC 2014*, 11-14 March 2014
- [2] H. H. Al Marhoon, I. Leevongwat and P. Rastgoufard, "A practical method for power systems transient stability and security analysis," *Transmission and Distribution Conference and Exposition (T&D), 2012 IEEE PES* , vol., no., pp.1,6, 7-10 May 2012
- [3] H. H. Al Marhoon, "A practical method for power systems transient stability and security," M.S. Thesis, Elect. and Computer Eng. Dept., Univ. of New Orleans, New Orleans, 2011
- [4] N. Beeravolu, "Predicting Voltage Abnormality Using Power Systems Dynamic Response," Ph. D. Dissertation, Elect. Eng. Dept., Univ. of New Orleans, New Orleans, 2013
- [5] P. Kundur, *Power System Stability and Control*, McGraw-Hill, Inc., New York, 1994
- [6] K. R. Padiyar, *Power System Dynamics Stability and Control*, BS Publications, Hyderabad, 2nd edition, 2008
- [7] P. W. Sauer and M. A. Pai, *Power System Dynamic and Stability*, Prentice-Hall, Inc. New Jersey, 1998
- [8] P. C. Magnusson, "Transient Energy Method of Calculating Stability," *AIEE Trans.*, Vol. 66, pp. 747-755, 1947
- [9] P. D. Aylett, "The Energy Integral-Criterion of Transient Stability Limits of Power Systems," *Proc. IEE*, Vol. 105c, No. 8, pp. 527-536, September 1958.
- [10] C. P. Steinmetz, "Power Control and Stability of Electric Generating Stations," *AIEE Trans.*, Vol. XXXIX, no.2, pp.1215-1287, July 1920
- [11] R. Wikins, "Practical Aspects of System Stability," *AIEE Trans.*, pp. 41-50, 1926
- [12] R. D. Evans, C. F. Wagner, "Further Studies of Transmission System Stability," *AIEE Trans.*, pp. 51-80, 1926
- [13] Edvard. (2010). Historical Review of Power System Stability Problems. Retrieved from <http://electrical-engineering-portal.com/historical-review-of-power-system-stability-problems>
- [14] A. R. Bergen, V. Vittal, *Power Systems Analysis*, Prentice-Hall, Inc, New Jersey, 2nd edition, 2000
- [15] Y. Xue, Th.V. Cutsem and M. Ribbens-Pavella, "Extended equal area criterion justifications, generalizations, applications," *IEEE Trans.*, 1989, PWRS-4, (1), pp. 44-52.

- [16] Lu Fang and Yu Ji-lai, "Transient stability analysis with equal area criterion directly used to a non-equivalent generator pair," *Power Engineering, Energy and Electrical Drives, 2009. POWERENG '09. International Conference on*, vol., no., pp.386-389, 18-20 March 2009.
- [17] A. Michel, A. Fouad and V. Vittal, "Power system transient stability using individual machine energy functions," *Circuits and Systems, IEEE Transactions on*, vol.30, no.5, pp. 266-276, May 1983.
- [18] P. Rastgoufard, A. Yazdankhah and R. A. Schlueter, "Multi-machine equal area based power system transient stability measure," *IEEE Transactions on Power Systems*, vol.3, no.1, pp.188-196, Feb 1988
- [19] T. Athay, R. Podmore and S. Virmani, "A Practical Method for the Direct Analysis of Transient Stability," *IEEE Transactions on Power Apparatus and Systems*, vol.PAS-98, no.2, pp.573-584, March 1979
- [20] M. H. Haque, "Equal-area criterion: an extension for multimachine power systems," *Generation, Transmission and Distribution, IEE Proceedings*, vol.141, no.3, pp.191-197, May 1994.
- [21] A. Priyadi, N. Yorino, M. Eghbal, Y. Zoka, Y. Sasaki, H. Yasuda, and H. Kakui Eghbal, "Transient stability assessment as boundary value problem," *Electric Power Conference, 2008. EPEC 2008. IEEE Canada*, vol., no., pp.1,6, 6-7 Oct. 2008.
- [22] A. Priyadi, N. Yorino, D. K. Jha, Y. Zoka, Y. Sasaki, H. Yasuda and H. Kakui, "Critical Trajectory Method for Transient Stability Analysis," *Computer and Electrical Engineering, 2008. ICCEE 2008. International Conference on*, vol., no., pp.291-295, 20-22 Dec. 2008.
- [23] M. H. Haque, "Application of energy function to assess the first-swing stability of a power system with a SVC," *Generation, Transmission and Distribution, IEE Proceedings-*, vol.152, no.6, pp. 806- 812, 4 Nov. 2005.
- [24] R. M. Iqbal and S. Krishna, "Online dynamic security assessment of power systems using critical group energy function," *Power India Conference, 2012 IEEE Fifth*, vol., no., pp.1,6, 19-22 Dec. 2012.
- [25] Zhenhua Wang, V. Aravnthan and E. B. Makram, "Generator cluster transient stability assessment using catastrophe theory," *Environment and Electrical Engineering (EEEIC), 2011 10th International Conference on*, vol., no., pp.1,4, 8-11 May 2011.
- [26] C. W. Taylor, *Power system voltage stability*, McGraw-Hill, New York, USA, 1994, pp. 273
- [27] G. K. Morison, B. Gao and P. Kundar, "Voltage stability analysis using static and dynamic approaches," *IEEE Tran. on Power Systems*, Vol. 8, No.3, August 1993, pp. 1159-1171
- [28] Y. G. Zeng, A. Berizzi and P. Marannino, "Voltage stability analysis considering dynamic load model," *Proceedings of the 4th International Conference on Advances in Power System Control, Operation and Management, APSCOM-97*, Hong Kong, November 1997.

- [29] Xu Wison and M. Yakout, "Voltage stability analysis using generic dynamic load models," *IEEE Transactions on Power Systems*. Vol. 9, No. 1, February 1994.
- [30] M. H. Haque and U. M. R. Pothula, "Evaluation of Dynamic Voltage Stability of a Power System," *POWERCON 2004*, Singapore.
- [31] C. C. Liu, "Characterization of a voltage collapse mechanism due to the effect of on-load tap changers," *Proc, 1986 IEEE International Symposium on Circuits and systems*, Vol.3, May 1986, pp. 1028-1030.
- [32] C. C. Liu and T. VU. KHOI, "Analysis of Tap-Changer Dynamics and Construction of voltage Stability Regions," *IEEE Transaction on circuits and systems*, Vol. 36, no. 4, April 1989.
- [33] Sekine. Y, Ohtsuki. H, Cascaded voltage collapse. *IEEE Trans. Power Systems*, Vol. 5, no. 1, February 1990, pp. 250-256.
- [34] Kai Sun, S. Likhate, V. Vittal, V. S. Kolluri and S. Mandal, "An Online Dynamic Security Assessment Scheme Using Phasor Measurements and Decision Trees," *Power Systems, IEEE Transactions on* , vol.22, no.4, pp.1935,1943, Nov. 2007
- [35] R. Diao, V. Vittal, Kai Sun, S. Kolluri, S. Mandal and F. Galvan, "Decision tree assisted controlled islanding for preventing cascading events," *Power Systems Conference and Exposition, 2009. PSCE '09. IEEE/PES* , vol., no., pp.1,8, 15-18 March 2009
- [36] R. Diao, Kai Sun, V. Vittal, R. J. O'Keefe, M. R. Richardson, N. Bhatt, D. Stradford and S. K. Sarawgi, "Decision Tree-Based Online Voltage Security Assessment Using PMU Measurements," *Power Systems, IEEE Transactions on* , vol.24, no.2, pp.832,839, May 2009
- [37] I. Genc, R. Diao, V. Vittal, S. Kolluri and S. Mandal, "Decision Tree-Based Preventive and Corrective Control Applications for Dynamic Security Enhancement in Power Systems," *Power Systems, IEEE Transactions on* , vol.25, no.3, pp.1611,1619, Aug. 2010
- [38] Ye Shengyong, Xin Li, Xiaoru Wang and Qingquan Qian, "Power System Transient Stability Assessment Based on Adaboost and Support Vector Machines," *Power and Energy Engineering Conference (APPEEC), 2012 Asia-Pacific* , vol., no., pp.1,4, 27-29 March 2012
- [39] T. Van Cutsem and C. Vournas, *Voltage stability of electric power systems*, Kluwer academic publishers, Boston, USA, 1998, pp. 378
- [40] D. N. Kosterev, C. W. Taylor and W. A. Mittelstadt, "Model validation for the August 10, 1996 WSCC system outage," *IEEE Transactions on Power Systems*, vol. 14, No. 3, August 1999, pp. 967-979.
- [41] K. S. Shetye, T. J. Overbye and J. F. Gronquist, "Validation of power system transient stability results," *Power and Energy Conference at Illinois (PECI), 2012 IEEE* , vol., no., pp.1,8, 24-25 Feb. 2012
- [42] J. Machowski, J. W. Bialek and J. R. Bumby, *Power System Dynamics Stability and Control*, John Wiley & Sons, Ltd., West Sussex, 2008

- [43] R. M. Rifkin, *Everything Old is New Age: A Fresh Look at Historical Approaches to Machine Learning*, *PhD thesis*, Massachusetts Institute of Technology, 2002
- [44] Ye Shengyong Xin Li, Xiaoru Wang and Qingquan Qian, "Power System Transient Stability Assessment Based on Adaboost and Support Vector Machines," *Power and Energy Engineering Conference (APPEEC), 2012 Asia-Pacific*, vol., no., pp.1,4, 27-29 March 2012
- [45] C. M. Bishop, *Pattern Recognition and Machine Learning*, Springer Science+Business Media, LLC, New York, 2006
- [46] T. Hastie, R. Tibshirani and J. Friedman, *The Elements of Statistical Learning: Data Mining, Inference, and Prediction*, Springer-Verlag, LLC, New York, 2nd Ed., 2011
- [47] S. T. Y. Lee and F. C. Schewpe, "Distance Measures and Coherency Recognition for Transient Stability Equivalents," *Power Apparatus and Systems, IEEE Transactions on*, vol.PAS-92, no.5, pp.1550,1557, Sept. 1973
- [48] L. Mariotto, H. Pinheiro, G. Cardoso, A. P. Morais and M. R. Muraro, "Power systems transient stability indices: an algorithm based on equivalent clusters of coherent generators," *Generation, Transmission & Distribution, IET*, vol.4, no.11, pp.1223,1235, November 2010
- [49] H. Bevrani, *Robust Power System Frequency Control*, Springer US, LLC, New York, 2009
- [50] M. Pavella, D. Ernst and D. Ruiz-Vega, *Transient Stability of Power Systems: A Unified Approach to Assessment and Control*, Kluwer Academic Publishers, Boston/Dordercht/London
- [51] F. Milano, *Power System Analysis Toolbox: Quick Reference Manual for PSAT version 2.1.2*, June 28, 2008

Vita

The author was born in 1982 in the Kingdom of Saudi Arabia. He completed his associate diploma in Electrical Power Engineering Technology from Jubail Industrial College, Jubail, Saudi Arabia in 2004 with first honor degree. He finished his Bachelor of Science degree in Electrical Engineering from the University of New Orleans in December 2008 with Cum Laude honor. He then received his M.S. in Electrical Engineering from the University of New Orleans in May 2011. He is expected to finish his Doctorate studies in Engineering and Applied Sciences (Electrical) in the University of New Orleans in August 2015.

He was a Graduate Assistant for Entergy's Protection Standard Automation project between August 2013 and May 2015. He is currently working as an Engineer at Entergy's Transmission Protection Department. His areas of interests are power systems modeling and simulation, on-line stability and security assessments, and power systems control and protection.

Mr. Al Marhoon is a student member of IEEE since 2008, a Sr. member of UNOES since 2015 and a member of Tau Beta Pi.